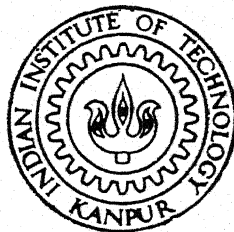# FORMATION AND GROWTH OF INTERMETALLIC COMPOUNDS IN DIFFUSION COUPLES OF FE AND TI WITH AL-12% SILICON EUTECTIC ALLOY

By

TANMOY MAITRA

DEPARTMENTS OF MATERIALS & METALLURGY

INDIAN INSTITUTE OF TECHNOLOGY, KANPUR

JUNE, 1998

FORMATION AND GROWTH OF INTERMETALLIC COMPOUNDS IN DIFFUSION COUPLES OF FE AND TI WITH AL-12%SILICON EUTECTIC ALLOY

A Thesis Submitted

in Partial Fulfillment of the Requirements

for the Degree of

Master of Technology

by

TANMOY MAITRA

DEPARTMENTS OF MATERIALS & METALLURGY

INDIAN INSTITUTE OF TECHNOLOGY KANPUR

JUNE 1998

MME - 1998 - M - MAI - FOR
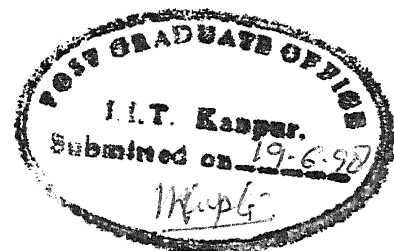
CERTIFICATE

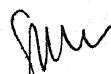It is certified that the work contained in this thesis entitled *"Formation and Growth of Intermetallic Compounds in Diffusion Couples of Fe and Ti with Al-12%Si Eutectic Alloy"*, by *Tanmoy Maitra*, has been carried out under my supervision and that this work has not been submitted elsewhere for any degree.

Dr. S. P. Gupta

Professor

Materials & Metallurgical Engineering

Indian Institute of Technology

Kanpur July, 1998

Abstract

Intermetallic coatings are of growing significance due to their high temperature oxidation and corrosion resistance properties. They find application in electronics, chemical and nuclear related industries. Dissimilar metal joining are carried out depending upon specific requirement. Whatever may be the application , a series of intermetallic layers form as a result of chemical reaction at the interface. For simple metal-metal and metal-ceramic or ceramic- ceramic systems a series of intermetallic compounds form according to the phase diagram. Thermodynamics and kinetics decides their formation and growth behaviour. Depending upon the initial compositions of the alloys, a wide range of intermetallics may form in ternary systems.

We have studied the formation and growth of intermetalic compounds in Fe-Al, Fe-Al-Si, Ti-Al and Ti-Al-Si systems.The diffusion couples were formed between Fe and Al or Fe and an Al-12.6 % Si alloy and annealed at 900°C. Similar experiments were carried out with Ti. The diffusion couples were either cooled in air or water quenched.

It·was found that formation and growth of some intermetallic compounds was preferentially very rapid. At the same time some of the intermetallic grew very slowly. Occurence of the phases depends on the diffusion path through the ternary isothermal section. Mostly Si substitutes Al in the lattice , both for Fe and Ti.

To the revered memory of my father

Late Sri Biswamoy Maitra

Acknowledgements

I thank my guide, Dr. S.P.Gupta, for his guidance, inspiration and encouragement during the course of this project.He has tought me the values of research and independent thinking. He spent tremendous time and effort on me and was always ready to help and dicuss my difficulties. It was a great pleasure working with him during the last two years.

I must take the oportunity to thank my friends kallol, sandip, dobu, sanjukt, pavitrada, anirban and kamalesh for their kind help in completing this thesis. I also would like to thank all the laboratory staffs who have helped me a lot without which this thesis could not have been a reality. Finally I must thank my lab-mates for their kind support to succesfully complete this work.

Contents

List of Figures

List of Tables

Nomenclature

D_B^A	: Diffusivity of B in A
D_A^B	: Diffusivity of A in B
ΔG	: Change in free energy
C_B	: Composition of B
a	: Surface area shape factor
b	: Volume shape factor
d	: Gradient energy term
g_v	: Volume free energy per unit volume
∇C	: Compositional Gradient
R^*	: Critical radius of nucleus
J_L	: Diffusion flux through lattice
J_{GB}	: Diffusion flux through grain boundary
D	: Diffusivity through lattice
$D^/$	: Diffusivity across the grain boundary
$M(t)$	: No. of atoms transported per unit area per unit time
A_L	: Area of the lattice
A_{GB}	: Area of the grain boundary
$\frac{dC}{dx}$	: Compositional gradient
δ	: Thickness of the grain boundary
d	: Average grain diameter
D_{eff}	: Effective diffusivity
$\tilde{J}_j^i$	: Interdiffusion fluxes of the species j in phase i
J_A^i	: Intrinsic flux of species A
J_B^i	: Intrinsic flux of species B
J_v^i	: Valency flux in the i phase
X_B^β	: Composition of B in β phase
X_B^α	: Composition of B in α phase
$\dot{N}$	: Rate of change in total no. of A and B atom per unit diffusion cross-section present in phases α and β
$\tilde{J}_{BI}^i$	: Interfacial interdiffusion flux of B in phase i
k^i	: rate of change of total no. of lattice sites of phases i per unit diffusion cross-section
J_{VI}^α	: Interfacial vacancy flux in α phase
J_{VI}^β	: Interfacial vacancy flux in β phase
ΔJ_{VI}	: Diffusional vacancy flux in α and β phases

Chapter 1

Introduction

Surface modification of metals and alloys by forming intermetallic coating is one of the new areas of research which has undergone tremendous improvement over last few years. As far as the high temperature oxidation and corrosion resistance under specific environment is concerned, different intermetallic coatings has shown tremendous applicability. Apart from surface modification, metal-ceramic, ceramic-ceramic joining, brazing of ceramics in electronic industry have found huge application.

Iron-aluminides are of high research interest because of its excellent oxidation and sulphidation resistance, relatively high-temperature strength and high work-hardening rate. It is being attracted as a new structural materials,because of its many good properties and low materials cost.

Studies of the phase stabilities in the Fe-Al-O system demonstrate that Al_2O_3 will form on iron-aluminides even at extremely low oxygen potentials. A pure alumina surface oxide can be truly protective in a variety of high-temperature environments. It is the thermodynamic stability of this Al_2O_3 scale ,its rate of formation and growth on iron-aluminides, and adherence to the underlying alloy that determines the actual high temperature corrosion behaviour.

As promising light weight alloys the titanium-aluminides are being considered for high temperature application. γ TiAl ($L1_0$ structure)based alloys with a small amount of Cr,Mn,Nb and Si are regarded as possible structural materials

in turbines and turbo-chargers and also as skin and heat protection shields of hypersonic spacecraft. In order to extend the development to higher application temperatures the Ti_3Al phase is combined with Ti_5Si_3. The Ti_5Si_3 phase has a low density and a very high melting temperature. Brittleness and a tendency to microcracking prevents its application as a single phase material.

Different coating procedures like Hot Isostatic Pressing(HIP) physical vapour deposition, chemical vapour deposition (CVD), laser surface modification, Reactive Ion Nitriding (RII)(for coating of ZrN etc.),high-velocity oxyfuel coating (HVOF)(recent devolopment as a substitute for hard Cr coating) are applied depending upon the type and nature of coating needed. Although the structure and properties of the aluminium coatings depend on the production process, the basic principle remains the same.

Some of the researchers(1-4) have earlier identified different equilibrium and non-equilibrium phases in the Fe-Al-Si system by Scanning Electron Microscopy(SEM),Transmission Electron Microscopy(TEM) and X-Ray Diffraction(XRD), but the complexity of this system has been the source of numerous contradictory reports.

Van-Loo et al(5) have studied the growth of intermetallics and diffusion in the Ti-Al system. Work has also been carried out on the Ti-Al-Si system(6,7) This study involves some fundamental investigations in the Fe-Al-Si , Ti-Al and Ti-Al-Si systems and characterization of the interface formed. We have also studied the solubility of Si in iron aluminides. intermetallic compounds.

1.1   Diffusion Couple

When pure metals are in contact at high temperature,diffusion of the metals take place at the interface giving rise to new phases if the two components have mutual solubility in each other. For lower temperature and lower diffusion time ,it may happen that some of the phases are missing. Thermodynamics and

kinetics of formation of intermetallic compounds are the deciding factors .

1.1.1   Binary Diffusion Couple

When a metal A is brought in contact with a metal B, and the diffusion couple allowed to anneal , the A and B atoms diffuse into each other. The phases that form in the couple is understood from the isothermal section at the annealing temperature. As a rule, an interface will represent two phase field separating single phase regions involving the same two phases.

The diffusion path is dictated by the concentration gradient that exists and can be obtained by the equilibrium phase diagram . A concentration gradient must exist to supply atom flux for the growth of phase regions through the interface.

With increase in time these interface migrate in such a manner that ultimately a particular phase outgrows the others. This particular phase is denoted in terms of the gross composition of the couple which is decided by the amount of solute present in the initial components of the diffusion couple. However, this would only happen if the time given for diffusion is sufficient for the metal A to diffuse across the entire metal B and vice- versa.Upon subsequent cooling different equilibrium phases and non-equilibrium phases may form. The former is dictated by the equilibrium phase diagram while the later by different thermodynamic and kinetic factors. When sufficient time is not given for these metals to diffuse across each other, the isothermal section of the phase diagram is considered and all the phases across it form.This is the simplest way of characterizing a binary diffusion couple.If a phase has very low growth rate then it may form as a thin layer and may not be visible. It becomes difficult to carry out the analysis of such phases and their transformation products. For example consider the phase diagram shown in the figure 1.1. The concentration-distance profile is shown in Fig 1.2 at temperatureT_1 . The diffusion couple will show two interfaces ($\alpha + \beta$) and ($\beta + L$).The concentration of liquid and β phases are shown as $X_{L/\beta}$ and $X_{\beta/L}$, respectively at the ($\beta + L$) interface. Similarly ,

compositions of α and β phases are shown as $X_{\beta/\alpha}$ and $X_{\alpha/\beta}$, respectively at the $(\alpha + \beta)$ interface in Fig 1.2.
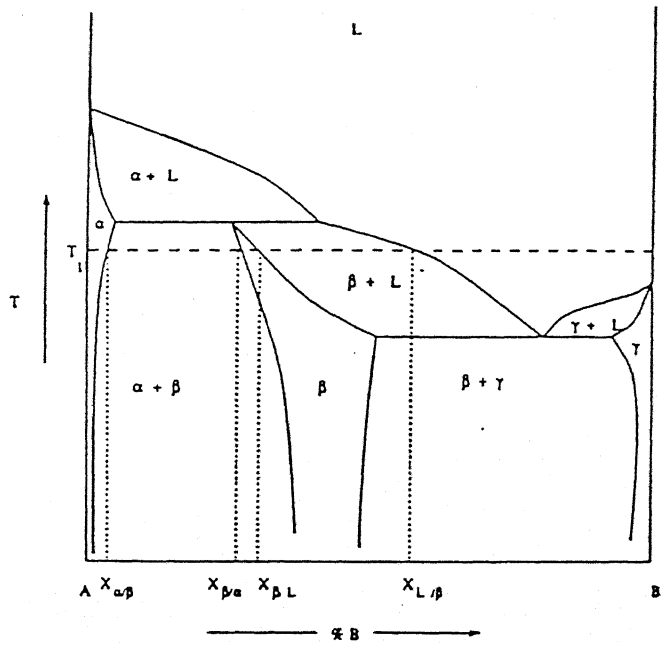
Figure 1.1: Hypothetical phase diagram
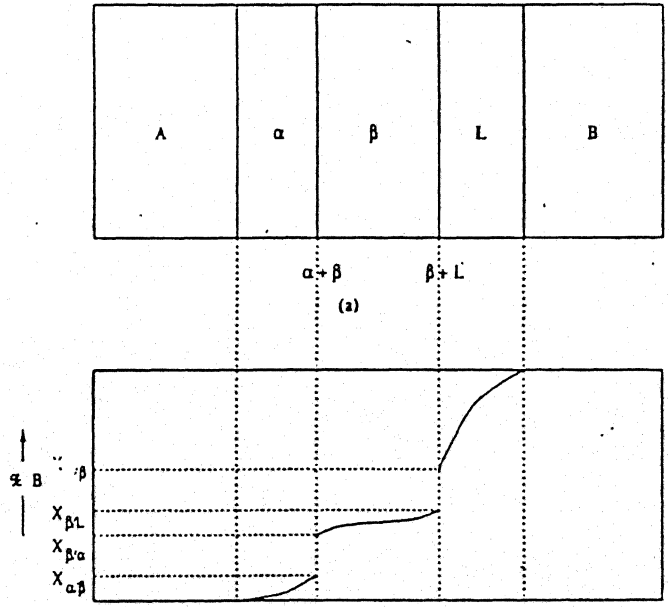
Figure 1.2: (a) Diffusion couple at temperature T_1;(b) Concentration-distance Profile

In the binary diffusion couples considered above members of the couple act as semi infinite bodies. However when one of the members of the couple becomes liquid then the assumption of the metals being semi-infinite bodies is no longer valid, because the diffusivities of the components is much higher

in the liquid as compared to that of the solid. The diffusion across the entire layer of the liquid occurs and the liquid homogenises in due course of time. The gradient in the liquid is modified due to enhanced diffusion and convection. The modified concentration profile is shown in Fig 1.3. There may however be some difference in the structure due to freezing of the liquid with gradient(which although nevertheless exists)or because certain phases would selectively float or sink in the liquid.
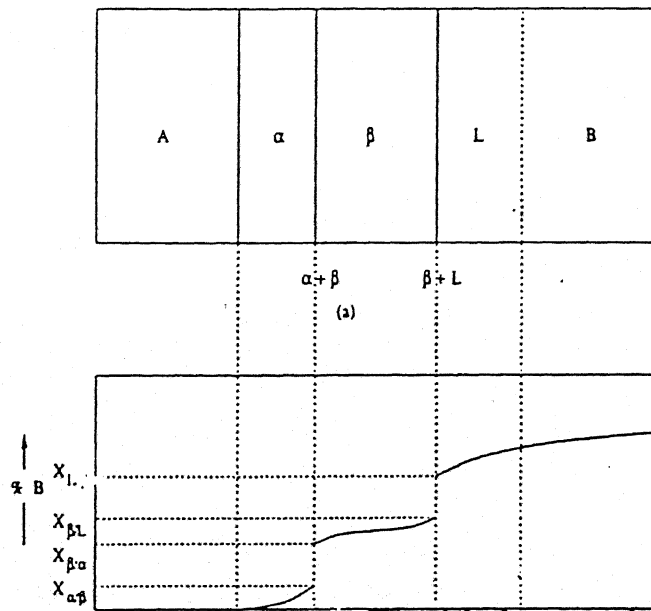
Figure 1.3: (a)Diffusion couple at temperature T_1 with homogenisation of liquid, (b) Concentration-distance profile of the diffusion couple at temperature T_1

1.2 Mechanism of Interface Migration

The mechanism of interface migration in diffusion couples has been proposed by Sergeev(8) and Luybov(9) . Accordingly, A atoms approach the interface by volume diffusion through the exchange with vacancies. The resultant flux of A atoms across the interface causes a composition change in the region adjacent to the interface. The crystal structure of the lattice changes due to supersaturation (or depletion) of the interface region, thus causing displacement of the phase boundary.

Thus, the phase composition depends on volume diffusion ,interface flux of atoms and lattice transformation, while the interface motion is governed only by

the lattice transformation.

1.2.1   Formation of The First Phase

Let us consider a binary system A-B and the diffusion couple A/B formed with the pure components. At a high enough temperature , diffusion begins to proceed at high enough rate. Let us assume for the sake of simplicity that the diffusivity of B in A is larger.The B component will dissolve in A resulting in the growth of α solid solution. At the interface α/B, the concentration of B in α will remain constant with time. However, the concentration gradient will decrease with increase in time of anneal. Let us now consider the free energy - composition diagrams($\triangle$G vsC_B) of the α and β phases and the formation of intermetallic phase η that may appear in the diffusion couple,Fig 1.4.
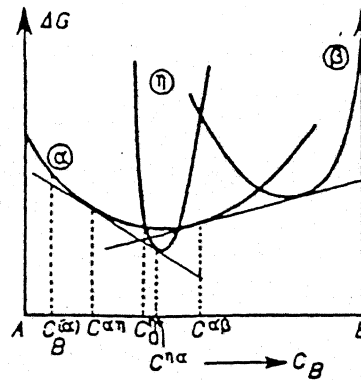
Figure 1.4: Free energy vs composition diagram

When the concentration of solute B attains the intersection point of the $\triangle$G curves of α and η phases, a polymorphic transition($\alpha' \to \alpha + \eta$) in principle is possible without change in composition. But because of the difference in the lattice structure, such a phase transition is controlled by some nucleation barrier and in most cases α' solid solution will grow further and become richer in B. This stage of the process is expected to proceed until the driving force for the phase transition becomes high enough so that the nucleation barrier becomes immaterial. Eventually, this nucleation will still be more favoured due to the gradient energy term (introduced by J.W.CAHN) that has to be added to the

free energy relative to a homogeneous solution.

According to Desre and Yavari(10,11) and Gusak(12); the condition for nucleation in this case are different from the classical ones , because of the concentration gradient.For instance , for a spherical nucleus of radius R ,the free energy of nucleation contains one more term besides the volume (in R^3) and the interfacial free energy (in R^2)terms :

$$\Delta G = aR^2 - BR^3 + dR^5$$

where b and a are volume and surface area shape factors combined into the free energy terms and d is the corresponding gradient energy term. The value of d depends on the concentration gradient in the supersaturated parent phase.According

$$d = \frac{2\pi g^{//}}{15L^2}$$

with $g^{//} = \frac{\delta^2 g_c}{\delta c^2}$ and L = 1/∇C. ∇C denotes the concentration gradient. Gusak has shown the dependence of ΔG(R) has a bifurcation at L = L^* = 3 R^*/Δ C where R^* is the critical radius of the nucleus in a homogeneous solid solution and Δ C is the composition range of the parent phase inside which the intermediate phase is more stable,FIG 1.5 . Some of the researcher have taken the elastic energy term in addition to the above terms in calculation of the free energy for nucleation.
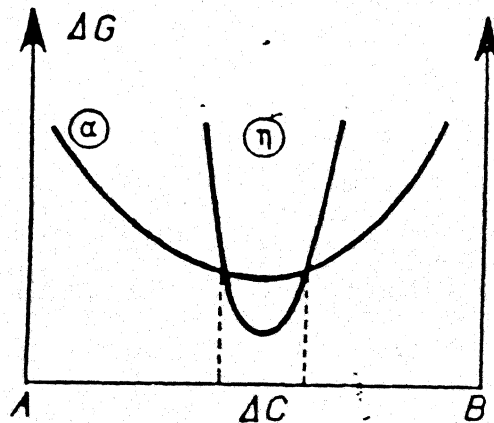
Figure 1.5: ΔG vs C diagram showing η is more stable than α over Δ C

1.2.2   Formation of Subsequent Phases

When the difference in the free energy for the formation of γ phase is large, the nucleation stage is not the controlling factor and the γ phase can grow easily. However it is easily shown that there is a critical thickness (Coselle and Tu(13))of compound η in order that γ will be able to grow.

It has been shown by Coselle et al (13) that the growth rate of one phase will not be positive until the thickness of the other one attains some critical value .

1.2.3   Role of Grain Boundary diffusion

It has been frequently claimed in the literature that the growth kinetics of the layered structure do not follow a time square root law. This is possible if the transport of atoms occur along the grain boundaries made possible from the polycrystalline structure of most interface layers. Let us consider the the growth of a phase with columnar grains allowing the diffusion paths with two different diffusivities D and $D^{/}$ along the lattice and grain boundary respectively having the two corresponding fluxes:
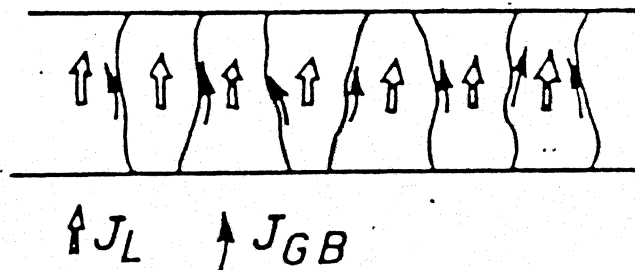
Figure 1.6: Schematic diagram showing lattice and grain boundary diffusion

J_{L} =-D dc/dx J_{GB} =-$D^{/}$ dc/dx

where the concentration gradient has a common value. The number of atoms transported per unit time, per unit area is given by:

M(t) = ($A_{L}J_{L}$ + $A_{GB}J_{GB}$)

where A_{L} and A_{GB} are respectively the areas of cross section of the lattice and grain boundary per unit area through which diffusion of atoms occurs. With a

conventional thickness δ for grain boundaries, $A_L = 1$ and $A_{GB} = 2\delta/\mathrm{d}$ where d is the average grain diameter.

Instead of lattice diffusivity, the transport is governed by an effective diffusivity:(14)

$$D_{eff} = D + \frac{2D^/\delta}{d}$$

Besides this increased value of the diffusivity, nothing is changed in the derivation of kinetic law . The parabolic regime is just faster as compared to simple diffusion in a volume diffusion controlled process. The grain boundary diffusion will become dominant when the grain diameter is small.

1.2.4   Interface Reaction

Interface reactions are the obliged companion of the diffusion process. They involve two kinds of elementary process
- ' chemical ' reactions expressing the construction and destruction of the phases.

- creation or destruction of point defects , as the net flux of point defects are different in each phase.The site balance needs a source or sink process .This requires some mechanism in the plane of the interface e.g. the climb of misfit dislocation, as suggested by Pieraggi and Rapp (15) . But the efficiency of such mechanism is not guaranted :

a) the misfit dislocations must be regenerated as long as they are climbing , a process that depends on the crystallography of the interface.

b) in many cases , the misfit dislocations are lying a few atomic distances off the interface.

c) the dislocation climb activity cannot necessarily respond to the required rate of creation and annihilation of point deffects.

1.2.5 Diffusion Induced Flow and Stress During Inter-Diffusion

During interdiffusion in system with components of different mobilities or partial molar volumes , the imbalance in diffusive transport can induce deformation and stress . Since , plastic deformation proceeds by relaxational rather than diffusional kinetics, interdiffusion over small distances can be non-Fickian in such systems. At small distance scales, the rapid diffusion of the ' fast ' component can cause pressure to build upto a quasi-steady state level, at which the pressure gradient term just cancels the composition gradient term in the driving force. Subsequent interdiffusion is rate limited by plastic deformation, which relaxes the stress . The evolution of the composition distribution is very different when plastic deformation rather than diffusion is rate limiting.

1.3 Interface Migration and the Kirkendall Effect

For the interdiffusion of solid-solutions in a binary isomorphous A-B system, unequal diffusion rates of the two components A and B induces a displacement in the lattice planes.This displacement induces the wellknown Kirkendall effect. For such isomorphous system two types of reference frames are used 1.frame centered on the number of mole(number-fixedframe),denoted as the N frame; 2. Kirkendall frame denoted as K frame.

Similarly, in the case of a two phase diffusion couple(Fig 1.7),the analysis of the Kirkendall effect would necessitate the use of two different sets of Kirkendall reference frames for the two contacting α and β phases.

The N frame ,common to the α and β phases, is defined by the flux equation

$$\tilde{J}_A^i + \tilde{J}_B^i = 0$$

(i= α or β) where $\tilde{J}_i^i$ are the interdiffusion fluxes of the species j (A or B). The fluxes are defined as positive for diffusion from α toward β phase. The origin of the N plane is the Matano plane, here defined as the plane separating a constant number of A plus B species. The K-frames are defined by the flux
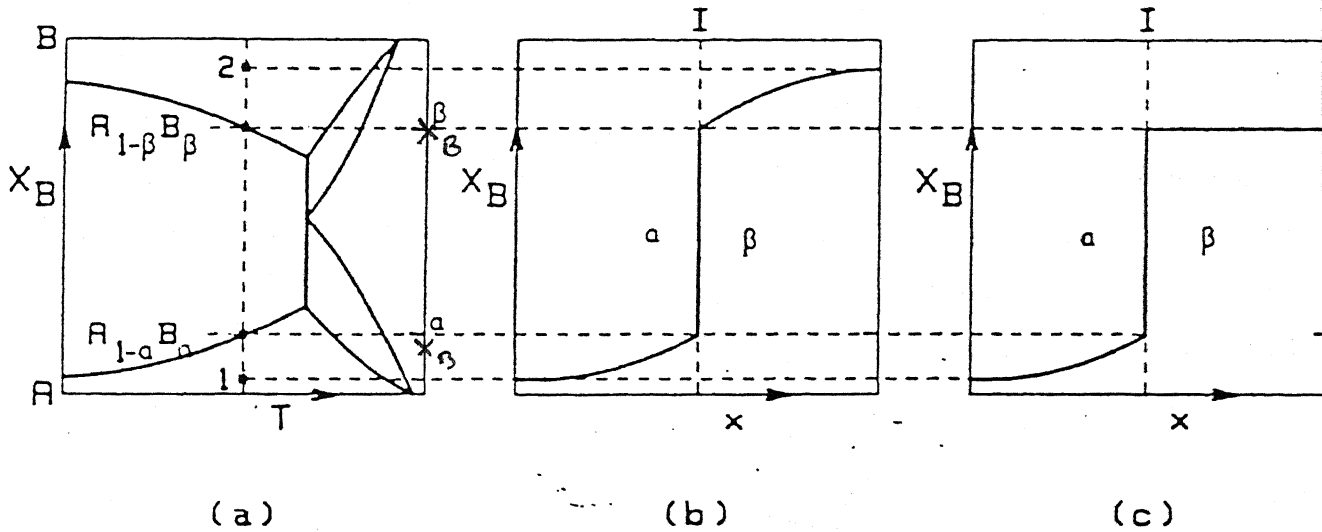
Figure 1.7: Schematic representation of (a) phase diagram and concentration profiles for diffusion reaction ; (b) between two unsaturated composition(1 and 2),or (c) between one saturated and one unsaturated composition

equation associated with the diffusion in the α and β phases

$J_A^i + J_B^i + J_V^i = 0$ where J_A^i and J_B^i are the intrinsic fluxes of species A and B, and the vacancy flux,associated with the lattice plane shift in the i phase (α orβ).The lattice plane at the original interface defines the origin of the two K-frames.

In a system such as that shown in the Fig 1.7, the interfacial diffusion fluxes of A and B would induce the growth or recession of the α orβ phases through the interfacial reaction describing the relative transformation of α into β and/or the reverse transformation. In the N frame , the rate of growth or recession is the rate of change $\dot{N}$ in the total number of A and B atoms per unit diffusion cross-section present in the phases α and β. This rate would be positive as the α phase grows. The atomic balance or equivalently the mole number balance, at the $\alpha - \beta$ interface can be expressed by the usual growth equation

$$(X_B^\beta - X_B^\alpha)\dot{N} = \tilde{J}_{BI}^\beta - \tilde{J}_{BI}^\alpha$$

where, as indicated in Fig 1.7 ;X_B^β and X_B^α are the mole fractions of B in β and α phases, respectively at equilibrium, and $\tilde{J}_{BI}^i$ the interfacial interdiffusion flux of B in phase i.

The rate of growth of the phase i relative to its K^i frame represents the rate of change of total number of lattice sites of phase i resulting from the atomic interfacial exchange reaction and/or other interface action(vacancy creation or annihilation). Because vacancies are the pre-dominant defects for the diffusion processes, the difference between $\dot{N}$ and $\dot{K}^i$ just corresponds to the interfacial flux of vacancies into the α and β phases so that

$$\dot{N} = \dot{K}^\alpha + J_{VI}^\alpha = -\dot{K}^\beta + J_{VI}^\beta$$

The relative magnitudes of $\dot{k}^\alpha$ and $\dot{k}^\beta$ depend on the difference between interfacial vacancy fluxes in the α and β phases.

$$\dot{k}^\alpha + \dot{k}^\beta = J_{VI}^\beta - J_{VI}^\alpha = \Delta J_{VI}$$

Van Loo et al (17) ; calculated the concentration profiles and the associated diffusion flux to show the dependencies of these specific quantities on the intrinsic diffusivities of the A and B components and the initial concentration of the α and β phases. In the calculation the partial molar volumes for A and B are assumed to be equal,so that the N frame and the volume–fixed frame are identical, and the origins of N frame and Matano frame coincide. The position of the origin of the k^α and k^β frame was determined and an evaluation of the interface displacement and the interface vacancy fluxes.

Their calculation of concentration profiles , vacancy flux and vacancy flux divergence, for different ratios of intrinsic diffusion coefficient and differing initial concentration for the α and β phases showed same interphase interface must be able to act as vacancy source or vacancy sink. This interfacial action must compensate for the difference in diffusion fluxes of the A and B species within α and β phases. The usual assumption of conservation of lattice sites can be
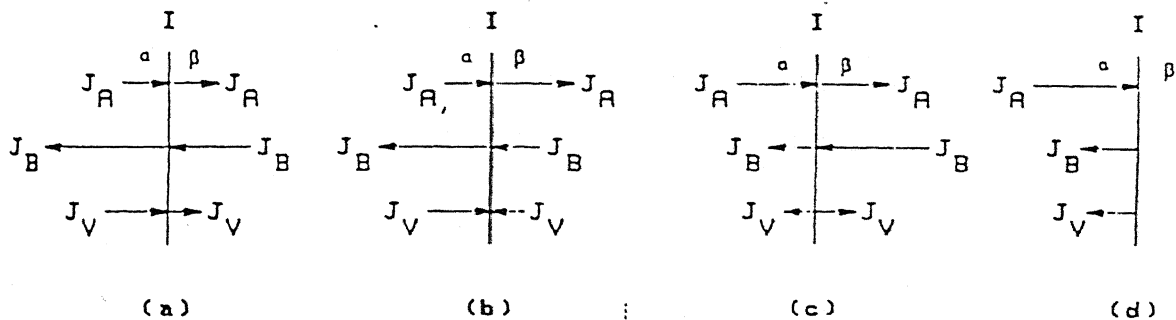
Figure 1.8: Some different cases for interfacial fluxes of $\alpha - \beta$ diffusion couple ; (a) B diffuses faster than A in both α and β phases so that $J_V^\alpha > 0$ and $J_V^\beta > 0$; (b) A diffuses faster than B in β phase and slower in α phase so that $J_V^\alpha > 0$ and $J_V^\beta < 0$; (c) A diffuses faster than B in α phase and slower inβ so that $J_V^\alpha < 0$ and $J_V^\beta > 0$. (d) Saturated β phase , $J_V^\beta = 0$ and $J_{V \cdot \alpha} < 0$ (A diffuses faster than B in α phase)

expressed as

$$\int_{-\infty}^{x_I} \delta J_V / \delta x dx + \int_{x_I}^{+\infty} \delta J_V / \delta x dx + Interface action = 0$$

so that Interface action = J_{VI}^β - J_{VI}^α = ΔJ_{VI}

1.4   Ternary Diffusion Couple

A ternary diffusion couple consists of a pure component, A ,in physical contact with a binary alloy of the other two components, B and C.The diffusion of species A,B and C into each other may proceed if the diffusion couple is kept at a sufficiently high temperature with appreciable rate of diffusion of the three components. Attempts to predict the sequence of diffusion layer formation by the expedient of drawing, upon the appropriate ternary isotherm, a straight line connecting the terminal composition of the diffusion couple and then noting the order and identity of one-phase and two-phase zones crossed.It has appeared to
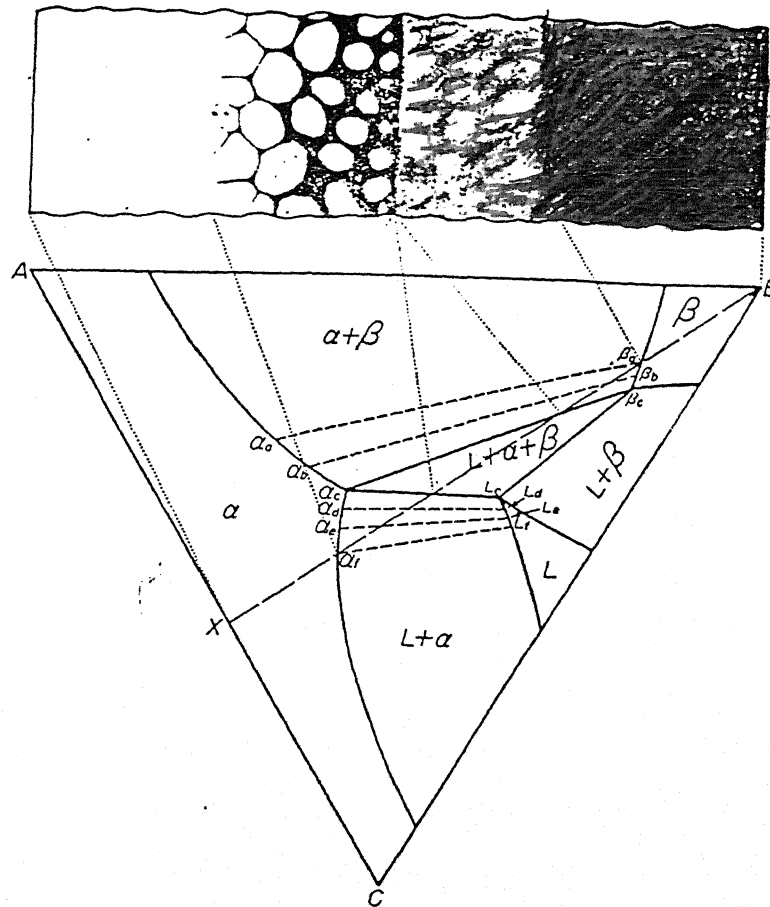
Figure 1.9: Schematic representation of the relation between the structure of a ternary diffusion couple and the phase diagram

succeed in some cases in which relatively simple constitutional relationship were involved. The assumption of a linear course of a gross composition path across a ternary diffusion couple is an oversimplification is clear from the condition that a linear composition path implies the unlikely restriction of equality among the diffusion rates of the three components. In ternary diffusion couple the intermediate layer may consists of a single phase and mixtures of two phases, while the three phase region form the interface.

1.4.1 One-phase equilibrium

The one-phase region of the phase diagram are represented in diffusion couple by single phase layers.Since, there are two degrees of freedom in isobaric, isothermal one-phase equilibrium , the composition path across the one-phase

layer may vary simultaneously with respect to components i.e. composition path may be curved.

1.4.2   Two-phase equilibrium

Each two phase region of the phase diagram is represented in the diffusion couple either by the interface between two single-phase layer, by a layer of definite thickness composed of alternating deposits of various proportion of the two phases,or by a combination of these modes. If the path lies parallel to a tie-line, there can be no composition gradient in either phase in crossing the field and nothing more than an interface between the two phases can develop. A possible explanation lies in the fact that the energy of the system is increased by the introduction of phase interface. A plane boundary between single-phase layers correspond to a minimum interfacial area,however a two phase layer forms large surface area. Thus it appears that the diffusion path as a whole, may be warped to seek minimum surface energy. (Clark and Rhines)(18)

When the path crosses all the tie-lines in the field, the two phase layer is composed of all conjugate compositions of the two phases. Each particle that extends from one boundary of the layer to the opposite boundary varies in composition over the complete range of the two phase field. Since there is one degree of freedom in two phase equilibrium at fixed temperature and pressure, the complete freedom of choice of composition path that is required in order to realize the condition that every diffusion couple shall follow a unique path across each field that it encounters. It requires that the diffusion sequence determine both the conjugate composition of the phases and their relative proportion at each position in the two phase layer.

The two phase layer is composed of a pair of conjugate phases each having a corresponding concentration gradient between the two surfaces of the layers. These gradients are so constructed that at any specified depth within the layer, each phase has the same activity. Thus, a gradient exists in a direction normal to the external boundary plane of the layer, but not parallel with these surfaces

and, there can, accordingly, be a net chemical transport only normal to the layer surface. Parity of the activity of the two phases , requires a lateral segregation of the components.This, however , results in no gross change in the composition in any plane in the layer parallel with the interface.

1.4.3 Three phase equilibrium

The three-phase equilibrium in an isobaric isotherm has no degree of freedom. The only control over the gross composition change across this field resides in the proportioning of the quantities of the three phases upon the two sides of the interface. It is possible for any point on one of the sides of a triangle in the phase diagram to be associated with any point on either of the other two sides.This provides unique transists for each diffusion couple and any number of paths through any point within the three-phase region.

1.5 Dependence of Diffusion Path for A_xB_y/C type diffusion couple

When an alloy BC is brought in contact with a pure metal A and annealed at high temperature the diffusion of A occurs into the alloy and the species B and C diffuse into the metal A. Although the layer structure of the phases formed between the two single phases in the binary diffusion couple is the only possible morphology, this is no longer true in a ternary diffusion couple.The additional component in the ternary diffusion couple provides one more degree of freedom which allows the occurrence of variety of structures within the diffusion zone.The simple layered, aggregate and periodic layer morphologies(19) are possible in the diffusion couple. The occurrence of any of these depends on the mobility of various species.

For example, consider the phase diagram shown in the figure 1.10. A solid solution of atoms from the alloy BC in the metal A can exists in equilibrium with

the compounds AC and BC. From the isotherm it can be seen that if a diffusion couple is made between A and BC a solid solution must be formed. Whether or not the compound AC will be formed depend on the relative diffusivities of B and C in the metal A. If C atoms diffuse faster than B atoms , they would further penetrate into the bulk of the slice A and the intermetallic layer AC may form.
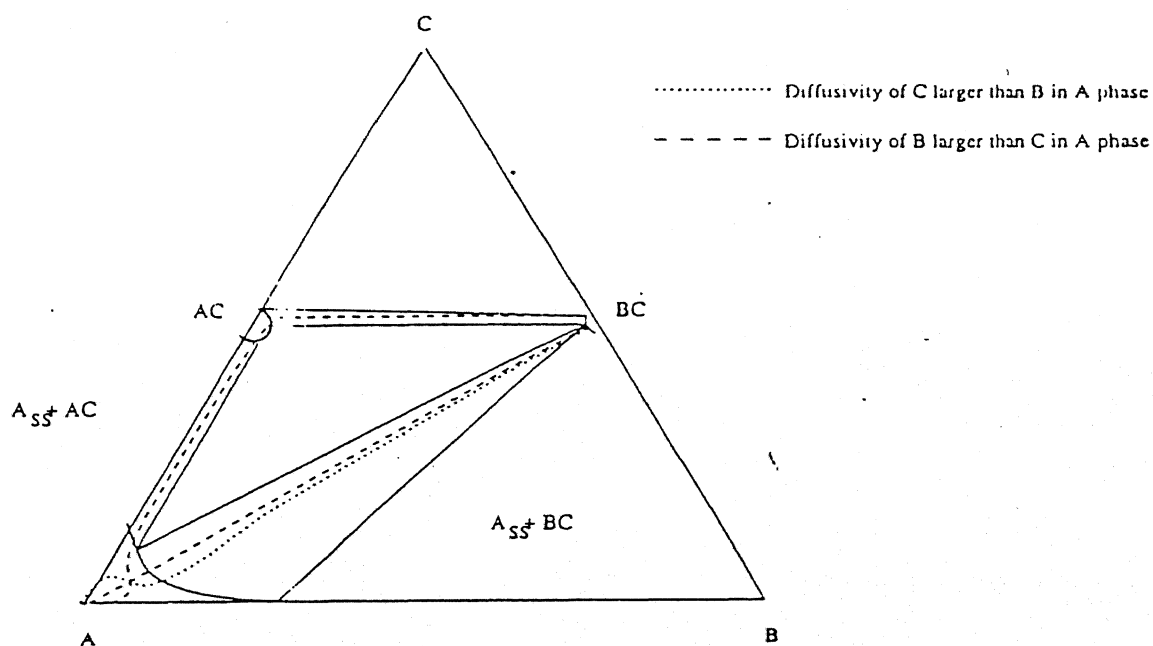
Figure 1.10: The diffusion paths for diffusion couple between A and BC for the cases when the B-atoms diffuse faster than C atoms and vice-versa.

The diffusion path, defined as the locus of the average composition found in the diffusion couple parallel to the original interface, will therefore, start from A in the direction of C. At a certain point, closer to the interface B atoms are also present and the diffusion path would turn towards the B corner of the isotherm. From mass balance consideration, the path must cross the line connecting A and BC because the number of atoms of B leaving BC must be equal to the atoms of C leaving BC. If the mobility of B and C are in reverse order, the path would be reversed.Thus the phase AC would be formed in one case and the intermetallic layer BC in the other case.

Consider another example as illustrated with consideration to the phase

diagram sown in Fig.11. In this diagram the prediction are much easier to make for the diffusion couple between A and BC. The only sequence possible for the diffusion couple is $A/A_2B/AB/C/BC$ from a thermodynamic point of view.
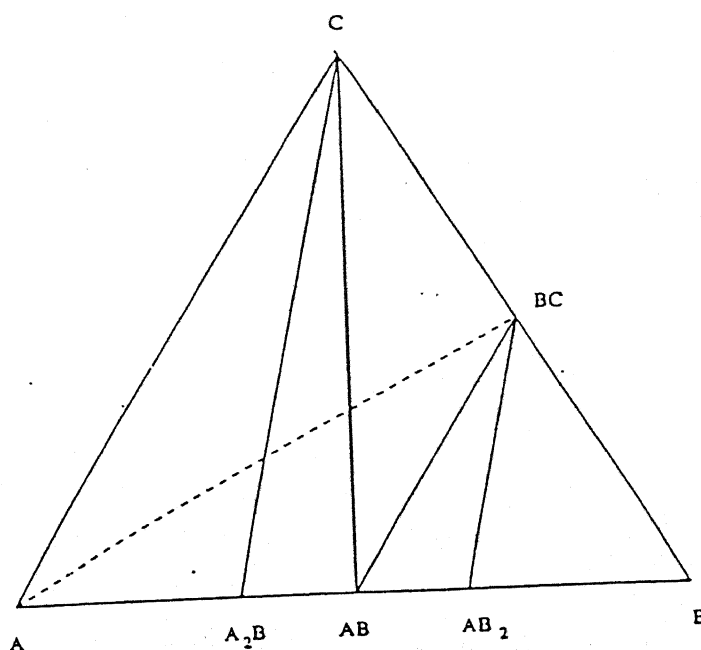
Figure 1.11: A hypothetical phase diagram where the difference in diffusivity of B and C would not effect the compounds formed in the diffusion couple A/BC

1.5.1 New Theories Regarding the Prediction of Sequence of Intermetallic Compounds

Van Loo et al.(20) developed an excellent model for prediction of intermetallic compounds in metal-ceramic combination. The key idea is the impossibility for atoms or ions to intrinsically diffuse into a direction where its own chemical activity is increased. Using this model, Li et al.(21) explained the layer sequence of their observed reaction zone qualitatively.

Recently B.J.Lee(22) showed a new scheme for prediction of interface reaction products at metal/ceramic interface, based on thermodynamic calculation and diffusion simulation.Basically a diffusion controlled reaction and a build-up

of a local equilibrium were assumed at the interface. The thermodynamic state at the interface before the formation of the reaction product was regarded as to correspond to a metastable equilibrium state between the two initial phases. Under the metastable equilibrium state , the driving forces of formation of all the other phases could be calculated. By selecting the phase with highest driving force of formation as the first- forming interface reaction product,the order of formation as well as the interface layer sequence could be predicted.

1.6 Fe-Al Binary and Fe-Al-Si Ternary System

1.6.1 Fe-Al System

Table 1.1: Intermetallic Phases in Fe-Al System(24)

Formation Temperature	Formula	Crystal Structure	Formation Energy(Kcal/mole)
552	Fe_3Al	Cubic (DO_3)	-
1310	$FeAl$	Ordered BCC(B_2)	-
1215	Fe_2Al_3	Cubic,	-
1154	$FeAl_2$	Triclinic	75.78
1171	Fe_2Al_5	Orthorombhic	121.4
1152	$FeAl_3$	Monoclinic	90.4

1.7 Fe-Al-Si System

The system contains many technologically important alloys, so the phase equilibria of the ternary system have been reviewed a number of times. The system is characterized by a number of ternary phases and at least nineteen ternary invariant reaction during solidification which make it difficult to establish the phase equilibria of the system. The complexity is further supplemented by super cooling , incomplete reactions and metastability.
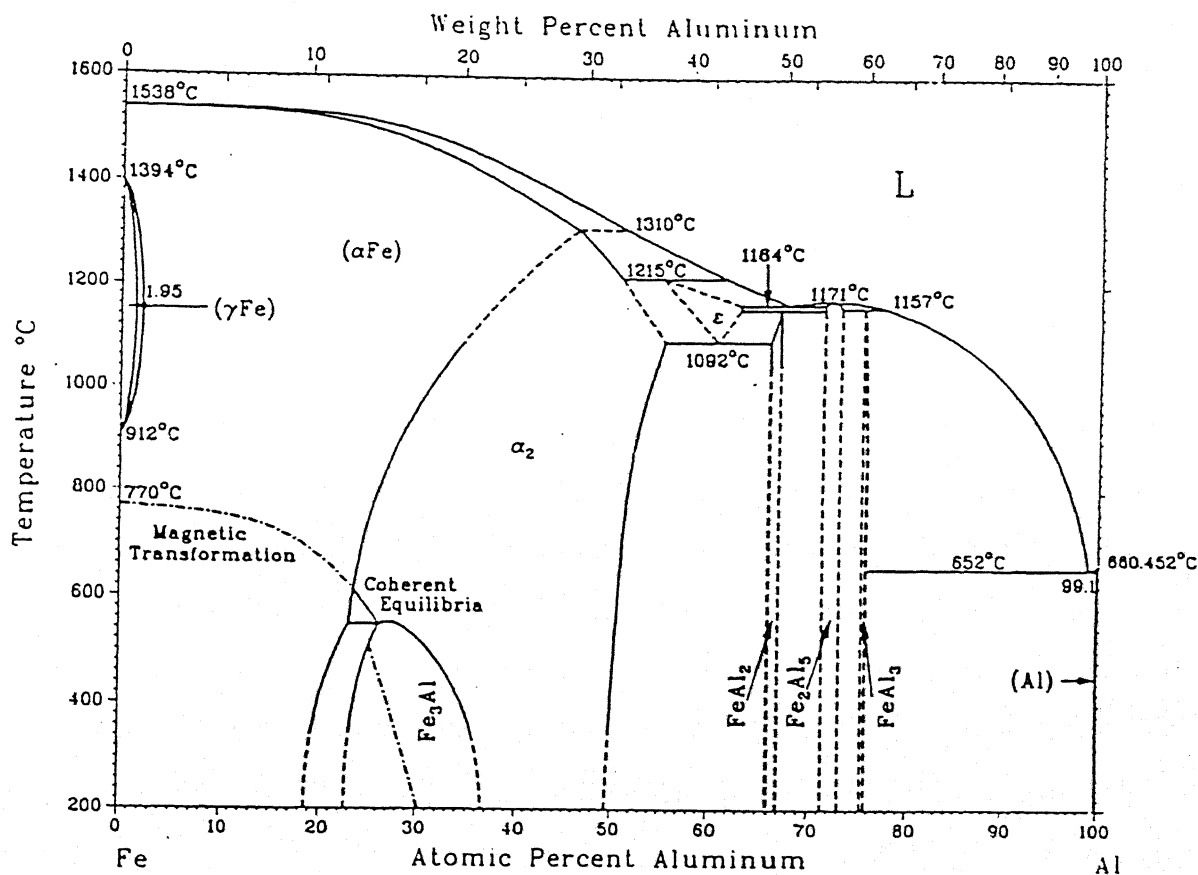
Figure 1.12: Phase diagram of Fe-Al(23)

1.7.1 Order-disorder Reaction

Mutual solid solubility between Fe_3Al and Fe_3Si is well established. The existence of the ordered phase $\alpha_1(Fe_3Al$ and Fe_3Si which have DO_3 structure or BiF_3 type order) and (FeAl and FeSi which have B_2 or CsCl type structure) along the end section , was studied by high temperature X-ray diffraction and recording the disappearance of the DO_3 superlattice {111} and {200} reflections as a function of temperature and composition. A ternary compound $Fe_3(AlSi)$ is also reported having DO_3 structure. With the addition Si in Fe_3Al the ordering energies increase monotonically.

Table 1.2: Ternary Solid Phases in Fe-Al-Si System (24)

Ternary phase		Composition, wt-%			Range of homogeneity
Symbol	Formula	Al	Fe	Si	
τ_1	$Al_3Fe_3Si_2$	26.6	55.0	18.4	...
τ_2	$Al_{12}Fe_6Si_5$	40.5	41.9	17.6	...
τ_3	$Al_9Fe_5Si_5$	36.6	42.1	21.2	2—3%
τ_4	Al_3FeSi_2	41.9	28.9	29.1	...
τ_5	$Al_{15}Fe_6Si_5$	46.0	38.1	16.0	About 5%Al
τ_6	Al_4FeSi	56.3	29.1	14.6	...

The results of Katsnelson et al(25); indicate that addition of Si in Fe_3Al increases the $\alpha_1(DO_3) \rightarrow \alpha_2(B_2)$ transition temperature while that of $\alpha_2(B_2) \rightarrow \alpha(Fe)$ increases upto about 12.5 % beyond which it levels off. On the other hand, recent result of magnetic measurement by Takahasi (26) indicate that $\alpha(Fe) \rightarrow \alpha_2(B_2)$ and $\alpha_2(B_2) \rightarrow \alpha_1(DO_3)$ transition temperatures, initially increase upto about 6 at % Si and then decreases, Fig 1.13. Even though in general the nucleation and growth of $\alpha_1(DO_3)$ domain in $\alpha_2(B_2)$ domain is easier than in α matrix, the direct $\alpha(Fe) \rightarrow \alpha_1(D0_3)$ transformation in certain composition range has been attributed to the lowering of atomic potential energy when Al atoms are substituted by Si atoms.
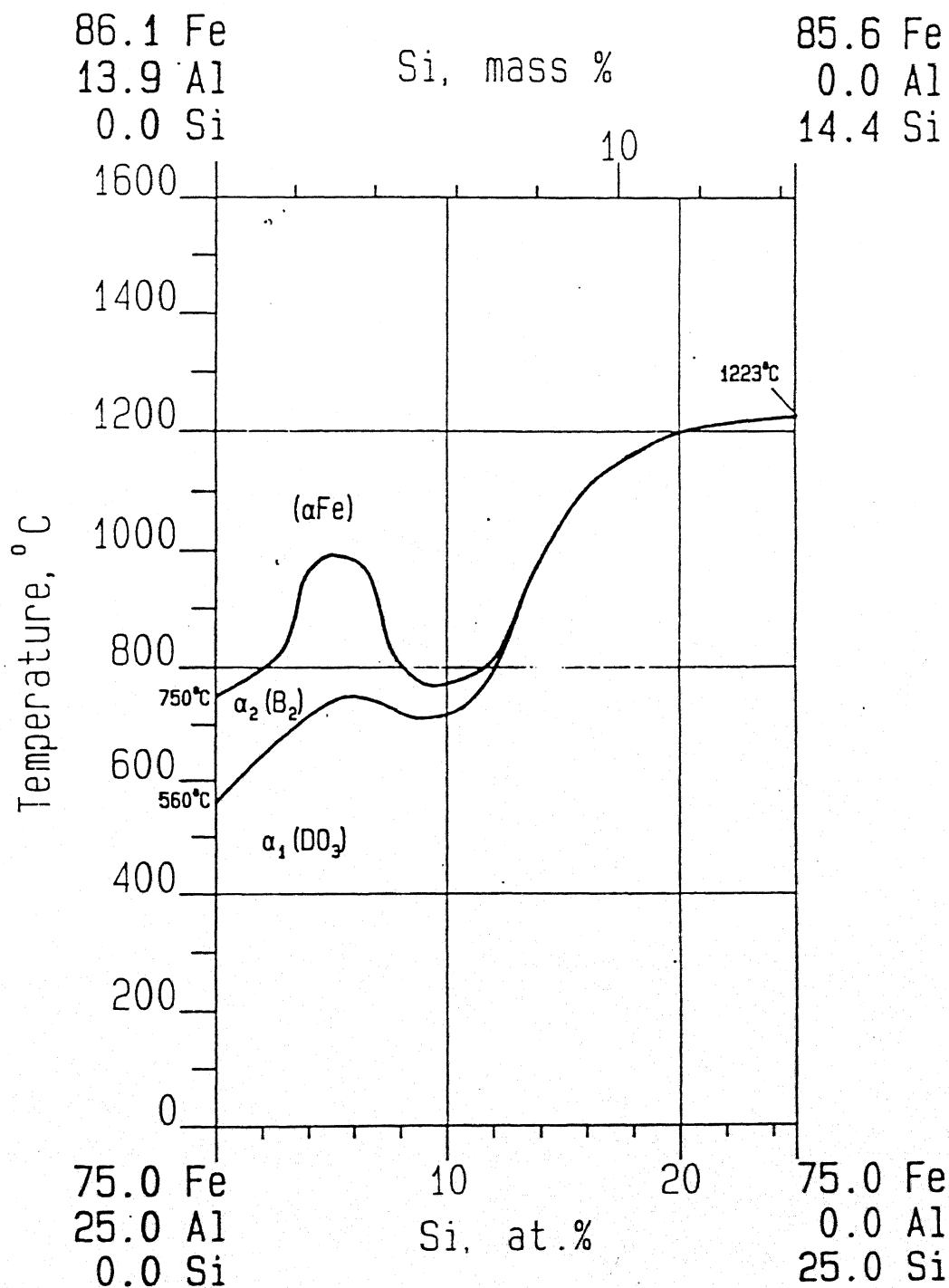
Figure 1.13: The $Fe_3Al - Fe_3Si$ section showing the boundaries of α_1, α_2 and α(Fe) phase

Figure 1.14: Isothermal section of the Fe-Al-Si system at 600°C(27)
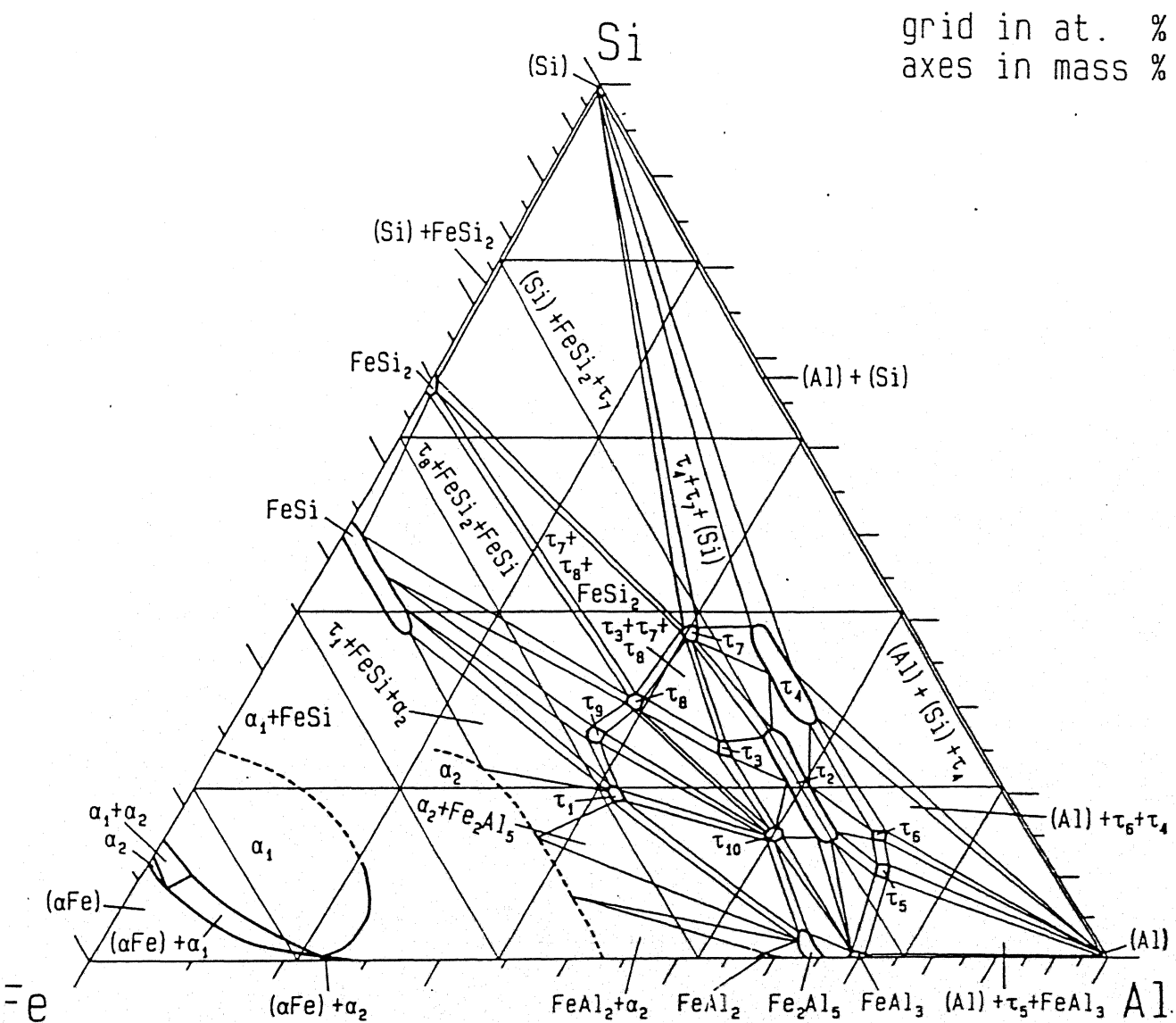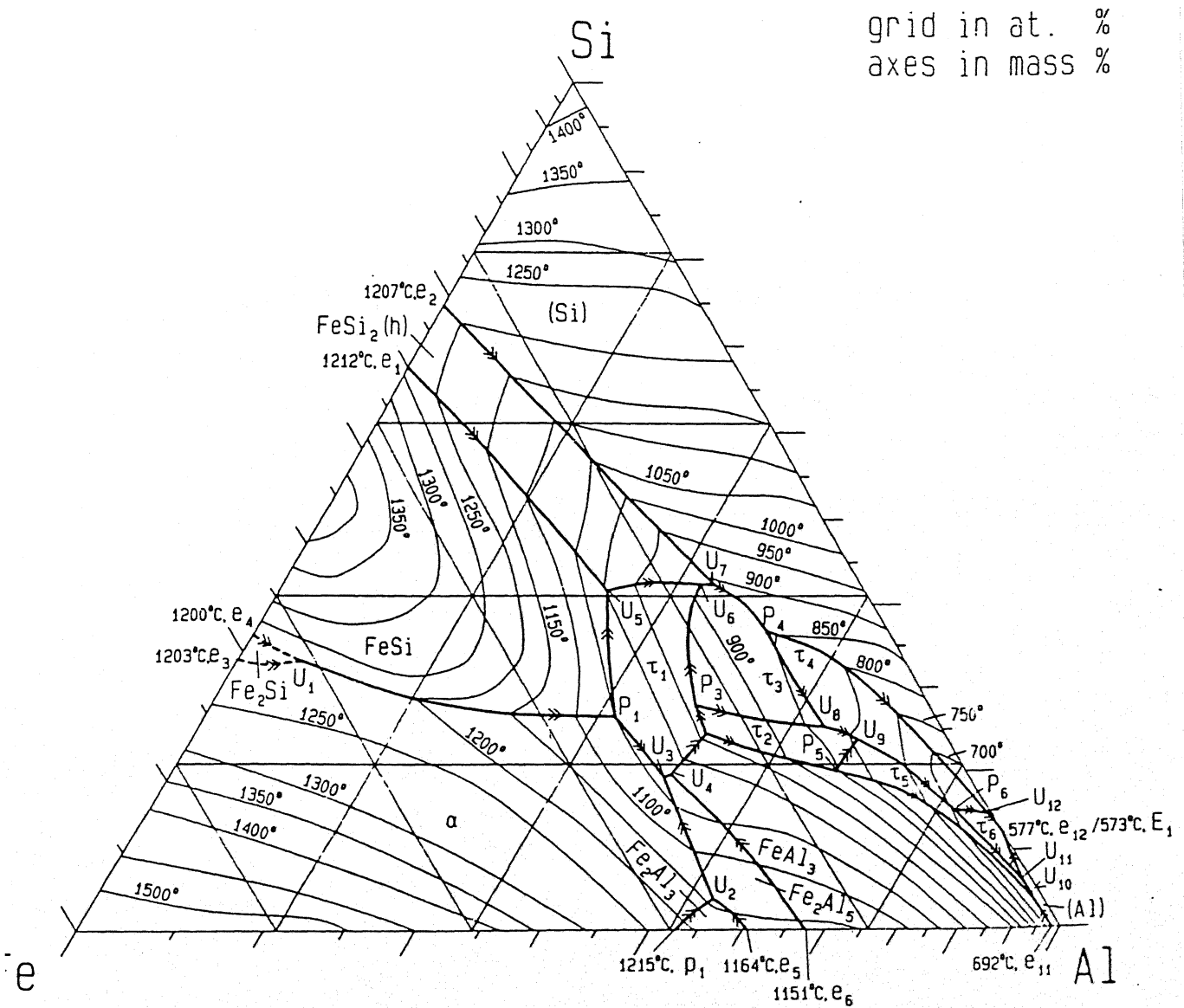
Figure 1.15: Liquidus surface of the Fe-Al-Si system (27)
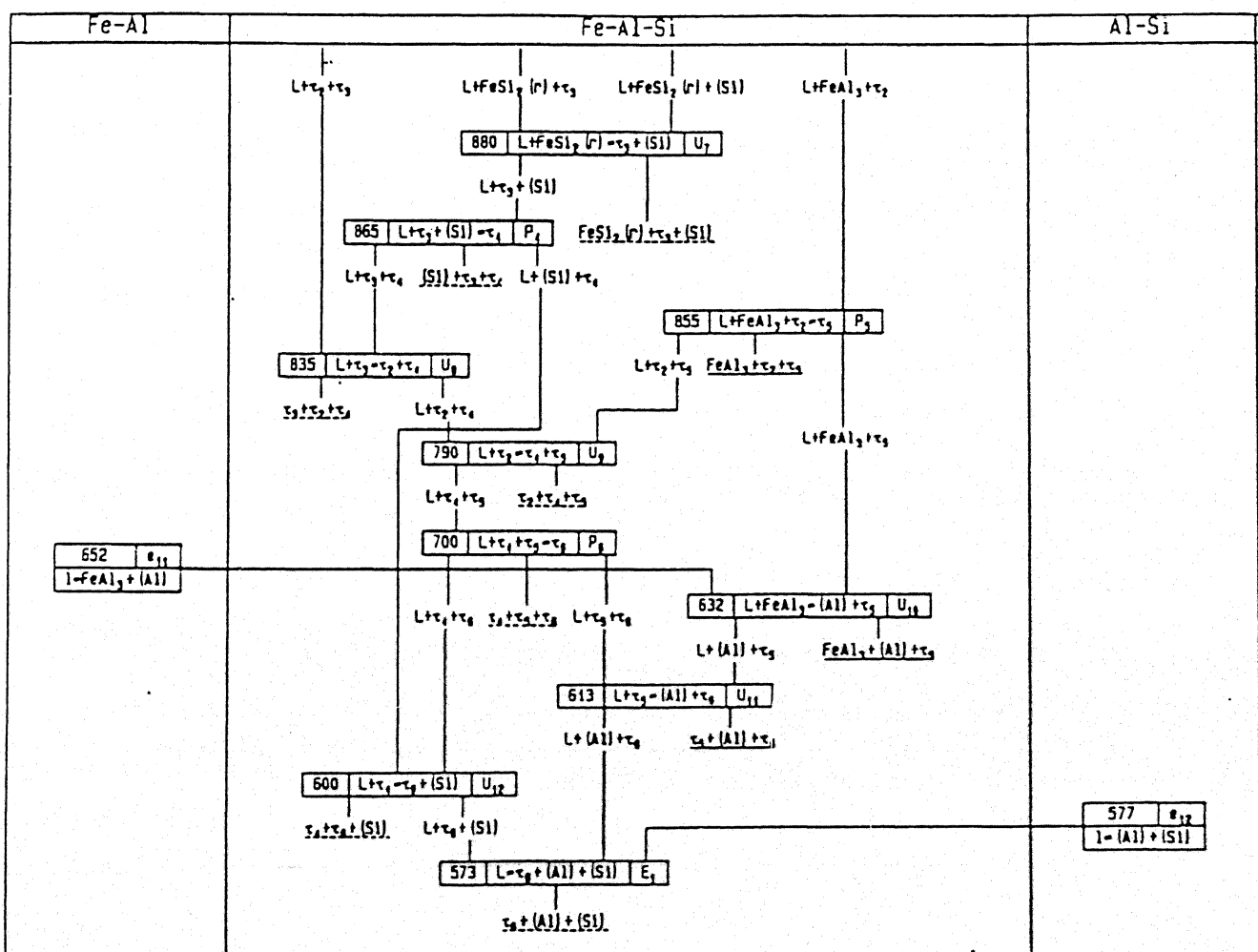
Figure 1.16: Reaction scheme of Fe-Al-Si system below 900°C

1.8 Ti-Al and Ti-Al-Si System

1.8.1 Ti-Al System
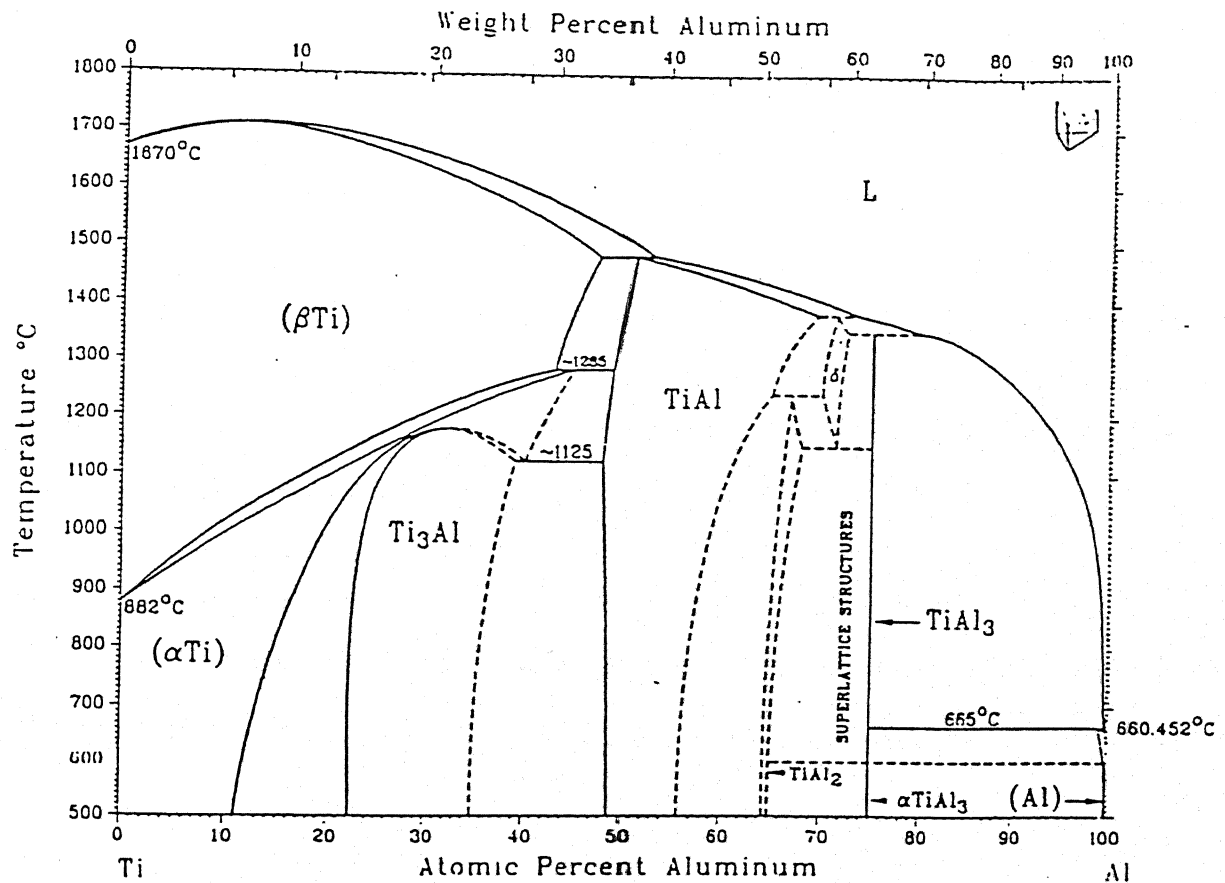
Figure 1.17: Titanium-Aluminium binary phase diagram after (23)

Table 1.3: Titanium aluminides , their structure and formation temperature(28)

Phase	Formation Temperature(C)	Structure	Symbol
Ti_3Al	1180	DO_{19}(hcp)	α_2
$TiAl_2$	1216	DO_{22}(tetragonal)	
$TiAl$	1460	$L1_O$(fct)	γ
Ti_2Al_5	1215	-	δ
$TiAl_3$	1387	$L1_2$	

1.8.2 Ti-Al-Si System

Crossley(29) investigated the Ti rich corner of the Ti-Al-Si system upto 13at% Al and 3at% Si from 600 to 1200° C and presented partial isothermal sections at 600,800,900,1000 and 1200° C .Al has little , if any, effect upon the solubility of Si in the α -Ti phase and but decreases the solubility of Si in β Ti phase.The solubility of Si at 840° C decreases from 0.6 at% to 0.4 at% by the addition of Al to Ti-Si alloy. At1200° C , the solubility of Si in the β phase decreases from 4 at% Si for Al free β Ti to 1.75 at% Si for β (Ti -Al 25). The TiAl phase dissolves less than 1 at% Si. Panseri (30) observed the precipitation of a ternary compound when adding 0.6 at% Ti to an Al-Si eutectic alloy . Brukl(31) identified a ternary compound as $Ti(Al_{1-x}Si_x)_2 (0.15 \leq x \leq 0.3)$ and pseudotetragonal structure using X-ray powder diffraction analysis. He observed a solubility of Si in$TiAl_3$ of upto the composition $Ti(Al_{0.85}Si_{0.15})_3$ A solubility range from $TiAl_3$ to$Ti(Al_{0.8}Si_{0.2})$ at700° C was also reported. An invariant ternary reaction was reported at 579° C.

$$L + Ti_2Al_3Si_2 = (Al) + Si$$
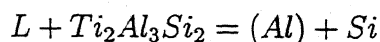
Ternary solid phases are tabulated below

Table 1.4: Ternary compounds of Ti-Al-Si system

Phase	Formation Temperature	Formula	Remarks
τ_1	900^0C	$(Ti_{1-x}Al_x)_8(Al_{1-y}Si_y)_6$ $Ti_7Al_5Si_{12}$	$x \approx 0.12$ (32,33) $0.06 \leq y \leq 0.25$ (31) at x=0.12,y =0.25
τ_2	-	$Ti(Al_{1-x}Si_x)_2$	$0.15 \leq x \leq 0.3$ (33)
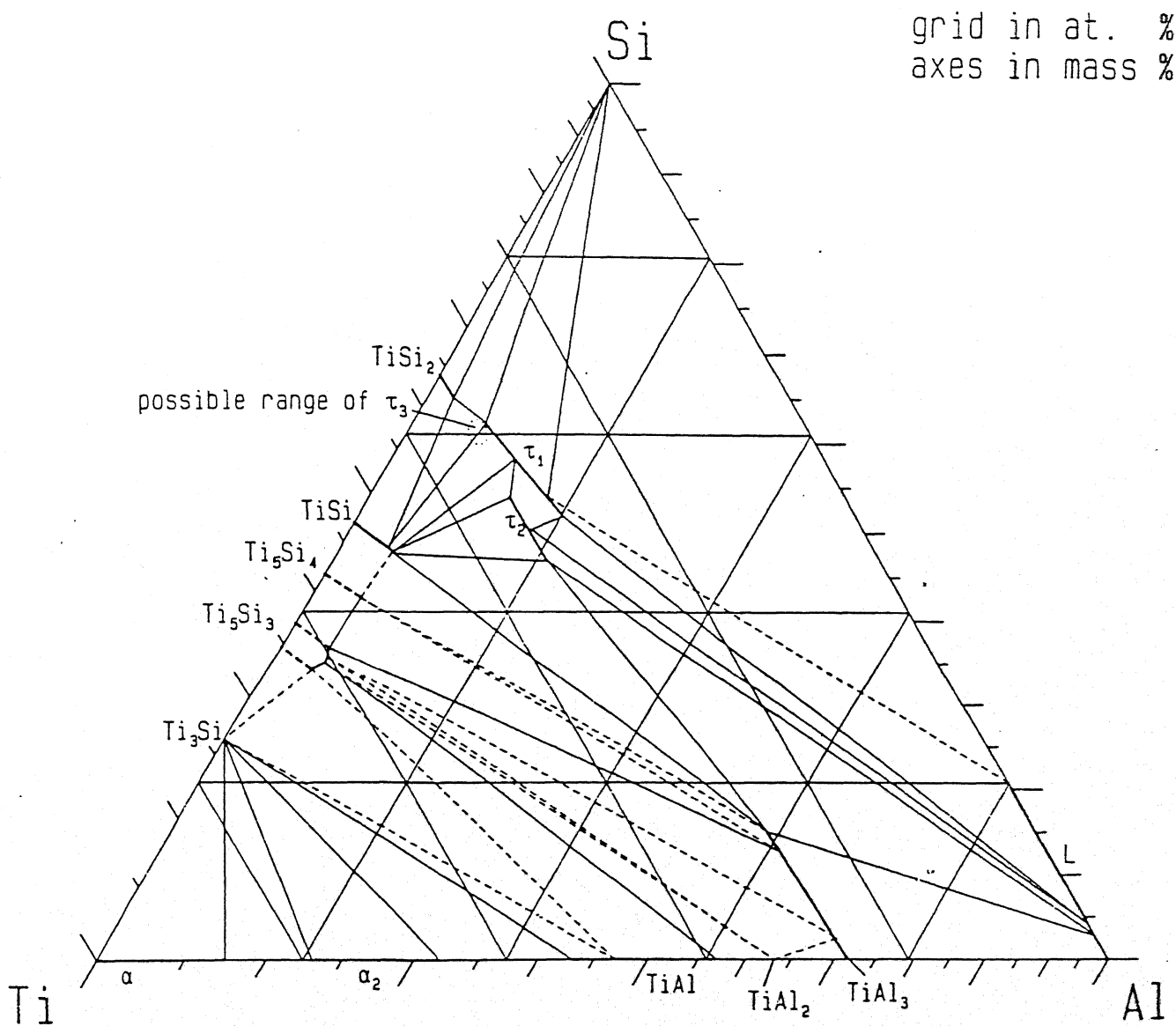
Figure 1.18: Isothermal section at 700°C.
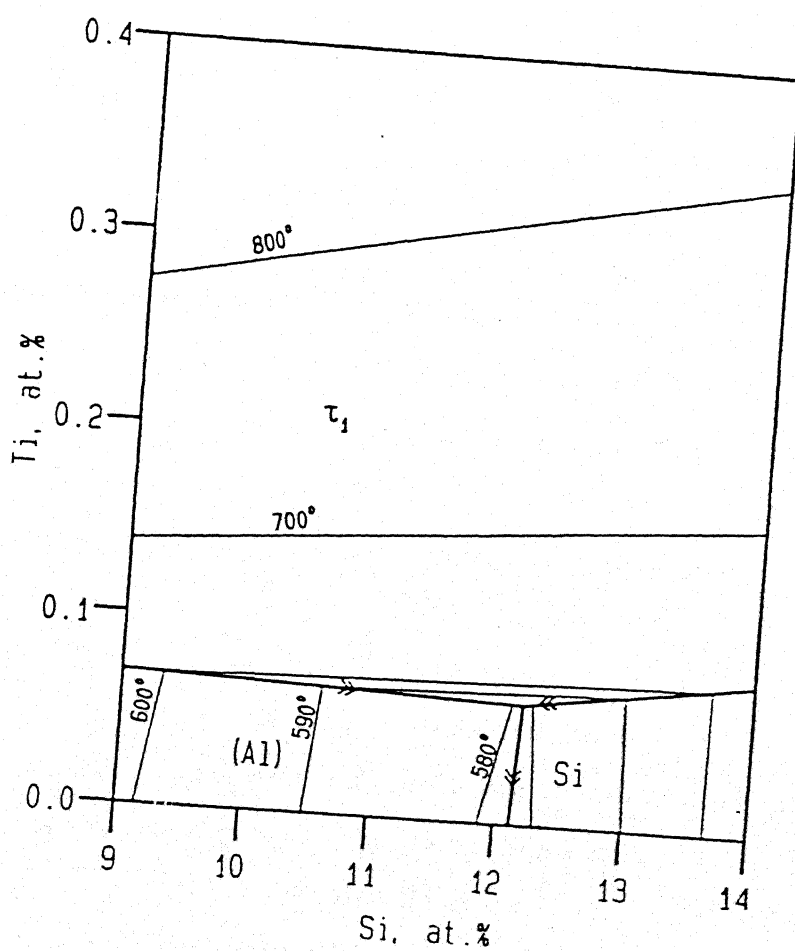
Figure 1.19: Liquidus surface near the Al-Si binary eutectic (28)

Chapter 2

Experimental Procedure

The metals used in this investigation were of very high purity (Fe and Ti of four 9 purity).An Al-Si eutectic alloy of composition 12.2 at % Si was made in the induction melting furnace.While making the alloy the melt was continuously stirred to ensure the formation of a homogeneous alloy and no segregation of the liquids. This alloy ingot was then cut into several small pieces to make Fe-AlSi and Ti-AlSi ternary diffusion couple.

For the binary couple pure Al was used .In the Fe and Ti ingot which had nearly circular cross section of 8mm dia. a preliminary cut was made along the cross section using the diamond cutter to make its surface flat.This surface was then polished using standard metallographic techniques to ensure optically flat surface for good bonding. Then another cut was made parallel to the former to get a slice of 2mm thickness. These slices of Fe and Ti were used as the base metals in the diffusion couple. Wettability is purely dependent on the particular combination of the solid and liquid composition used(for a given temperature and pressure). To ensure maximum area of bonding Al and Al-Si samples of maximum permissible base area was used and to make immediate and effective bonding their surfaces were also polished. Base metal (Fe/Ti) and Al/ Al-Si alloy were then cleaned in Ultrasonic Cleaner to make sure there is no unwanted debris on the surface which could hinder bonding.

The samples were then kept in an assembly as shown in the Fig 2.1 . The base metal was put on a graphite block. Al/Al-Si alloy was put on the base metal and was surrounded by a graphite disk of 6mm outer dia.(inner dia 4mm approximately).Another graphite block was put on the graphite disc and made screw tight . Both the graphite blocks and the graphite disc were polished to ensure no air leakage. Graphite blocks were used to lower the oxygen potentials while hollow graphite disc for prevention of liquid flowing out of the base metal.

Metal Assembly Holder

Screw

Carbon Blocks

Al/AlSi alloy

Graphite disc

metal
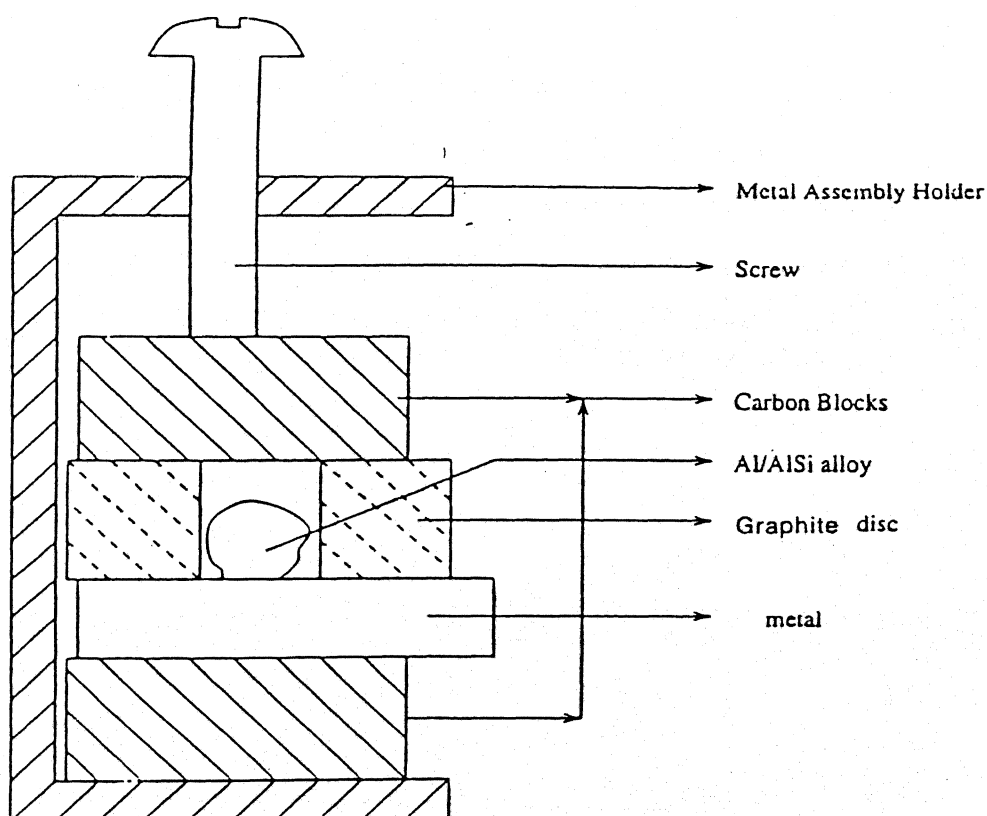
Figure 2.1: Section of the assembly in which the couples were prepared.

This assembly was then put in a quartz tube which was connected to a rotary vacuum pump. Vacuum of around 10^{-3} to 10^{-4} torr was obtained thereby ensuring little high temperature oxidation of the metals.The quartz tube then

put inside a vertical furnace and kept at a fixed temperature and annealed.

Fe-AlSi was kept at 900°C for 9 , 16 ,25 Hrs. and at 600°C for 36 hours while the Ti-AlSi was kept at 900°C for 4,9 and 16 hours and at 1000°C for 9 and 25 hours.

One each of Fe-AlSi and Ti-AlSi were water quenched following diffusion at 900°C for 25 hrs. and at 900°C for 9 hrs. Rest of the samples were air cooled keeping the vacuum pump running to ensure no oxidation and air entrapment in the liquid during cooling.

Once the diffusion couple cooled down to room temperature it was removed from the quartz tube and retrieved from the assembly and cut with the help of a diamond cutter to expose the interface region as shown in the Fig 2.2. It was then mounted and polished using the standard metallographic techniques.The interface region was then studied using Electron Probe Microanalyser (EPMA) where the composition of the various phases were determined.Scanning Electron Microscopy (SEM)was also carried out on these samples to study the microstructure of various phases formed during solidification and the intermetallic layers.
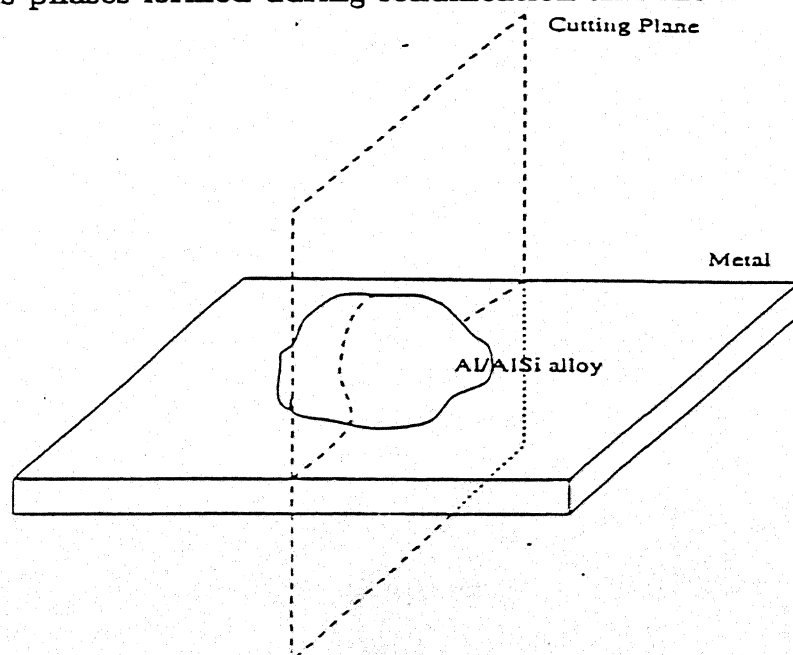
Figure 2.2: The plane along which the diffusion couple was cut to expose the interface

Chapter 3

Results and Discussion

3.1   The Binary Diffusion Couple, Fe-Al

The Fe-Al forms a solid-liquid diffusion couple at 900°C. The Al atoms from the liquid diffuse fast and cross over the solid-liquid interface to join the Fe lattice and vice-versa.The liquid quickly gets enriched with Fe and a saturated inhomogeneous liquid solution is formed.The gradient in the liquid as predicted by the phase diagram can not exist as it is modified due to the convection in the liquid.

Primary $FeAl_3$ forms during cooling from 900°C to relive the supersaturation of Fe that exists at that temperature according to L=L_0+FeAl$_3$. As we scan the solidification microstructure different morphologies of $FeAl_3$ are seen; Figs **3.1** to **3.3**. The primary $FeAl_3$ appears as dendrites with wavy interface (non-faceted), Fig3.1.

The plate type of morphology with facets was also prevalent , Fig 3.2. The plates taper off and become needle like during the terminating stage of solidifications .This shows the transitions of plates to needles type morphology and vice-versa. Liang and Jones(42) have found that the initial partially twinned faceted and non-faceted growth of an FeAl$_3$ would evidently be favoured over faceted growth of an $FeAl_3$ plate , because it requires much smaller undercool-
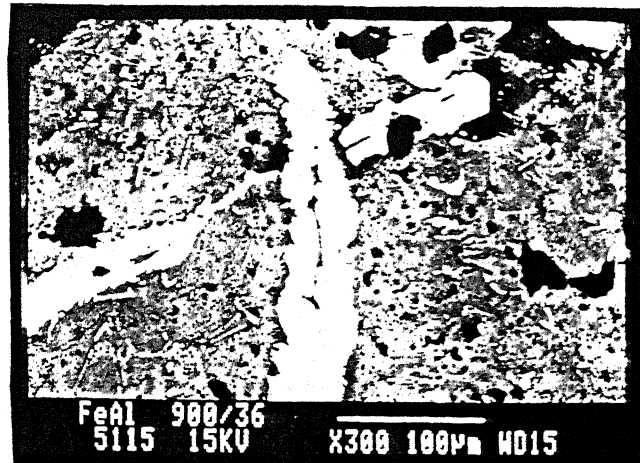
Figure 3.1: Primary $FeAl_3$ wavy interface

Figure 3.2: Plate and needle type $FeAl_3$
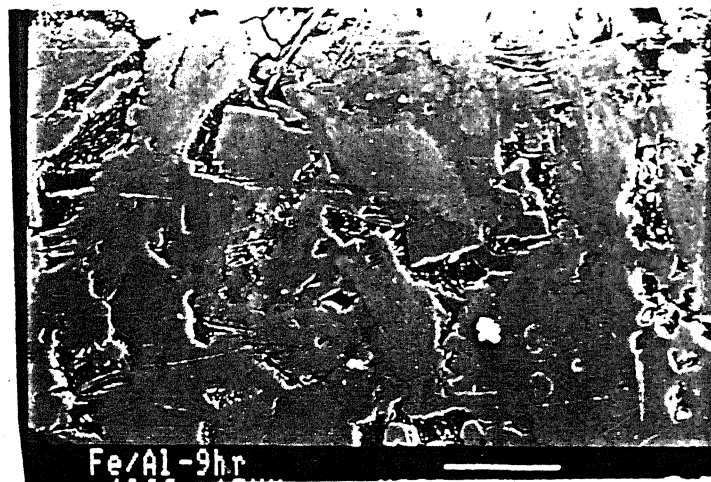
Figure 3.3: Polyhedral $FeAl_3$

ing. The same group (43) found that the final morphology of primary $FeAl_3$ changes from plate to needle-like with an increase in growth velocity. Two different types of $FeAl_3$ morphologies are also seen as in **Fig 3.3**

The faceted polyhedra of different sizes, among which some are homogeneous and a few are heterogeneously nucleated. These have much larger particle size compared to those nucleated homogeneously. The grains are almost polyhedral with a few exception of sharp dendritic arm protruding into the liquid. Few of them show facets. Towards the solid part of the diffusion couple, the relative volume fraction of $FeAl_3$ increases continuously with decreasing distance from the solid-liquid interface, which shows that the liquid is not completely homogeneous, rather has composition gradient, however small it may be.

The liquid adjacent to the $FeAl_3$ interface first rejects Fe, because this part of the liquid has maximum Fe content. So , $FeAl_3$ polyhedra forms first near the interface. Earlier, it must have dendrite type structure, but later as solidification proceeds towards the top, it becomes polyhedral due to continuous latent heat generation by the newly solidified $FeAl_3$. The $FeAl_3$ dendrites towards the top

have relatively larger volume fraction of the liquid compared to that at lower part near the interface. The liquid forms lamellar eutectic structure adjacent to $FeAl_3$ dendrites, Fig **3.3**

As the liquid gets cooled, its compositions follow the liquidus curve and ultimately reaches the eutectic composition where it forms $FeAl_3$ and (Al) from the following reaction, L = (Al) +FeAl$_3$. Some part of the liquid (preferably the upper half)has lower Fe concentration, so that the average composition of that part of the liquid lies on the hypoeutectic side,(with respect to Al as the base metal). The primary dendrites of aluminium solid solutions form from the liquid during cooling.

According to the binary phase diagram of the Fe-Al system (23), the solidification of the liquid starts at **660°C** and ends at **652°C**. The temperature range will be slightly increased due to **air** cooling, nevertheless, the driving force for formation of primary (Al) dendrites is very small compared to the$FeAl_3$ primary dendrites. The characteristics long primary arms of (Al) are not very prominent in the solidification structure, Fig **3.4**
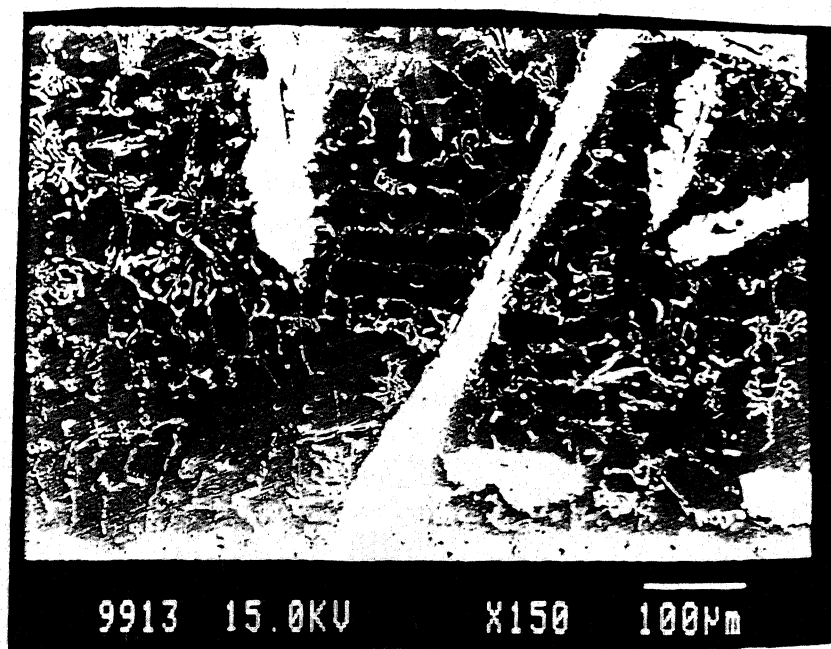
Figure 3.4: (Al) dendrites with divorced eutectic structure

As the liquid rejects primary aluminium, its composition moves along the liquidus with cooling and ultimately reaches the eutectic composition. From the observed microstructure , Fig 3.4, it is clear that the volume fraction of the liquid forming on the hypoeutectic side of the phase diagram is very small, so that the spacing between the primary dendrite phase is comparable to the $FeAl_3 - Al$ eutectic spacing.(44) The lamellar structure characteristics of the eutectic liquid solidification is not observed. The eutectic aluminium solid solution (α) is continuous with primary dendrites. The remaining liquid gets enriched with iron and solidifies as $FeAl_3$, Fig 3.4. The structure is that of a divorced eutectic as observed in Ag-Cu alloys. Some liquid pockets between primary (Al) shows lamellar eutectic structure, probably because the width between primary (Al) is larger than the eutectic spacing in those pockets or simply those pockets have eutectic composition such that a eutectic structure forms directly during cooling.

Diffusivity of Fe in molten Al decreases with decreasing temperature, while driving force for primary $FeAl_3$ formation decreases, because of thermal diffusion from previously solidified $FeAl_3$. This decreases the solidification rate (velocity) of $FeAl_3$. That means the characteristics diffusion length for Fe (here Fe is solute) $l_{Fe}(= \frac{D_{Fe}^{liq}}{R})$ changes with cooling . R is the solidification rate and D_{Fe}^{liq} is the diffusivity of Fe in liquid . Complex composition fluctuation because of natural convection (initial composition difference aided by gravitational force) and l_{Fe} play an important role in deciding the solidifying microstructure.

Next to the liquid layer, $FeAl_3$ layer shows large grained structure next to the primary $FeAl_3$. Layers of Fe_2Al_5 and FeAl form next to the $FeAl_3$ in the diffusion couple, Fig 3.5.

A fine precipitate of Fe_3Al forms on FeAl during cooling, Fig 3.5. Next to the Fe_2Al_5 layer there is a region of small thickness showing diffusion induced recrystallisation (DIR). According to the coherency strain theory proposed by Hillert(45), the boundary diffusion of solute results in a concentration gradient infront of the migrating Fe_2Al_5 boundary which inturn results in this region being elastically strained if the lattice parameter of the grain varies with solute

Figure 3.5: Microstructure showing iron aluminides layer

Figure 3.6: Kirkendall plane Fe-Al binary diffusion couple

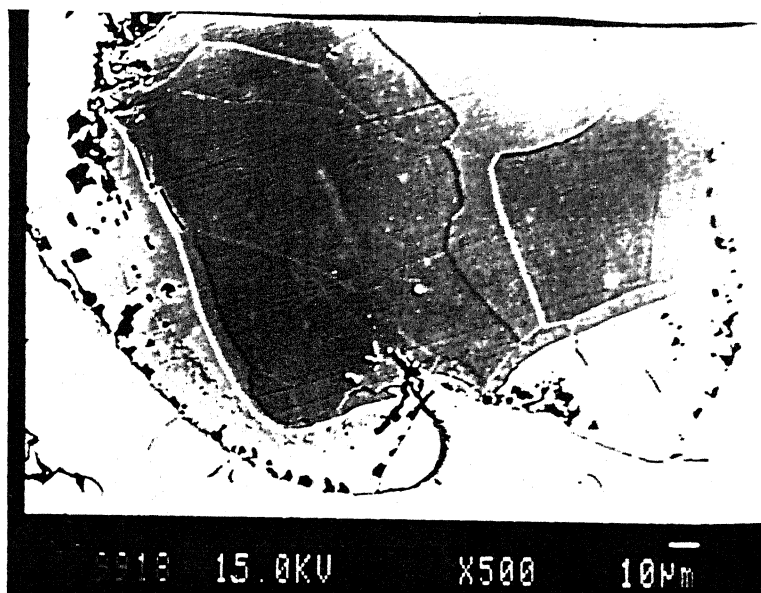concentration. The rest of the grain is supposed to be relaxed as the energy is accommodated by misfit dislocation and interstitial deffects. If the strained part of an $FeAl_3$ grain remains coherent with rest of the grain , then this stored energy

is released as diffusion induced recrystallisation occurs. Another interesting observation regarding Fe-Al binary diffusion couple is the appearance of two Kirkendall planes in (Fe)/FeAl and $FeAl/Fe_2Al_5$ interfaces(Fig 3.6).

This implies net vacancy flux at these interfaces are zero so that the Kirkendall planes coincide with the new position of the interfaces.Similar observation was reported by Van Loo et al(17); for interdiffusion of A and B atoms with given interfacial concentrations X_b^α=0.2 and X_B^β=0.7 for given intrinsic diffusion coefficient.

For the Kirkendall plane at (Fe)/FeAl interface, it can be inferred that the Fe is faster diffusing in Fe rich part of FeAl (whose non-stoichiometry is very large = 25 at as in the Fe rich part of FeAl , three type of deffects are possible

<blockquote>

i) Vacancy in Al sublattice.

ii) Fe in Al sublattice.

iii) Fe in interstitial position.

</blockquote>

The last one is quite unlikely, because it needs very high energy compared to the other two. For the diffusion of both the species Fe and Al in FeAl, nearest neighbour jump is likely because of higher jump distance of both the species (0.865 a compared to a, a is the lattice parameter) in like sublattices compared to the unlike ones Fig 3.7. Though it appears that the like bond formaton increases energy, but at 900°C the atom movements are more likely to be random i.e; encourage like bondings. For both the cases i) and ii) , Fe diffusion is preffered over Al diffusion , as for the later to predominate , there should be sufficient vacancies in Fe sublattice, which is quite unlikely for the Fe rich part of FeAl. The reverse is true for the Al rich part of FeAl. According to Chang and Neumann (38) FeAl shows triple defect (in which divacancy and antisite defec t form an elementary unit of diffusion)at low temperature configuaration and antistructure defect at high temperature . In our temperature of diffusion , it is more likely that the later would be followed as explained.

$FeAl_2$ phase is not found.
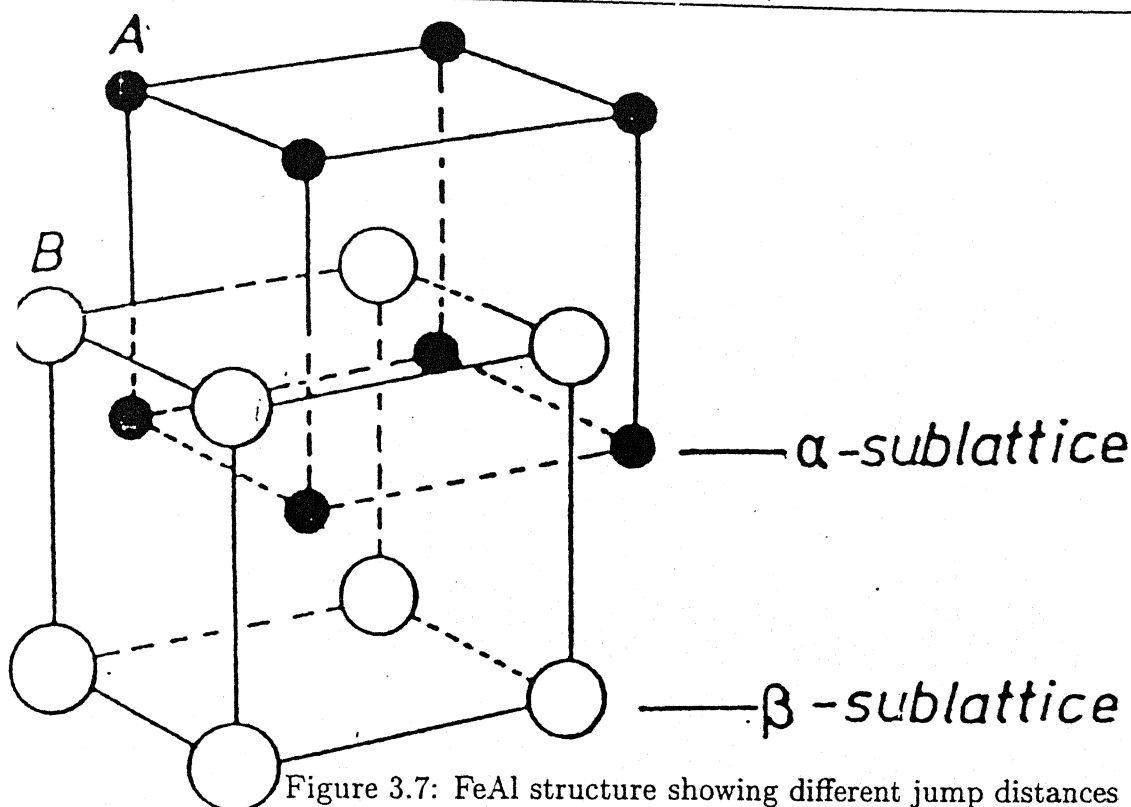
Figure 3.7: FeAl structure showing different jump distances

Enthalpy of formation of $FeAl_2$ (81.6 KJ/mol) (39) is lower compared to other iron aluminides. $FeAl_3$, Fe_2Al_5 , $FeAl$ have formation energies of 112.4, 197.82 and 81.6 KJ/mol, respectively. So, there should not be any problem of nucleation of $FeAl_2$.

The sublattices of $FeAl_2$ may be such that diffusion jump in like sublattices are impossible. Again jump to unlike sublattice may cause high energy barrier, so that this is feasible. This possibly makes the growth kinetics very slow.

3.2　Ternary Diffusion Couple, Fe-Al-Si (Air Cooled)

As soon as the Al-12 %Si eutectic alloy ($T_E = 577^oC$) is kept at 900^oC, it becomes liquid and starts diffusing into iron . As observed from the microstructure taken as per sequence from solid/liquid interface to the top of the liquid, primary $FeAl_3$ forms first as expected, Fig 3.8 .

As the primary $FeAl_3$ forms, solute gets partitioned between liquid and $FeAl_3$, but will not follow equilibrium diagram, because of air cooling. The partition

Figure 3.8: Primary $FeAl_3$ with other reaction products

coefficient depends on growth velocity . As growth velocity tends to 'zero', partition coefficient tries to attend its equilibrium value.Partition coefficient also depend on the crystallographic orientation of the growing interface. If a crystal grows with a faceted solid/liquid interface, the incorporation of solute into the crystal behind the facet can be quite different from the rest of the crystal.Brice(40) called this the facet effect. The dependence of partition coefficient on curvature is thought to be negligible(41). Thus, a concentration - distance profile builds up infront of the primary $FeAl_3$ dendrites ,which would be different for Al and Si, as their diffusivity in liquid are different. There will also be a thermal gradient, because of $FeAl_3$ formation. Now since the liquid has a range of composition,that too has changed by primary $FeAl_3$ formation, the secondary solidified product phases($FeAl_3 + \tau_2$) appear in the microstructure during cooling, Fig 3.9.

The secondary $(FeAl_3 + \tau_2)$ phases may or may not form through the reaction P_5 depending upon the composition in that portion of the liquid.Different phases for possible liquid composition are shown in table 3.1 for the four phase plane
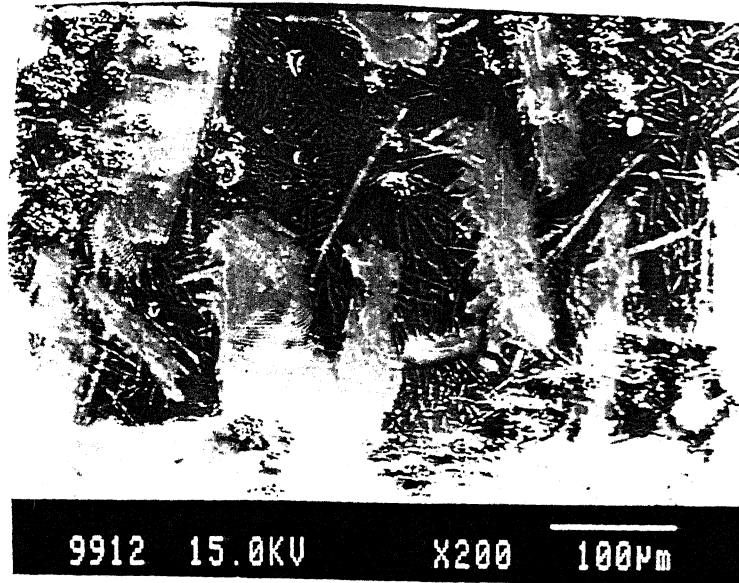
Figure 3.9: Secondary $FeAl_3$ and τ_2 phase

showing peritectic reaction.
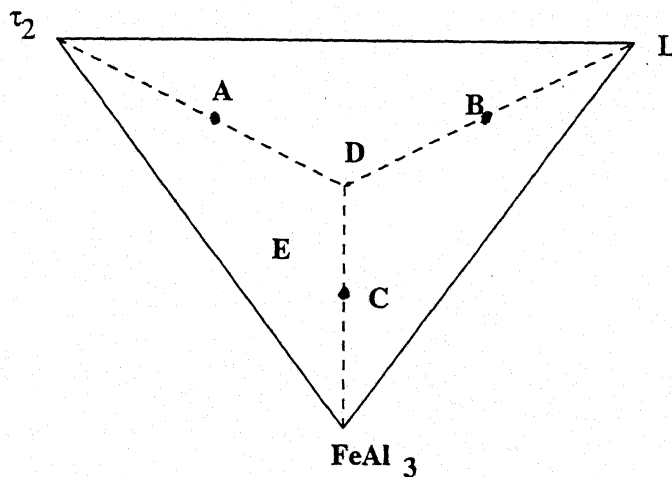
Figure 3.10: Schematic diagram showing P_5 reaction plane

Since the composition of different parts of the liquid are not known, it is difficult to identify the combination of phases. Again, what is supposed to be excess τ_2 (bright small sized precipitates)on peritectic morphology , may well have been secondary $FeAl_3 + \tau_2$, because peritectic τ_2 is in the middle of the $FeAl_3$ dendrites and appears as long rods ,Fig 3.11.

Table 3.1: Peritectic reaction scheme

Gross Composition	Microstructure
A	Excess $\tau_?$ +Peritectic
B	Excess liquid + Peritectic
C	Excess $FeAl_3$ + Peritectic
D	Only peritectic
E	Primary $FeAl_3/\tau_2$
	Secondary $FeAl_3$ and τ_2
	and peritectic.
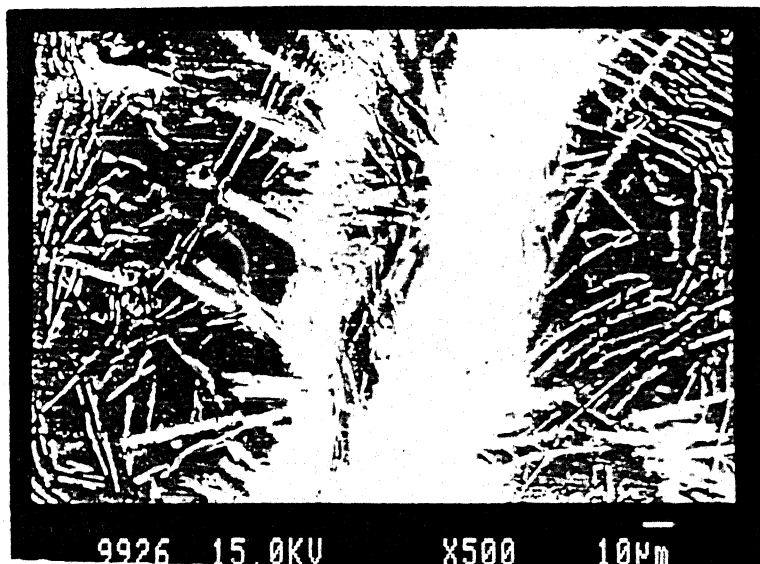
Figure 3.11: P_5 morphology

This reaction never completes because of air cooling. The unreacted liquid goes below the invariant plane corresponding to P_5 gives other solidifications products. The bottom most layer shows thick coarse grained $FeAl_3$, because it forms first during solidification and gets annealed in the sense that continuous latent heat generation comes from the solidifying phases as we go to the top of the liquid pool. From the liquidus projection diagram, it is quite obvious that, some of the four phase planes are likely to overlap each other when viewed from

the top. This causes two or three associated reaction morphologies . Other possible reasons are overlapping of several other diffusion and thermal fields and natural convection associated with it. As noticed from the photographs, the interdendritic liquids are of E_1 composition which means high fluidity of these liquid pockets that aid in further convection . Random distribution of dendrites (anisotropy in growth direction is not clear) makes this fluid flow different in different regions, giving rise to variation in gross composition and also in reaction products, even in the same horizontal coordinates.
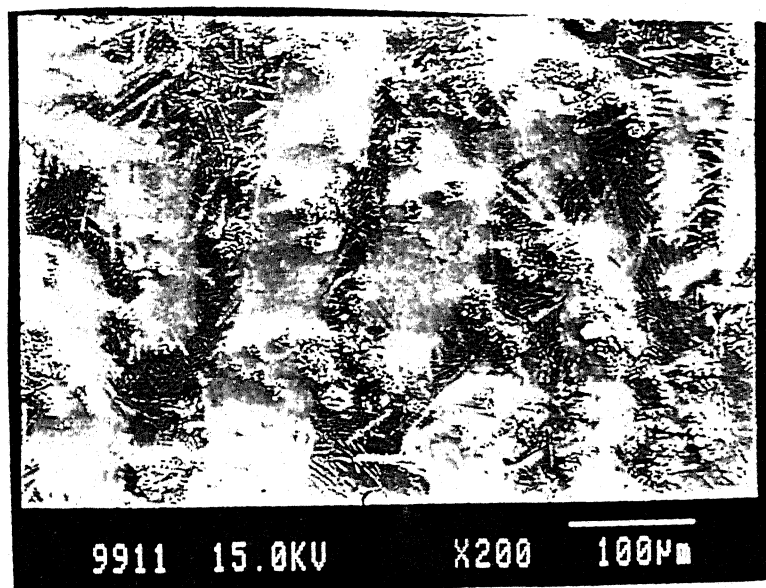
Figure 3.12: Clustered τ_2 and τ_4 phases

Clustered black and white dots as noticed in the next series of photographs (bottom to top) are found to be τ_2 and τ_4 mixture, Fig 3.12. The phase τ_4 is found to be white dots and it is different from greyish τ_2. A closer look at τ_2 reveals square shape with rounded corners which indicates reaction with liquid during cooling. The τ_2 and τ_4 cluster which lies on or adjacent to enveloped τ_4 (formed by P_5 reacion) is also observed in the solidified liquid. The τ_5 phase formed in the U_9 reaction is supposed to be continuous with τ_5 formed from P_5 reaction , as the former can't be separated by different morphology, Fig 3.12.
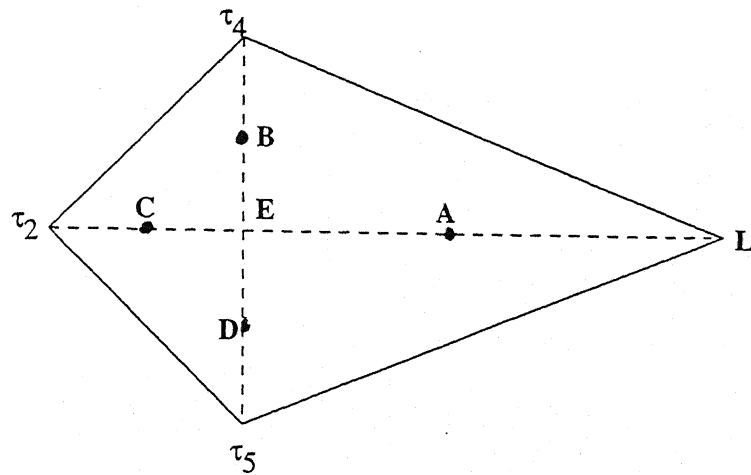
Figure 3.13: Schematic diagram showing U_9 invariant plane

Possible phases for quasiperitectic reaction are given in Table- 3.2

Table 3.2: Quasiperitectic reaction scheme

Gross composition	Phase Combinations
A	Excess liquid (=AE) + Quasiperitectic morphology
B	Excess τ_4(=BE)+ do
C	Excess τ_2(=CE)+ do
D	Excess τ_5(=DE)+ do
E	Primary τ_2 + do
Any other composition	Primary + Secondary+do Phases

The type of microstructure indicate that the gross composition may lie close to EL .Here also the interdendritic spaces show eutectic reaction, with a few solute depleted area.

Fig 3.14 shows both the P_6 and U_{12} reaction products. τ_4 phase appears as small bright squares and is dispersed throughout. In the microstructre shown in Fig 3.14 the inner envelop is $FeAl_3$, intermediate layer is τ_5 and the outermost layer is of τ_6 composition. The lower half of this figure shows product of the reaction $U_{12}$and it shows envelopment of the primary phase. The products of

Figure 3.14: Microstructure showing P_6 and U_{12} reaction characteristics

the reaction U_{12} also shows envelopment of τ_4 phase. It is expected that the liquid, τ_4 and τ_5 phases required for the ternary peritectic reaction P_6 , comes from U_9 reacion which is supposed to occur at higher temperatures. ($790^0 C$ for equilibrium cooling) compared to U_{12} reaction(600^0C). Similarly liquid, τ_4 and τ_6 phases for the U_{12} reaction come from P_6. U_{12} reaction is characterized by τ_4 precipitates in particular crystallographic alignment and appears as a row of particles. The τ_4 phase precipitates on τ_6 and appear as random precipitates. One of the interesting observation is that , adjacent to the products of P_6 and U_{12} reactions, no eutectic microstructure exists, which shows liquid depletion. This is probably because of high Si content of τ_4.

Fig 3.15 ; shows products of the combined P_5 and U_{10} reactions. The τ_5 phase of the reaction U_{10} shows an acicular morphology, presumably due to high temperature gradient infront of its tip.The adjacent depleted liquid forms α (Al) according to the reaction U_{10}.The three phase field of (L+ $FeAl_3 + \tau_5$) and (L+ $FeAl_3+$ (Al)) required for the $U_{1}0$ reaction are expected to come from P_5 and e_{11} ,respectively.

L+FeAl$_3$ =(Al) +τ_5 .... U$_{10}$
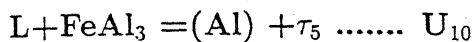
Products of the reaction U_{11} with τ_5 at the core and τ_6 enveloping it, are shown in Fig 3.16. Two three phase fields of (L+tau_5+τ_6)and (L+ (Al) +τ_5) are expected to come from reactions P_6 and U_{10},respectively which give the following reaction on just crossing the four phase plane

L + τ_5 = (Al) +τ_6...... U_{11}
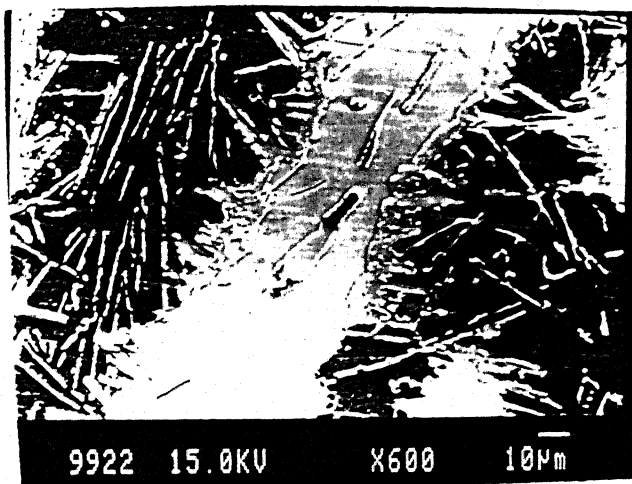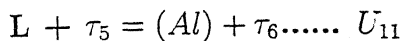
Figure 3.15: Microstructure showing P_5 and U_{10} reaction characteristics

Figure 3.16: U_{11} reaction characteristics morphology

The fibrous branches are mostly primary τ_6.   Primary τ_6 are faceted plates , Fig 3.14. Its mode of nucleation is not known. The liquid adjacent to the U_{11} morphology, also shows the eutectic structure, Fig 3.16, the three phase fields L+τ_6+Si from U_{12} and L+(Al) +τ_6 from U_{11} are expected to terminate on the ternary eutectic plane E_1 which ultimately gives microstructure corresponding to E_1 upon solidification $L = (Al) + \tau_6 + Si$ ...... E_1

The liquidus projection shows that e_1 and E_1 are very close to each other . It is expected that some liquid pockets will have composition corresponding to e_1 and others E_1 and they may overlap as suggested by McCartney et al(49).
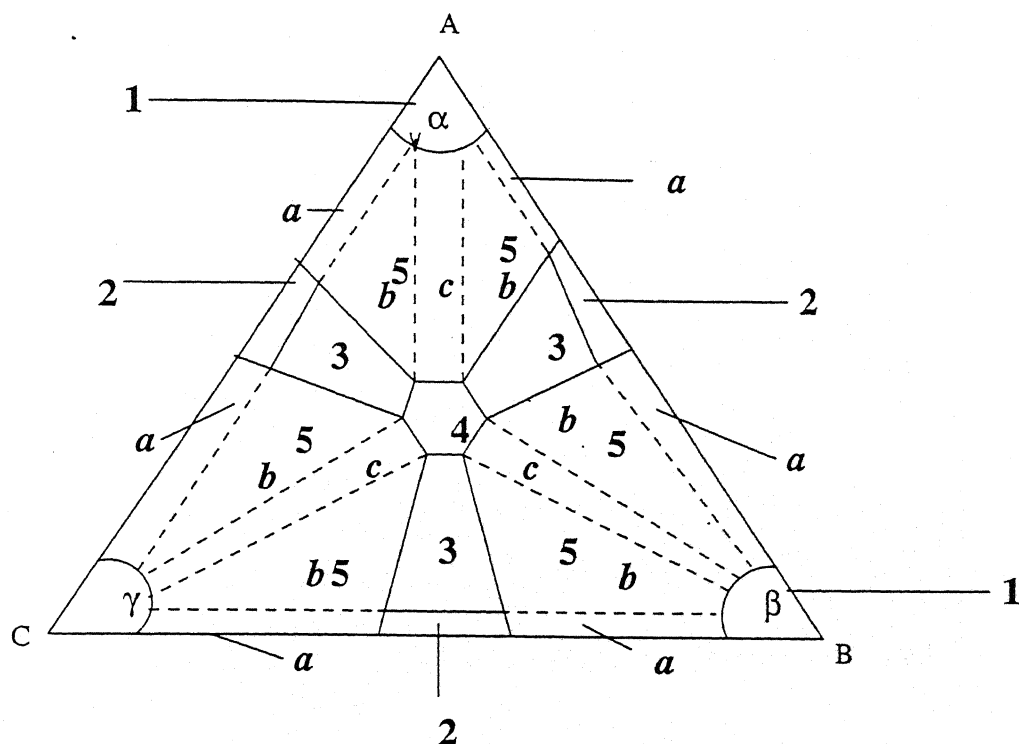
Figure 3.17: Schematic representation of the composition boundaries of the various structural regions(dotted and solid lines) for a fixed velocity and fixed velocity and temperature gradient.

Possible phase combination for different regions are tabulated below

Table 3.3: Ternary eutectic reaction

Domain	Phases
1	Single phase
2	Two phase eutectic
3	Secondary solidification and ternary eutectic
4	Ternary eutectic
5a	Single phase and binary eutectic
5b	Primary and Secondary and ternary eutectic
5c	Primary and ternary eutectic

Microstructures of the ternary eutectic consists of of rod shaped τ_6 phase in association with plates (acicular) of Si in the matrix of α (Al) ,Fig3.18.
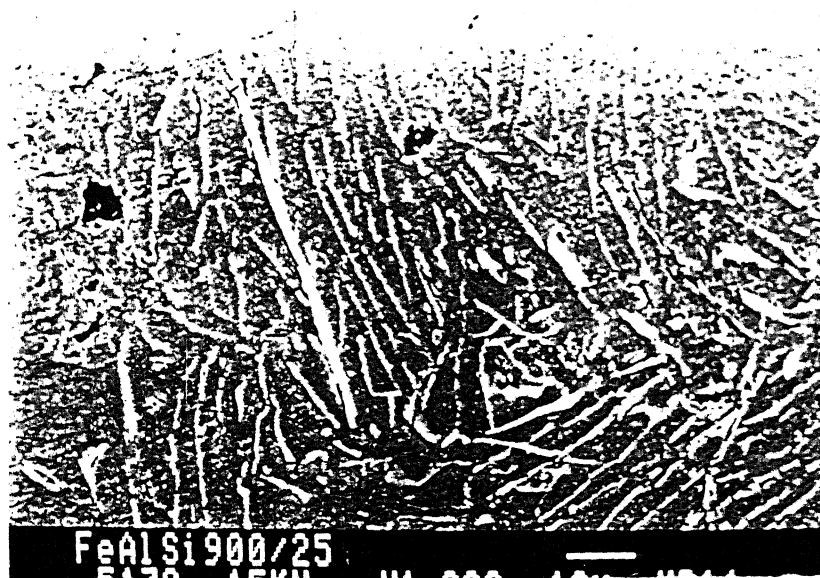
Figure 3.18: Microstructure showing ternary eutectic.

The edges of τ_6 are undulated. Comparison with Al-Si binary eutectic structure shows no difference of Si morphology which means Fe does not seem to modify its TPRE structure (Twin Plane Re-entrant Edge mechanism) which was first identified by Wagner(43),Hamilton and Seidenstichen[44]. They have found that the presence of internal deffects such as twins provide important sites for molecular attachment. Presence of {111} twins give rise to reentrant edges and grooves on growing surfaces which are self-perpetuating. It was further pointed out by these author that twinning on more than one plane will be necessary for continuous three dimensional propagation in the absence of any other mechanism and both primary and eutectic Si do include more than one twin. The instability of the rod morphology of τ_6 occurred because of surface energy consideration as suggested by Maquin et al(45). They considered an infinitely long cylindrical second phase embedded in the surrounding matrix of the other phase. The shape varies periodically as shown in Fig 3.19. The atoms diffuse from B to G (from $d\mu/dz > 0$) as $\mu_B > \mu_G$ where μ is the chemical potential just beneath an arbitrary point of a curved surface. There are only two possibilities
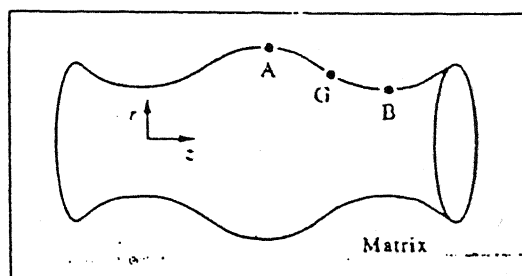
Figure 3.19: Instability of the cylindrical second phase

that μ_B and μ_A can follow i.e; either $d\mu/dz > 0$ continues until the cylinder breaks up at B or reaches a disturbed stable state for $\mu_B = \mu_A$. But, the same group has proved the later is impossible to attain. The former concept is noticed in the morphology of Fig 3.18 . Maquins et al(45) have further shown by similar analysis for $d\mu/dz < 0$, that the perturbation decays and tends to zero. The later can not be differentiated from the observed microstructure because it is hard to know whether it is going to break or straighten (by perturbation decaying) in the midway of the process. The Fe_2Al_5 phase appears as small fibres in the matrix of $FeAl_3$. The region marked A in Fig 3.2) is $FeAl_2$. In the work of Muraeva et al (46) , a new phase τ_{10} has been reported. However this has not been confirmed and numbers of authors including Rivlin and Reynor (24) have not considered τ_{10} as a separate phase. The analysis carried out on this phase confirms that it consists of 33 at % Fe, and balance Al and Si with the silicon being approximately 14.63 at %.Accordingly τ_{10} phase is nothing but the extension of the $FeAl_2$ intermetallics.It has been observed that Si atoms substitute for many of these of intermetallics of M-Al-Si where M is the base metal. The τ_{10} phase is therefore the intermetallic $Fe(Al_{1-x}Si_x)_2$. The isothermal section is modified accordingly as shown in Fig 3.20. Single phase layers of Fe_2Al_5 and FeAl form next to $FeAL_3$ and $FeAl_2$ layer, Fig 3.21 .The Fe_3Al phase is observed to precipitate as fine dispersion on the intermetallic FeAl.
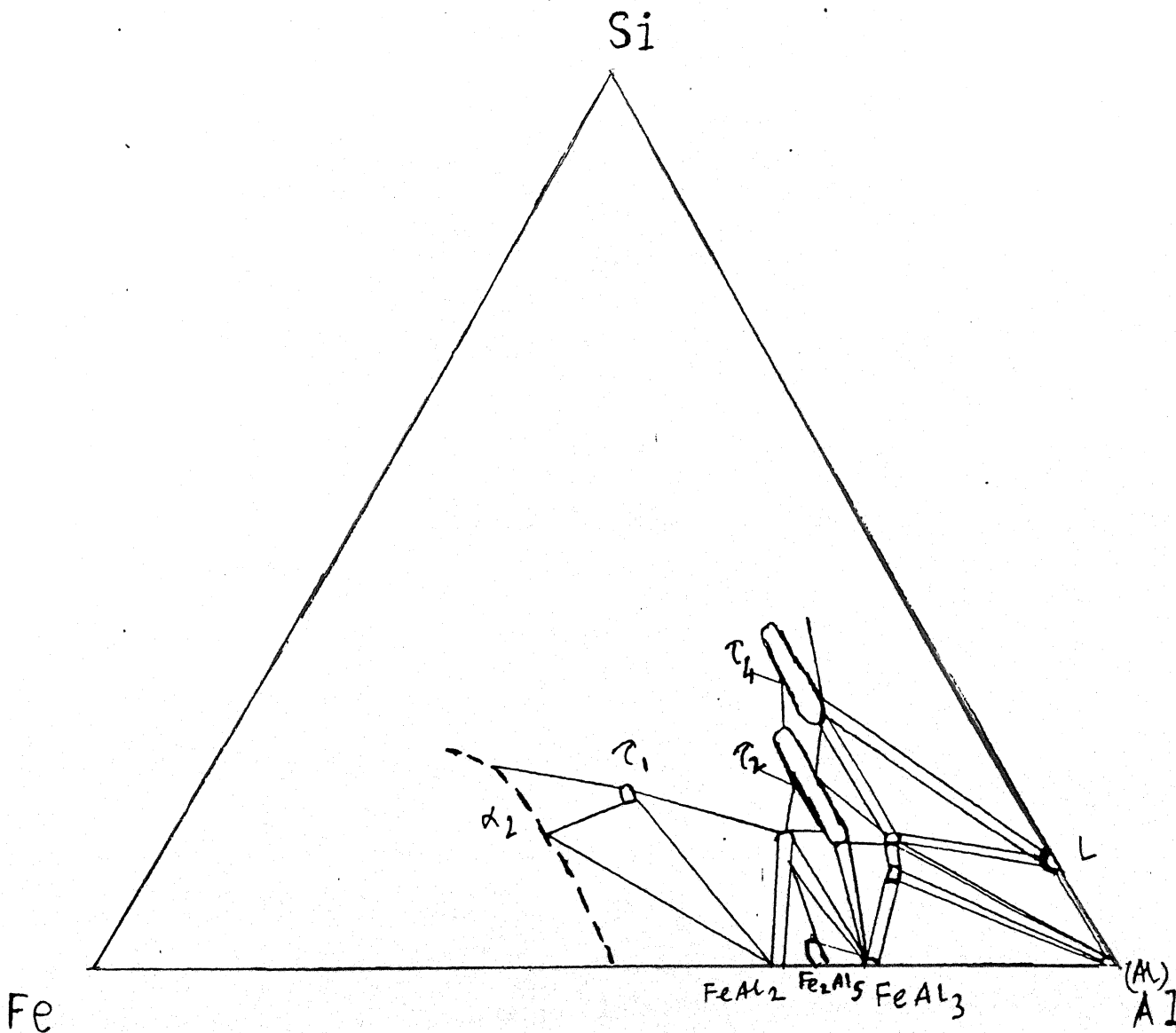
Figure 3.20: Modified Isothermal Section at 600° C
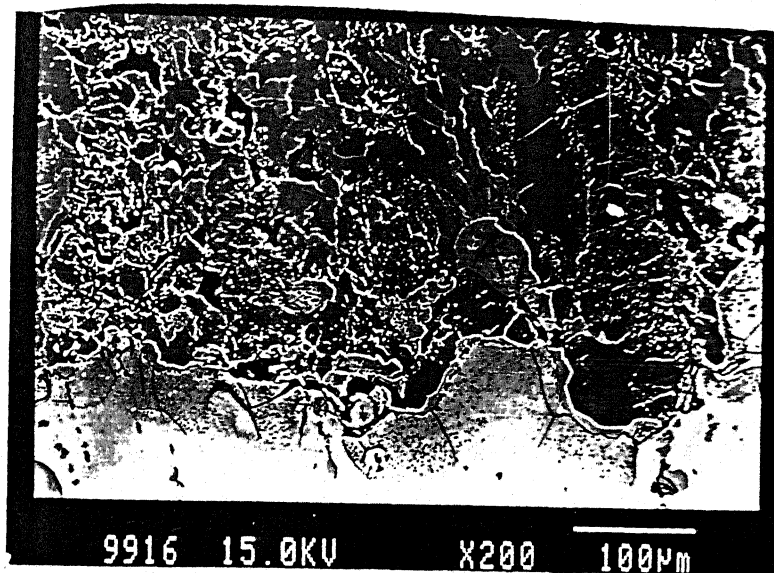
Figure 3.21: Solid state diffusion products

This iron solid solution with a steep gradient forms next to the FeAl layer, Fig 3.22 .As we increase the time of isothermal anneal of the diffusion couple, the Kirkendall plane shifts from the middle of FeAl(Fig 3.22) to the Fe_2Al_5 interface, Fig 3.23 . This indicates that Al is faster diffusing component towards the Al rich part of FeAl as discussed earlier for Fe-Al binary system. There is no kirkendall plane at the (Fe)/FeAl interface unlike the Fe-Al binary diffusion couple. Fe which is supposed to be the faster diffusing towards the Fe rich side of FeAl, may start diffusing slowly because Si is supposed to increase the potential energy of Al sublattice. In the ternary , Fe-Al-Si the nearest neighbour jump is discouraged by the system for Fe atoms unlike Fe-Al binary system.
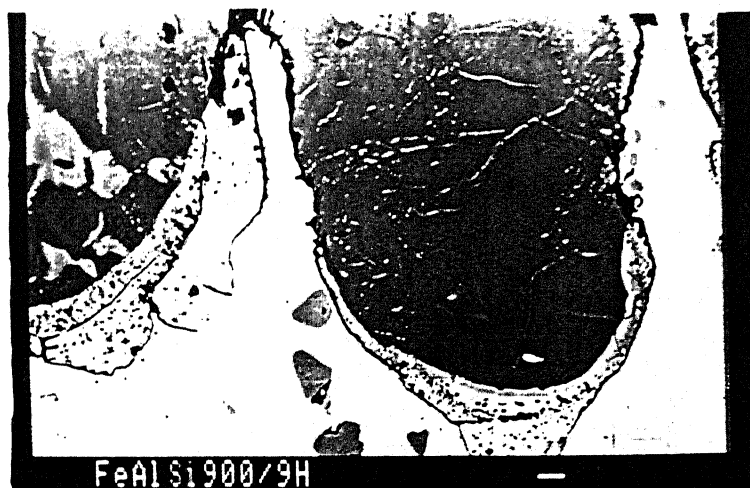
Figure 3.22: Kirkendall plane in 9 Hrs diffusion couple
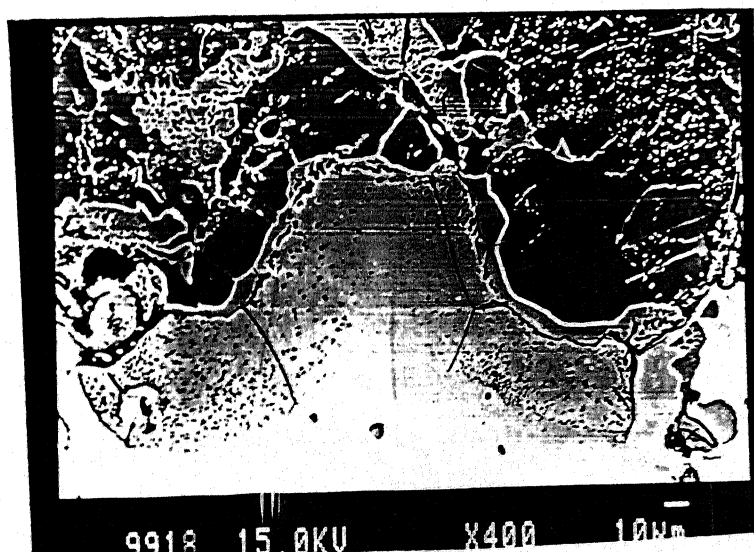
Figure 3.23: Kirkendall plane in 25 Hrs diffusion couple

3.3 The Ternary Diffusion Couple, Fe-Al-Si(water quenched)

A sample of the ternary diffusion couple was water quenched after 25 hours diffusion anneal at 900^0C. It shows layer of L and $L + FeAl_3$ followed by solid state reaction products. The occurrence of the product phase is decided by super or undersaturation of the diffusing elements, similar to those observed in the air-cooled sample. Very fast cooling rate , gives very high solidification rate for the primary solidification of $FeAl_3$ dendrites. The growth of these dendrites are arrested by impingements with other growing dendrites,3.23. Solidification
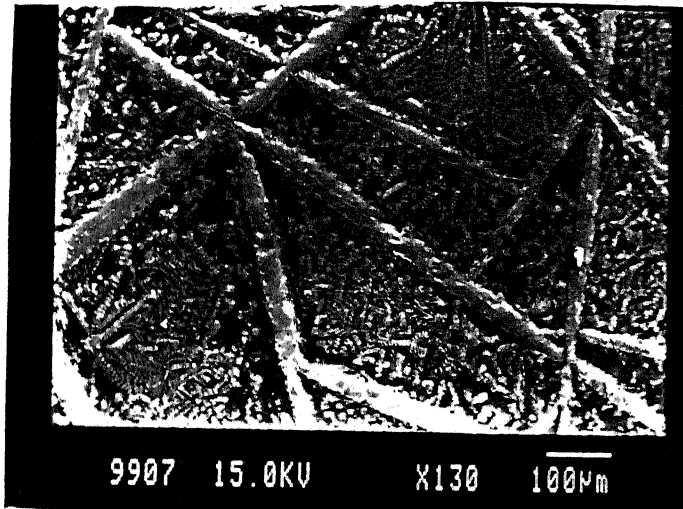
Figure 3.24: Impingement of the primary dendrites

of primary dendrites , change the fluid flow around them and therefore the local temperature gradient, because of its latent heat generation. It also causes the local change in composition of the liquid and thereby the morphologies of the newly developing phases.

Near the L/L+$FeAl_3$ interface (no physical meaning) the $FeAl_3$ dendrites form, as the nearby composition crosses the liquidus first.The $FeAl_3$ becomes coarse grained polyhedra and mostly lose their characteristics dendritic structure. Some of the $FeAl_3$ dendrites nucleated heterogeneously on the isothermally

formed $FeAl_3$, Fig 3.24. It becomes difficult to separate those that formed in the liquid during the quench from those existing at the isothermal diffusion temperature. The $FeAl_3$ and τ_2 phases are observed to occur next to the $FeAl_3$ as secondary constituents, Fig 3.25. Some of the secondary $FeAl_3$ are nucleated on
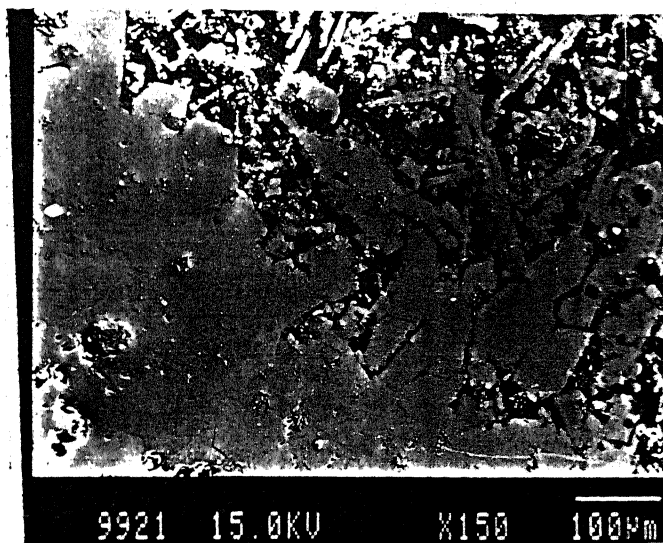
Figure 3.25: Primary and secondary $FeAl_3$

the primary and they are mostly interconnected showing heterogeneous nucleation on the edge of one another . As expected from the reaction scheme and the liquidus projection diagram, L+FeAl$_3$ +τ_2 phase terminates on the peritectic four phase plane (P_5 reaction)and ultimately undergoes the reaction

$$L + FeAl_3 + \tau_2 = \tau_5 \ldots\ldots P_5$$
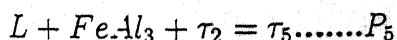
This can be easily identified by the envelopment of τ_5 , Fig 3.26. The τ_2 phase appears as long cylinder along the $FeAl_3$ axis and sometimes τ_2 is discontinuous, proving the reaction has partially occurred as expected. Other non-variant ternary reactions are suppressed because of very high cooling rate. The ternary peritectic reaction P_5 occurs at the highest temperature. The enveloped τ_5 phase occurs in various morphologies.The faceted τ_5 like secondary dendritic arms are shown in Fig 3.26. Faceted τ_5 needs higher undercooling than the non-faceted
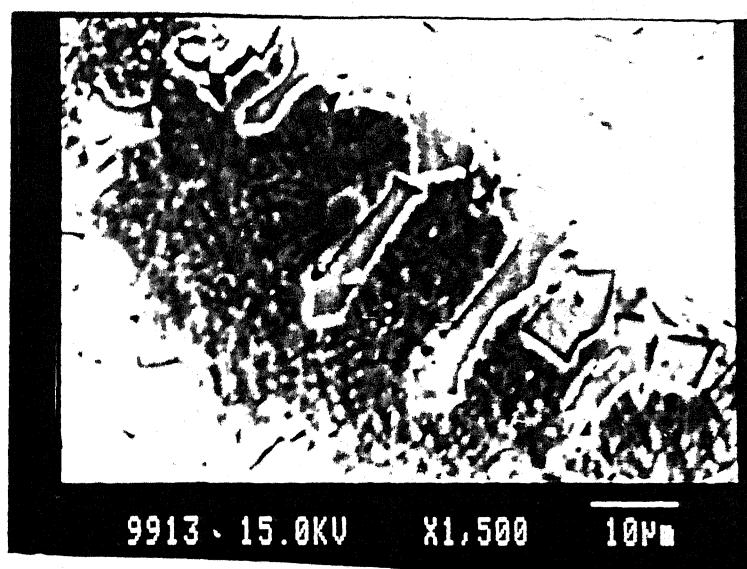
Figure 3.26: P_5 reaction morphology

structure and therefore will form late during cooling. The phase in between the dendrites are identified to be τ_5, which is expected to appear as a product of the ternary peritectic reaction P_5. They show planer interface , Fig3.27 . Some of
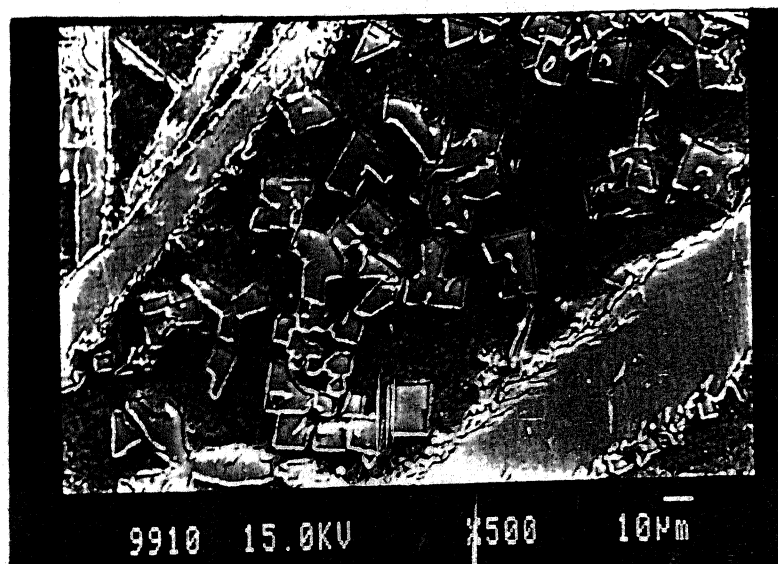
Figure 3.27: Different morphologies of τ_5

them have triangular, square and rectangular shapes. The faceted τ_5 have nucleated both homogeneously and heterogeneously in the liquid and on the existing τ_5, at the isothermal diffusion anneal temperature, respectively. Some of these appear interconnected with a reduction in surface energy of the liquid/solid interface. The presence of Si in the τ_5 phase presumably lead to the formation of faceted structure. A spinal chord type morphology is also observed for the τ_5 phase in some regions, Fig 3.28. These are also interconnected . The nucleation
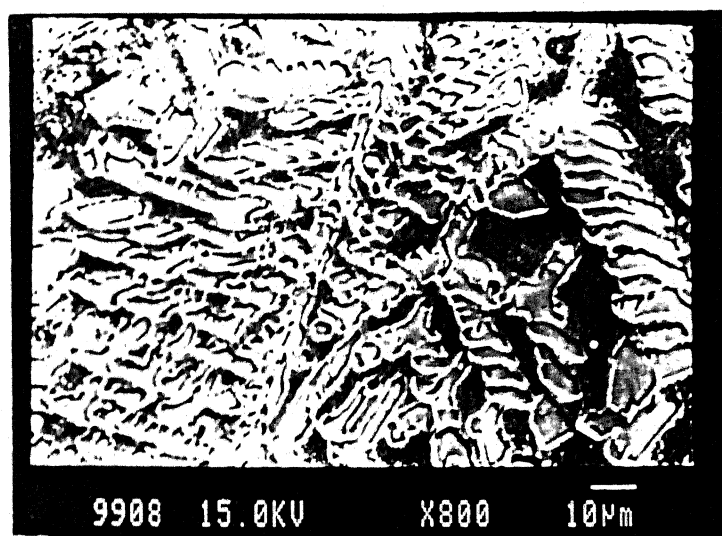
Figure 3.28: Spinal chord type τ_5

of these morphology of τ_5 has occurred homogeneously in the liquid as seen in Fig 3.28. A two phase layer of ($FeAl_3 + FeAl_2$) is observed. A small volume fraction of Fe_2Al_5 forms on it during cooling. From the morphology it is clear that $FeAl_3$ and $FeAl_2$ forms isothermally , followed by single layer of Fe_2Al_5 as expected . The Fe_3Al phase precipitates on FeAl . Next to it , there is a solid solution of Al and Si in Fe , Fig 3.29.
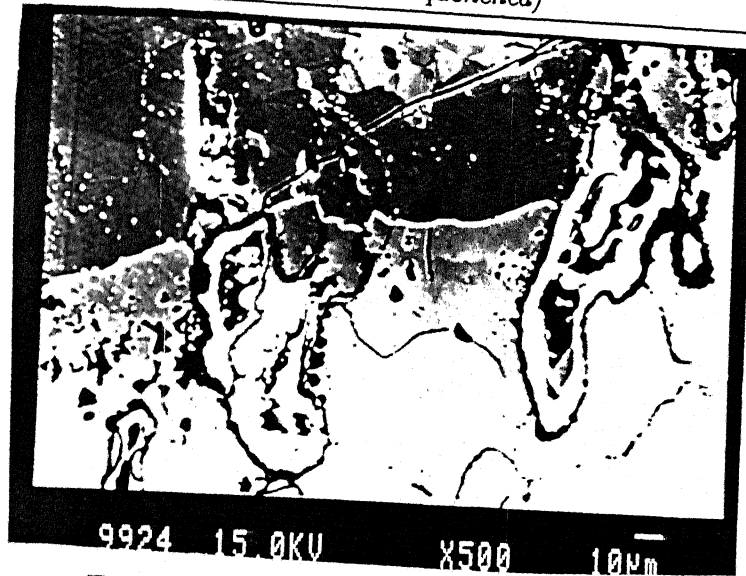
Figure 3.29: Solid state diffusion product
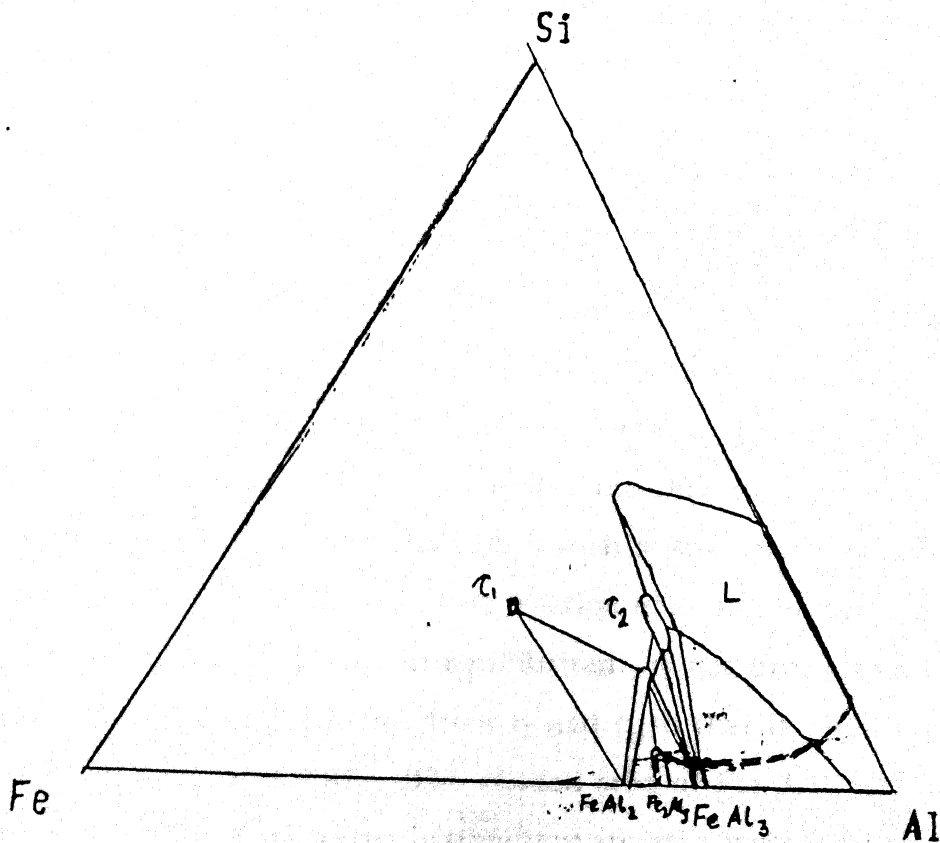
Figure 3.30: Schematic isothermal section at 900°C showing diffusion path

3.4 Ternary Diffusion Couple,Fe-Al-Si at 600°C (air cooled)

Investigation of this system at $600°C$ give some idea of the low temperature transformation and corresponding solidification microstructure along with the morphology of the other solid state reaction products. As before a gradient in liquid is set up which dictates the whole range of microstructures. Liquid near the top have higher Si and Al content compared to that near the interface region. First a τ_6 layer forms in the liquid next to the liquid /solid interface (Fig 3.31) , as the liquid becomes supersaturated in Fe. One interesting aspect is that the τ_6 phase forms along preferred crystallographic direction,fig 3.31. As we go towards the top part of the liquid,part of the diffusion couple elongated τ_4 phase is seen . $\tau_4$phase is expected to be present as L+τ_4. During cooling τ_4 and $\tau_6$form from the liquid ,fig 3.31. Few secondary τ_4 remain nucleated with initial one,but others are associated with secondary $\tau_6$as noticed in the microstructure.During further cooling ,the liquid undergoes the quasiperitectic reaction L $+\tau_4 = \tau_6$ +(Si) The enveloped morphology is clearly observed in fig 3.32. Again ,τ_6 of this reaction remain continuous with the secondary τ_6.that formed during cooling.Polyhedral Si is clearly seen just above the quasiperitectic morphology on the liquid,fig 3.32. This is understandable as Si is lighter and therefore floats up in the liquid. The diffusion path must have moved in such a way that it crossed the $\tau_5 + \tau_6$ two phase field.It gives minor volume fraction of τ_5 and τ_6. At the temperature of diffusion,only τ_5 and τ_6 exist in equilibrium. τ_2 get precipitated as shown in Fig 3.33. Due to cooling τ_2 forms from τ_5 and τ_6,so that it remain as an envelop surrounding τ_5 (Fig 3,31,3.32). The shaded area of Fig 3.33 shows the volume fraction of τ_2. The ternary eutectic structure appears away from the interface (at the top most part) of the diffusion couple. Microstructure of the top most part of diffusion couple shows primary (Al) dendrites ,Fig 3.34. It can be concluded that the liquid composition near top of the diffusion couple is on hypoeutectic sides.Secondary (Al)can not be traced as it is continuous with the primary (Al),
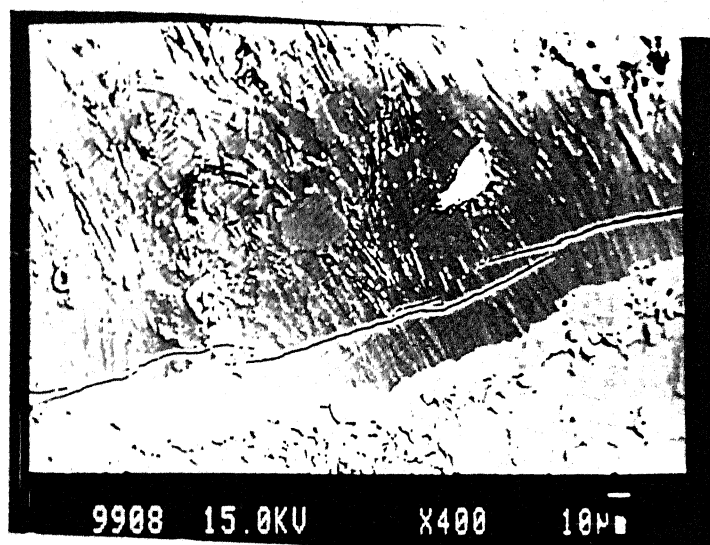
Figure 3.31: Microstructure showing τ_6 layer
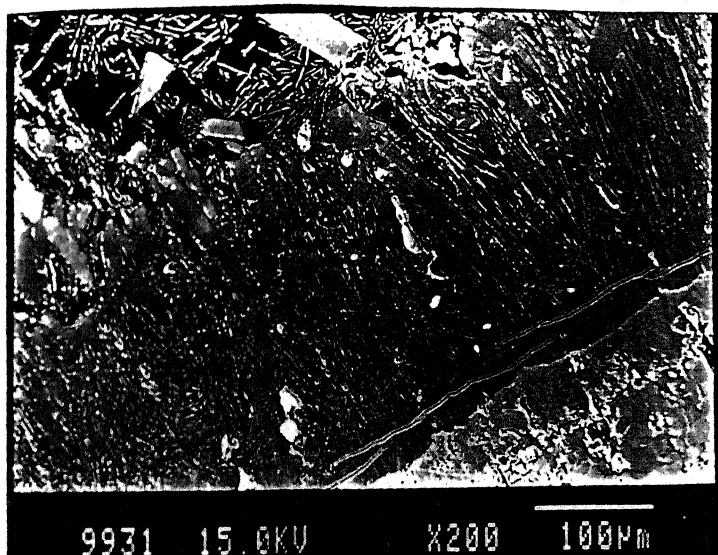
Figure 3.32: Quasiperitectic reaction morphology

while the secondary τ_6 start growing adjacent to the secondary (Al),Fig 3.35. Perhaps one end of τ_6 lies on (Al)is actually secondary (Al).The remaining liquid transforms to ternary eutectic as shown in the microstructure.During cooling the liquid composition moves along the eutectic valley and ultimately reaches the eutectic plane where it undergoes ternary reaction,E_1, L=(AL) $+\tau_6$ +(Si) Two there phase combination (L+τ_6+Si) and (l+(Al)+τ_6) descend on the ternary eutectic plane from the reaction U_{12} (near the interface, described earlier) and the
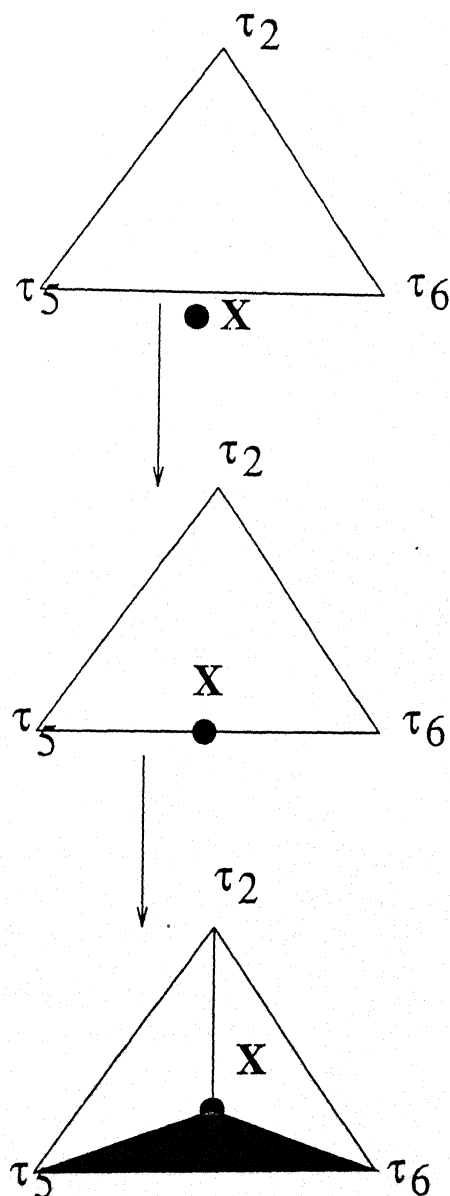
Figure 3.33: Schematic diagram showing formation of τ_2 out of τ_5 and τ_6

third (L+(Al) +Si) comes from the binary eutectic reaction of Al-Si system.The binary Al-Si composition and the ternary E_1 composition are almost the same .

Liquid composition in mass % (27)

E_1(ternary)	0.5	87.8	11.7
e_{12}(binary)	-	88	12

So,the cross over from e_{12} to E_1 is not precisely identified. It is rather mixed
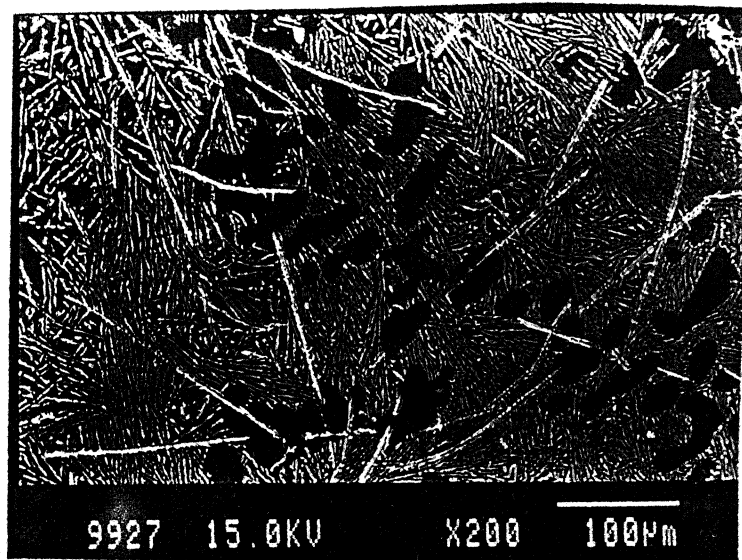
Figure 3.34: Microstructure showing primary (Al), secondary (Al) and τ_6 and mostly binary eutectic
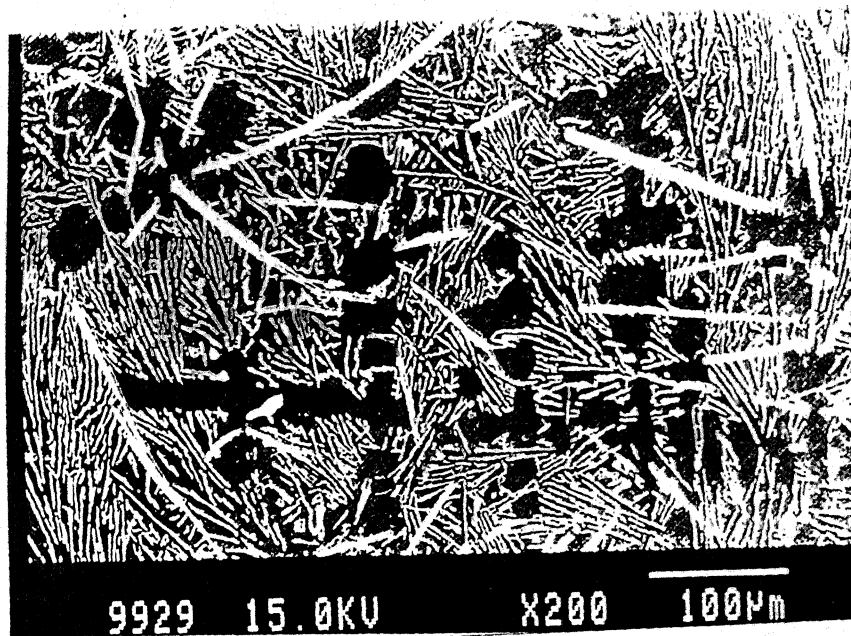
Figure 3.35: Microstructure showing ternary eutectic

because of convection in liquid. Generally eutectic composition is reached in the inter dendritic region spaces, where the liquid is richer in Fe and Si. Most of the interdendritic region show binary Al-Si eutectic as expected near the top of diffusion couple, Fig 3.34. The composition of the ternary eutectic, E_1 is reached in some part of the liquid. As the temperature is further decreased, ternary eutectic (E_1) composition is reached in the interdendritic region spaces, so that

there is an abundance of ternary eutectic structure , Fig 3,35,Next to the $(L+\tau_6)$ layer there are solid reaction products.A two phase layer of $(\tau_6+Al)$is expected to form .However, the volume fraction may be so small that it could not identified,although only τ_6 single layer is noticed ,Fig 3.36. Next to it, a single phase,τ_5 ,layer form,Fig 3.36.   Clear crystalline nature of of τ_5 is revealed in
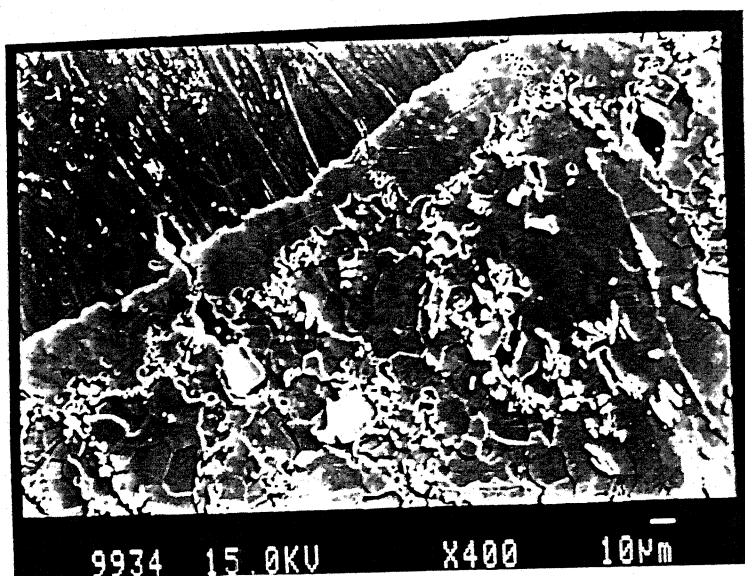
Figure 3.36: Microstructure showing τ_5 single layer and other phases

microstructure shown in Figs 3.36. τ_5 on τ_6 near τ_5/τ_6 interface is continuous with τ_5 single phase layer,Fig 3.31. A two phase layer of $Fe.1l_3+\tau_5$ forms next to τ_5, Fig 3.37.During cooling ,τ_2 gets precipitated as shown below
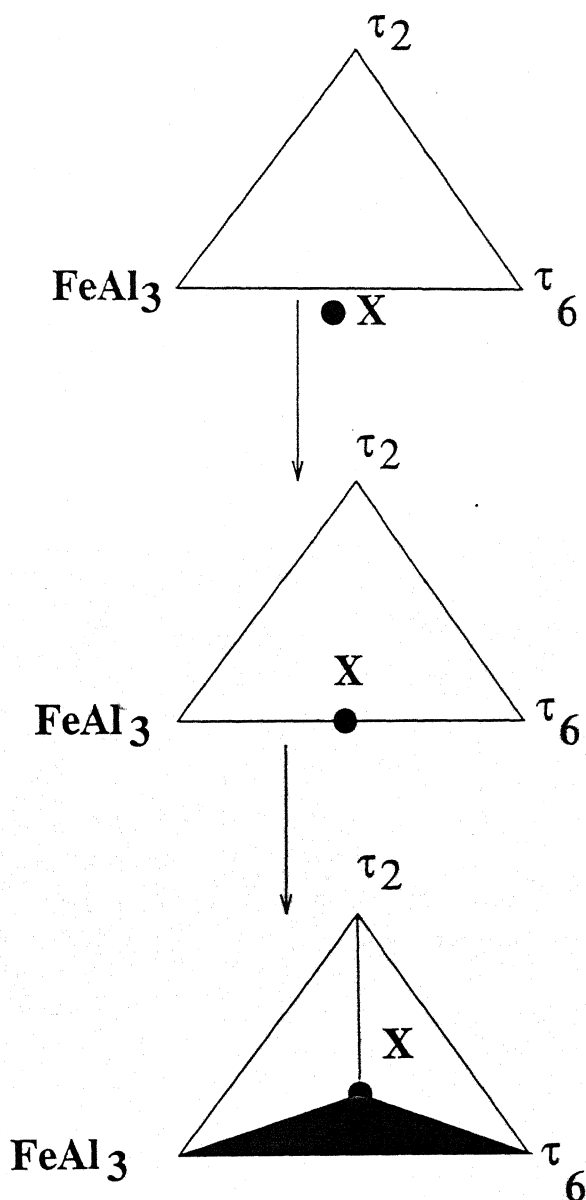
Figure 3.37: Formation of τ_2 out of $FeAl_3$ and τ_5

τ_2 forms from the reaction between $FeAl_3$ and τ_5 therefore ,it appears physically at the interface of$FeAl_3$ and τ_5 .The shaded area schematically shows the volume fraction of τ_2 pre-cipitated, Fig 3.37. Next to this layer, no other Fe-aluminides form, which indicates very slow kinetics which in turn supports their high formation energies, Fig 3.38. The isothermal diagram at 600°C is changed accordingly to explain the findings . The diffusion path is also indicated.
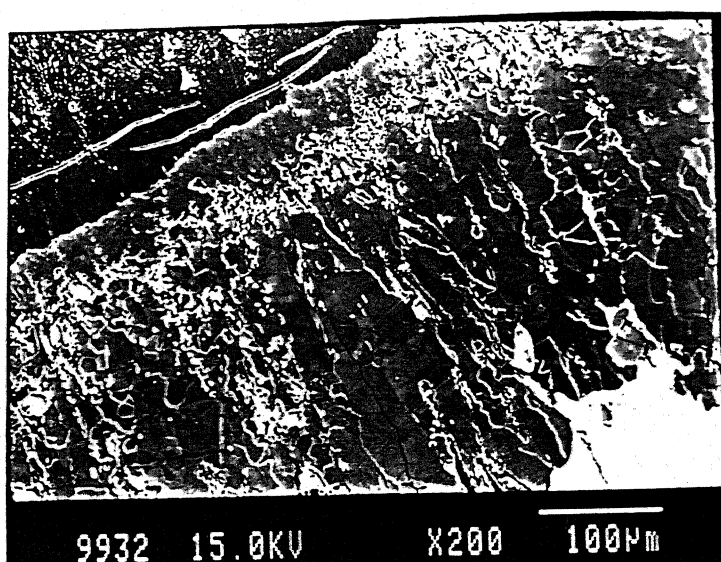
Figure 3.38: (Fe) solid solution next to FeAl$_3$ and τ_5 layer
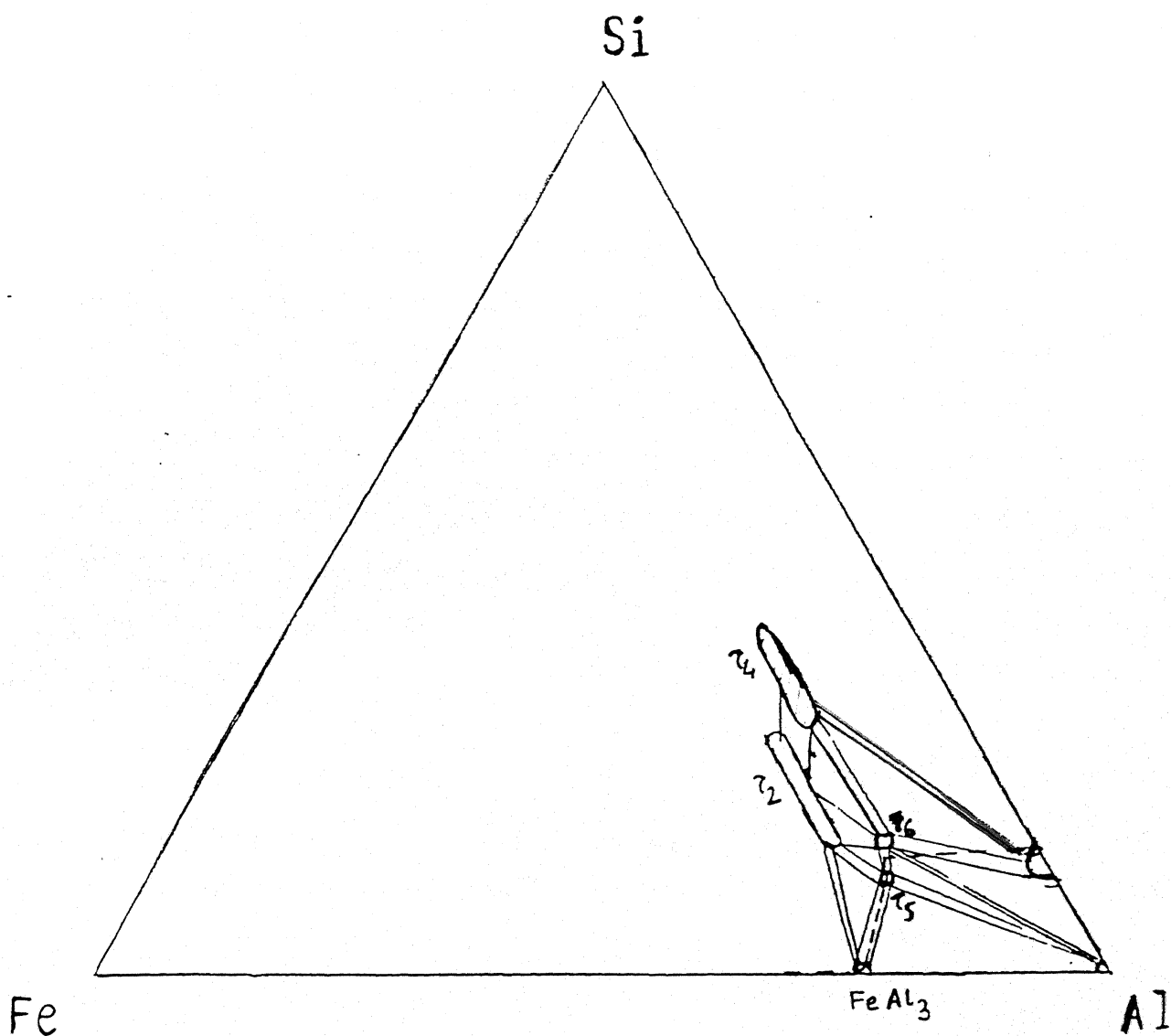
Figure 3.39: Isothermal section of Fe-Al-Si at 600°C towards the Al rich end

3.5 Compositions of Iron Aluminides and Ternary Compounds of Fe-Al-Si Diffusion Couple

The analysis of different intermetallics of Fe-Al and ternary compounds were carried out for Fe-Al-Si ternary diffusion couple, using EPMA unit. These are shown in table 3.4 and 3.5, respectively. Analysis of (Fe),(Al) and (Si) solid solution is shown in table 3.6 Si atoms substitute the Al positions in the lattice. Except for the $Fe(Al_{1-x}Si_x)_2$ phase, the solubility of Si in these phases is in the range 3.5 to 5.5 at %. The $Fe(Al_{1-x}Si_x)_2$ phase shows Si solubility of 14.62 at%. Since, the diffusion couple is air cooled, non-equilibrium cooling may lead to solute trapping which inturn gives higher solubility than equilibrium values. The $FeAl_3$ phase is reported to dissolve 0.975 at % Si(47);0.24 at% Si(48); 1.2225 at% Si(49); 3.5975 at% Si(50) and 7.35 at% Si at 600°C (51).The calculated values of x from these data are 0.0130, 0.0032, 0.0473 and 0.0980 respectively which are partly comparable with our results shown in Table 3.4. As we go towards off-stoichiometric,i.e.,towards Fe lean part of FeAl₃, Al is expected to go to Fe sublattice as antisite defects whereas Si atoms fractions remain almost constant. This indicates Si goes preferentially to Al sublattice. Had it gone to Fe sublattice, its at% could have shown much larger variation in solubility as compared to small variation observed. Towards the Fe rich side, iron atoms are supposed to go to Al sublattice as antisite defects and thereby would decrease the Si solubility as it has already preoccupied the site of Si atoms.This general trend is noticed from our result. Fe_2Al_5 phase shows Si solubility upto 5.88 at% in our analysis. But, Si solubility upto 3 at% is reported in the ternary isothermal section (at 600°C) referred by Ghosh (27). Air cooling may give rise to higher solubility of Si in Fe_2Al_5. The behaviour of Si in Fe_2Al_5 is similar to that in the compound $FeAl_3$ on the Fe-rich side.Towards the Fe-lean part of Fe_2Al_5, Si atom percent is on the higher side. The solubility of Si in the intermetallic FeAl is 3.32 at isothermal section(at 600°C) shows a solubility of upto 27 at % in FeAl. This value may be an approximation as it is indicated by dotted

line in the phase diagram. Further, in the same diagram, Fe_3Al shows a solubility upto 28 at% Si, possibly because Fe_3Al and Fe_3Si show mutual solid solubility, with Si atoms replacing Al atoms gradually and thereby changing the lattice parameter. Our analysis shows Si solubility of 5.50 at % in Fe_3Al which is well within the reported range. Among the ternary phases τ_2, τ_5 and τ_6 were identified convincingly, but τ_4 was difficult to analyse because of its small size. When the electron beam strike particles of τ_4, it also covers the surrounding area as a part of its analysis. So, variable compositions were obtained for τ_4. (Al),(Si) solid solution form as a part of different reaction in the liquid part of the diffusion couple. Air cooling may give solubility, values for these phases which are non equilibrium. The electron beam may not have hit the acicular Si which forms from ternary and binary eutectic reactions and therefore may not give the right composition. On the other hand, polyhedral Si formed as primary or as other reaction products gives the right composition values. (Fe) solid solution shows a gradual decrease in Al and Si at per as we move away from the (Fe)/FeAl interface towards the Fe base metal, table 3.6.

Table 3.4: Composition of intermetallic compounds formed in Fe-Al-Si diffusion couple

	Atomic %			
Binary Aluminides	Fe	Al	Si	x
$Fe(Al_{1-x}Si_x)_3$	21.4086	73.3753	5.2161	0.0695
	22.9413	71.8701	5.1886	0.0692
	22.5468	73.0549	4.3983	0.0586
	22.7801	72.7253	4.4946	0.0599
	22.6011	72.8162	4.5828	0.0611
	22.3790	73.1470	4.1470	0.0553
	22.2304	73.2212	4.5844	0.0611
	23.1997	72.4201	4.3802	0.0584
	25.0144	69.4265	5.5592	0.0741
	25.3604	72.2078	2.4319	0.0324
$Fe_2(Al_{1-x}Si_x)_5$	26.4365	69.0370	4.5365	0.0634
	27.0224	67.9699	5.0076	0.0701
	27.3918	67.0386	5.5696	0.0779
	28.4624	66.6390	4.8987	0.0686
	28.6941	67.9324	3.3735	0.0472
	29.2771	64.8438	5.8791	0.0823
$Fe(Al_{1-x}Si_x)_2$	33.7003	51.6810	14.6288	0.22
$FeAl_{1-x}Si_x$	63.2635	33.4182	3.3183	.09
$Fe_3Al_{1-x}Si_x$	74.3127	20.1819	5.5059	0.2207

Table 3.5: Composition of ternary compounds formed in Fe-Al-Si system

Ternary Compounds	Atomic%		
	Fe	Al	Si
τ_2	12.8224	69.4623	17.7133
τ_5	18.8024	69.1348	12.0628
	17.8186	71.9840	10.1974
	16.6269	66.4963	16.8768
	18.6605	68.2892	13.0503
τ_6	17.4404	64.4625	18.0971

Table 3.6: Composition of solid solution formed in Fe-Al-Si system

Solid Solution	Atomic%		
	Fe	Al	Si
(Fe)	99.0833	0.7054	0.2112
	99.0865	0.8194	0.0941
	99.8760	0.0477	0.0762
	99.9239	0.0421	0.3900
	99.9532	0.0021	0.0446
	99.9707	0.0000	0.0233
	99.9846	0.0000	0.0154
	99.9875	0.0125	0.0000
	100.000	0.0000	0.0000
(Al)	0.0754	99.1663	0.7583
	0.0391	98.6530	1.3079
	0.5261	98.1963	1.2776
	0.8190	98.9964	0.9216
	0.1047	97.5161	2.3992
(Si)	0.1010	0.7894	99.1095
	0.1281	0.6209	99.2509
	0.2396	0.5677	99.1927
	0.0447	0.5004	99.4549

3.6   The Binary Diffusion Couple, Ti-Al

When a diffusion couple is made between pure Ti and Al at 900^0C, the latter becomes molten . Molten aluminium has high wettability on Ti surface at 900^0C. It forms a vanishingly thin liquid film over Ti surface and completely covers the surface. At 900^0C the diffusion couple shows the following sequence of phases -

liquid, $TiAl_3$, $TiAl_2$, $TiAl$, Ti_3Al, Ti.

From the Ti-Al phase diagram, it is quite expected that a small composition gradient is set up from top of the liquid(pure Al) to $TiAl_3$ interface. This ideal composition gradient is likely to be smaller, because of convection. As the liquid is cooled , it rejects excess Ti as primary $TiAl_3$ form from the reaction L= L_0 +$TiAl_3$. Liquid composition follows the liquidus and ultimately- reaches the peritectic composition which is expected to be just below the equilibrium peritectic isotherm (660.452^oC) because of air cooling.

The liquid that reached the Ti solubility limit (i.e adjacent to $TiAl_3$ interface) until first reject Ti to form $TiAl_3$ at the interface of L/$TiAl_3$. The secondary$TiAl_3$ mostly nucleate heterogeneously on already exis ting $TiAl_3$ which is a solid state reaction product , thus making it continuous with the primary. From the Ti-Al phase diagram, it is clearly seen that the volume fraction of $TiAl_3$ that forms first is very small because its composi- tion is close to the peritectic composition and almost all $TiAl_3$ is consumed during the peritectic reaction, Fig 3.40.

Presence of small amount of liquids can be explained by off-peritectic com- position of the solidifying liquid and as incomplete peritectic reaction during air-cooling . The liquid nearest to the top of the diffusion couple forms $TiAl_3$ at lower temperature during cooling. From the phase diagram, it is quite clear that $TiAl_3$ formed near the top of the diffusion couple is less than that required for complete peritectic reaction at equilibrium . So, there must be excess liquid , which would be unreacted , as clearly seen in Fig 3.40. The excess liquid ulti- mately forms aluminium solid solution of certain composition which on further cooling rejects Ti due to sloping solvus (Al corner of Ti-Al phase diagram)in
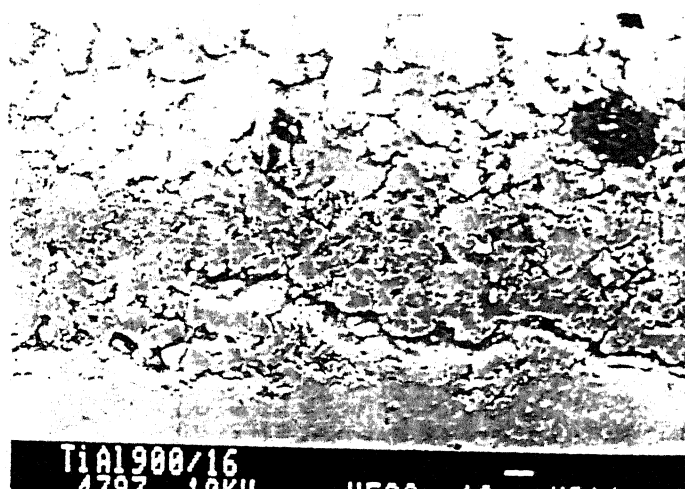
Figure 3.40: Microstructure showing different volume fraction of TiAl$_3$ near the interface and the top

the form of $TiAl_3$ as seen at higher magnification in Fig 3.41

Figure 3.41: TiAl$_3$ precipitate and peritectic reaction morphology(first type)

Peritectic reaction as mentioned earlier gives two type of morphologies. In the first, liquid pockets in $TiAl_3$ are surrounded by (Al),Fig3.41. The second morphology shows $TiAl_3$ surrounded by Al within liquid pools,Fig 3.42. Series of other intermetallic compounds follows $TiAl_3$ according to the phase diagram (Fig 3.43).
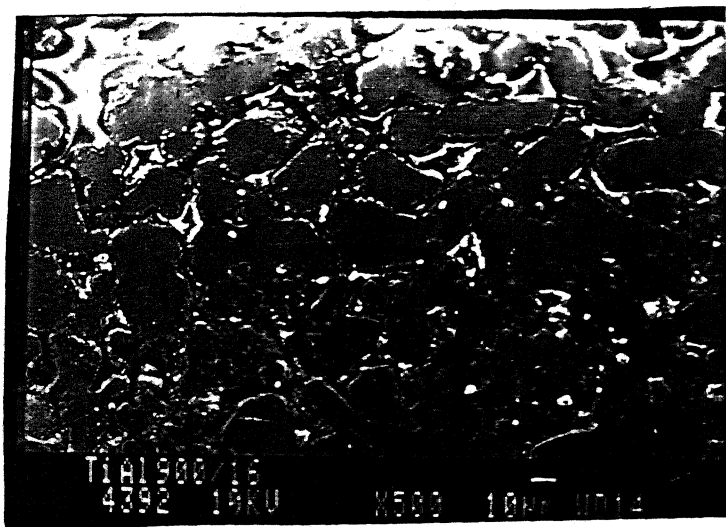
Figure 3.42: Peritectic reaction morphology (Second type)

The interfaces of the intermetallic phases are wavy and thickness of the layers are not constant although its length .The layers grow as hemispheres, Fig3.41.It can be explained by nucleation of intermetallic phase as individual units. Shape of the nucleus depends upon the wettability of the nucleating phase in contact with the other two phases . The former is defined by the contact angle with respect to one of the phases from which it starts growing . This contact angle depends upon the surface tension of the interfaces in contact with each other which varies with temperature and pressure. Though $TiAl_3$ is a compound of fixed stoichiometry it shows small gradient from 74 to 77 at% Al.The average thickness of $TiAl_3$ is much greater compared to other intermetallic phases present in the diffusion couple. It shows high growth rate of $TiAl_3$ compared to other

Figure 3.43: Series of titanium aluminides

intermetallic compounds as reported by Van Loo et al (5). They found the activation energy as well as frequency factor are low for $TiAl_3$. They concluded that there is a strong indication for the influence of grain boundary or more generally short circuit diffusion. Kidson et al(52) proposed that very fast diffusion along a lattice direction with an abnormally high vacancy concentration may lead to the low activation energy and frequency factor values. Al which is the major component in $TiAl_3$ is the faster diffusing element, because it can move in its own sublattice without disturbing Ti sublattice .But , for Ti, it must make some "wrong bonds " by going via Al sublattice temporarily (for the nearest neighbour jump), which increases the energy . The high growth rate suggests that,Ti diffusion via Al sublattice , encouraged at high temperatures (eg 900°C) causing randomness on ordering behaviour.

Hancock (56) has shown that six jump vacancy cycle is possible in L1$_2$ lattice for an α and β vacancy, which reasonably cause 'wrong' type of boning temporarily during diffusion. Though TiAl shows higher composition range (non-stoichiometry according to the phase diagram) compared to $TiAl_2$ and $TiAl_3$
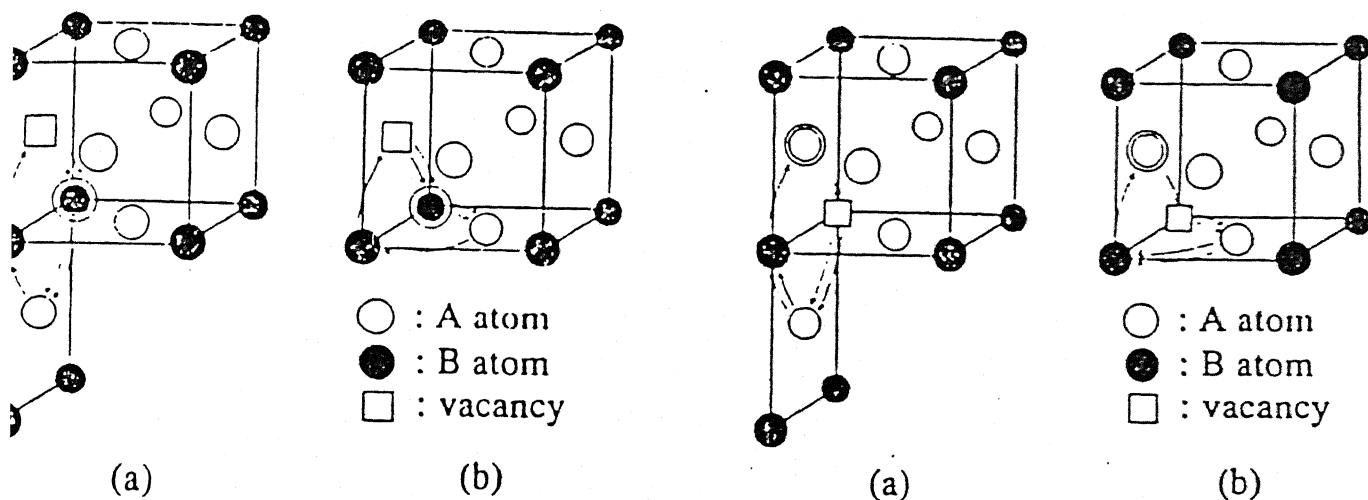
Figure 3.44: A_3B type $L1_2$ structure showing jump distance of atom

phases ,it forms a very thin layer , because the supply of Al through $TiAl_2$ gets reduced due to very low flux (because of low concentration gradient). On the other hand , $TiAl_3$ appears as thick layer , because of high flux of Ti from α(Ti) and high flux of aluminium from TiAl .In both the cases high concentration gradient causes higher flux of both Ti and Al.

3.7 Ternary Diffusion Couple, Ti-Al-Si

As Al-12 %Si eutectic alloy is kept in contact with Ti , due to formers high wettability , it forms a vanishingly flat liquid film , that surrounds the Ti all over the surface . Ti-Al-Si ternary isothermal diagram at 1200^0C as given by Perot(28) is slightly changed to get the schematic diagram at 900^0C/1000^0C because no major reaction or phase transformation occurs in the temperature range of 1200^oC–900^0C/1000^0C.

Ideal diffusion path shows , that τ_2 and $TiAl_3$ should exist in the liquid, however, water quenched sample does not show τ_2 , rather it shows $TiAl_3$.

That means , a liquid layer followed by (L+TiAl$_3$) layer forms . The nature
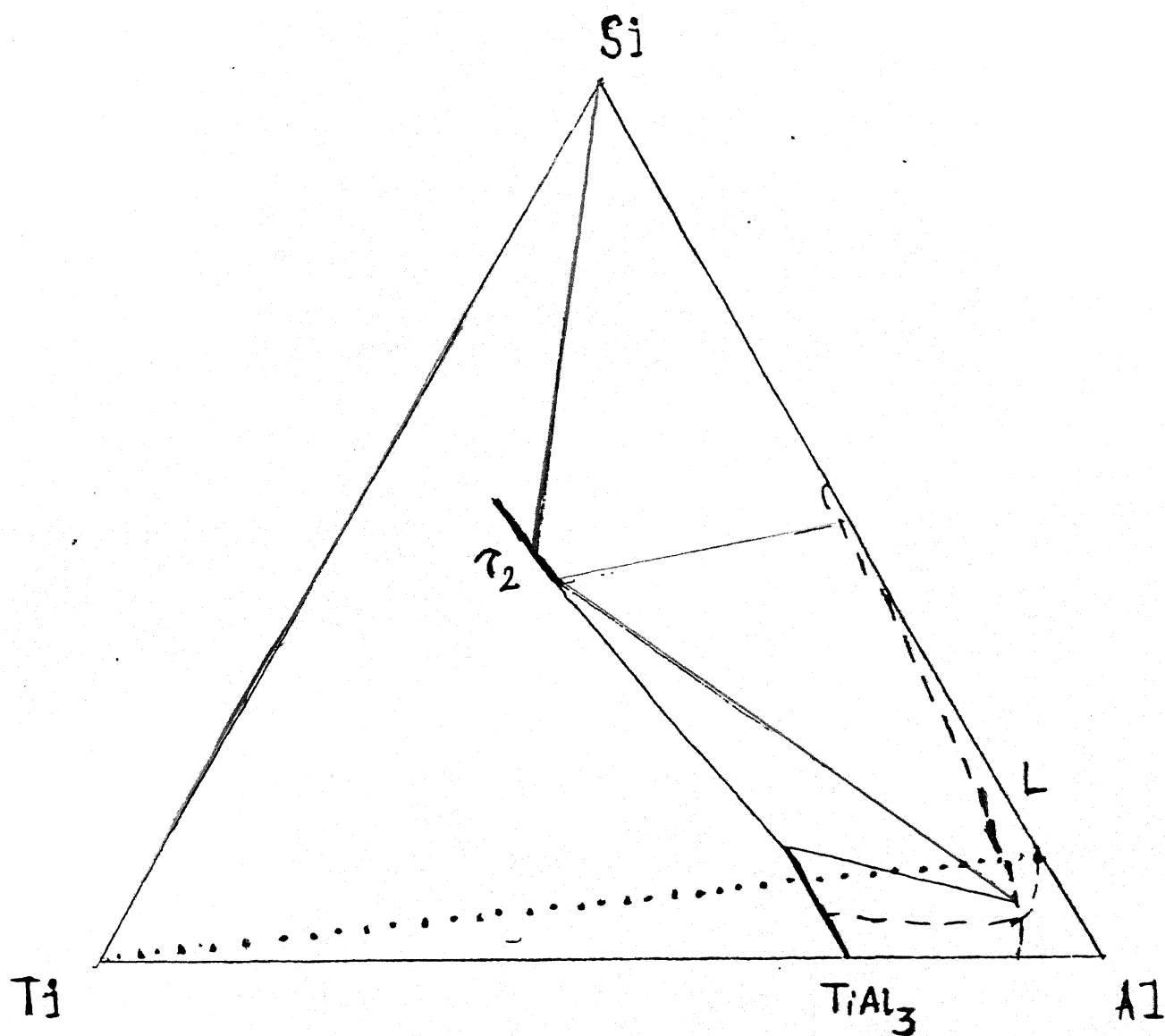
Figure 3.45: Schematic isothermal diagram at $900^{\circ}C/1000^{\circ}C$ towards the Al rich end

of the expected diffusion path through the liquid part can be explained by high diffusivity of Al compared to Si in the liquid . At the $(L+TiAl_3)$ /TiAl$_3$ interface TiAl$_3$ solidification starts, as Ti and Si cross the solubility limit .As we scan the
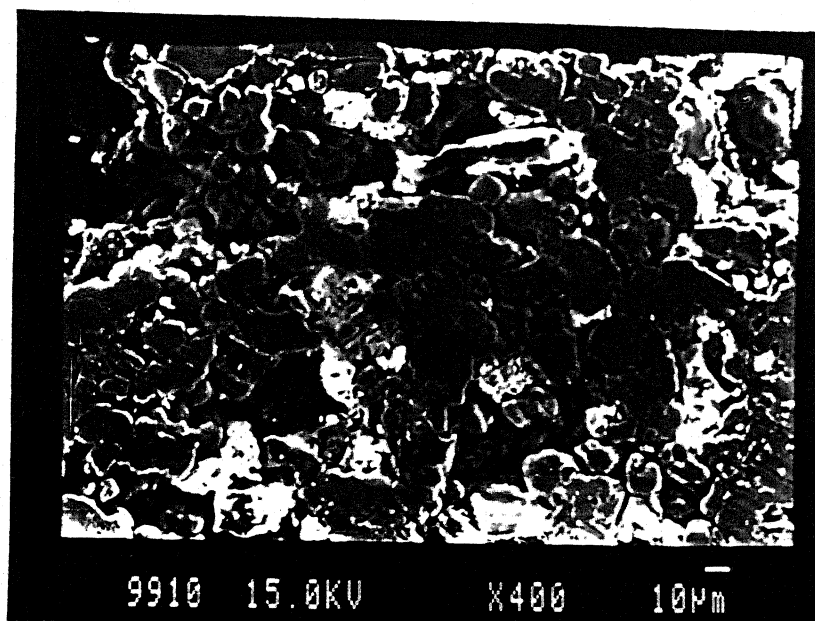
Figure 3.46: Water quenched diffusion couple showing $TiAl_3$ phase

microstructure towards the top of the diffusion couple τ_2 and (Al) form, Fig 3.47 and 3.48 .
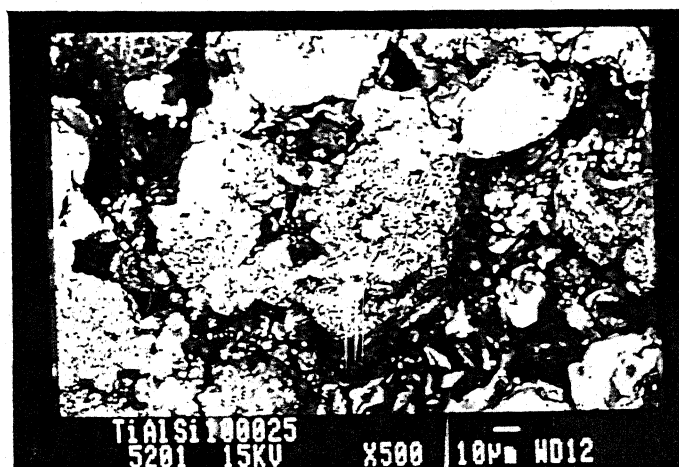
Figure 3.47: Microstructure showing τ_2 and (Al) phases.

Further cooling rotates the two phase field of τ_2 +(Al) and τ_1 +(Al) and both

Figure 3.48: Microstructure showing τ_2 and τ_1 phases

solidify from the liquid,Fig3.48. As observed in the microstructure, the volume fractions of τ_2 and τ_1 phases are very much smaller compared to $TiAl_3$. In the tentative ternary isothermal reaction proposed by Schubert et al(32) τ_1 appears below 900^0C ,but its exact temperature of formation is not known. Therefore, there must be a two phase field of L+τ_2 which helps $\tau_2$ to crystallise in the liquid before the formation of τ_1 .This is apparent from the microstructure,Fig 3.49 .

In few of the microstructure, products of the peritectic reaction L+TiAl$_3$= (Al) is noticed (Fig 3.49) where the liquid supposed to be extremely depleted of Si or the local composition fluctuation due to convection makes few liquid pockets with peritectic composition. Fig 3.49, also shows Al-Si eutectic structure. Though this structure is expected in the topmost part of the diffusion couple it is formed due to local liquid composition, diffusion and thermal field of the other solidifying phases. Binary Al-Si eutectic is the last to form , because at T_E liquidus surface shrinks to a point . The photomicrograph of Fig 3.50, shows τ_2 on $TiAl_3$.

Figure 3.49: Microstructure showing τ_2 phase, peritectic morphology of $TiAl_3$ and binary Al-Si eutectic

This is quite expected as the rotation of $\tau_2 + TiAl_3 +$ (Al) field makes the diffusion path cross this triangle . The τ_2 phase precipitates on TiAl$_3$ during cooling . Next to the L+TiAl$_3$ layer , different solid state reaction product forms isothermally . The first layer is that of the $TiAl_3$ phase which is relatively thick . This is followed by two phase mixture of $(TiAl_3 + Ti_5Si_3)$; $(TiAl + Ti_5Si_3)$ and Ti_3Al for diffusion couple annealed at 900^0 for 9 and 16 hours and at 1000^0C for 9 hours,Fig 3.51-3.53.
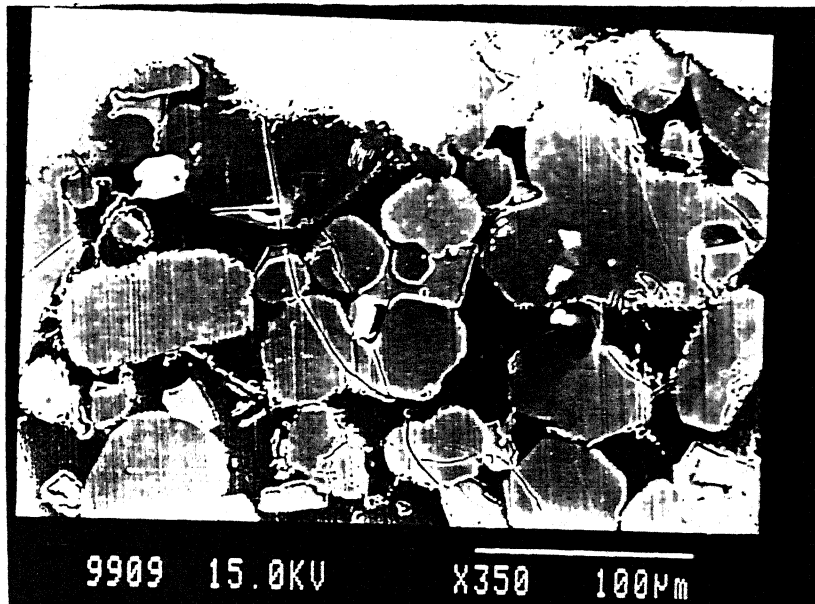
Figure 3.50: τ_2 phase on$TiAl_3$

The Ti_5Si_3 intermetallic layer forms a fibrous structure and its growth direction is parallel to the direction of diffusion. The growth of this phase is highly anisotropic. The Ti_5Si_3 structure, appears as a thick single layer also, Fig 3.53. In some places Ti_5Si_3 precipitates in random orientation, Fig 3.52. Next to ($TiAl_3$ $+Ti_5Si_3$) phase region, (Fig 3.52) a thick layer of TiAl forms with a precipitation of Ti_5Si_3 on it .Fraction of of the precipitates are very small denoting that
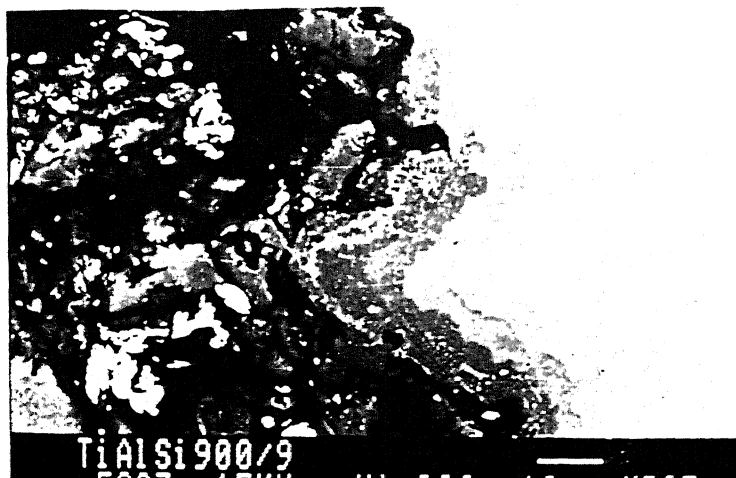
Figure 3.51: Microstructure showing different solid state reaction morphology

diffusion path crosses this phase field towards the TiAl corner and it almost touches the binary because it gives Ti_3Al with low Si solubility (0.3–0.5 at As already mentioned $TiAl_2$ intermetallic is not observed after analysing compositions of different layers that have formed in the diffusion couple experiment . Even analysis carried out at eight points at a spacing of 1μ m between ($TiAl+Ti_5Si_3$) and (Ti_3Al) . Heats of formation of TiAl(74.0 KJ /mole) is *lower* than that of $TiAl_3$ (142.4KJ/mole) and Ti_3Al(110.4KJ/mole) . The heat formation of for the $TiAl_2$ phase is not available .But ,in the diffusion couple annealed at 1000^0C for 25 hours ,$TiAl_2$ phase forms randomly in few regions . It appears that nucleation is easier in some part of the diffusion couple and difficult in some other parts . The formation energy of an intermetallic is independent of time of annealing of the diffusion couple. The problem lies in the growth kinetics , which is very slow for $TiAl_2$. That is why it ultimately starts appearing along the interface with increase in the diffusion time . From the isothermal diagram at 700°C (28)it appears that the ($TiAl_2+Ti_5Si_3$) phase reaction shows a very narrow phase field towards the $TiAl_2$ corner .May be this two phase field enlarges at higher tem-

Figure 3.52: Solid state diffusion products
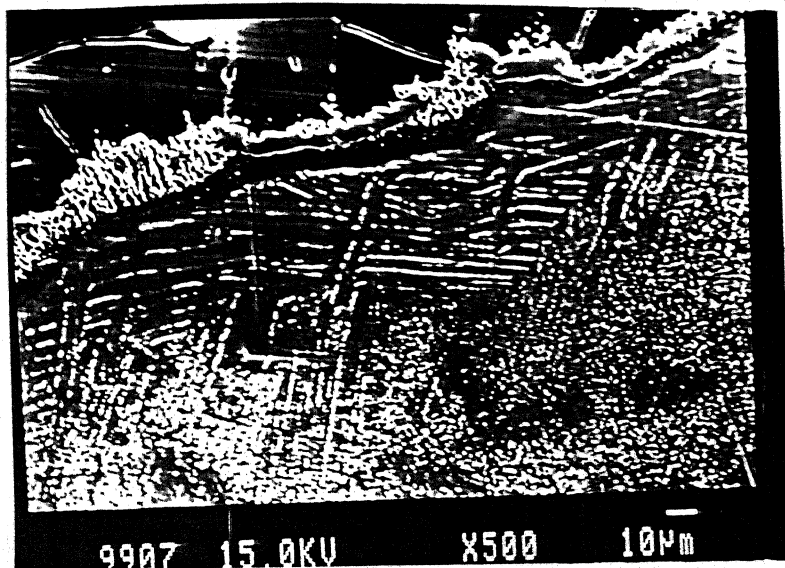
Figure 3.53: Intermetallics layers formed in Ti-Al-Si system

perature (900°C and 1000°C). The ideal diffusion path through it still shows a very negligible concentration gradient . This may be partly responsible for the absence of TiAl$_2$ in other diffusion couples .

A solid solution of α(Ti) forms next to the Ti_3Al layer . A precipitate of β(Ti) is formed on α(Ti) during cooling which is prominent for diffusion couple annealed at 1000^oC. Because higher fraction of β Ti forms isothermally in equi-

Figure 3.54: β (Ti) and α (Ti) showing orientation relation
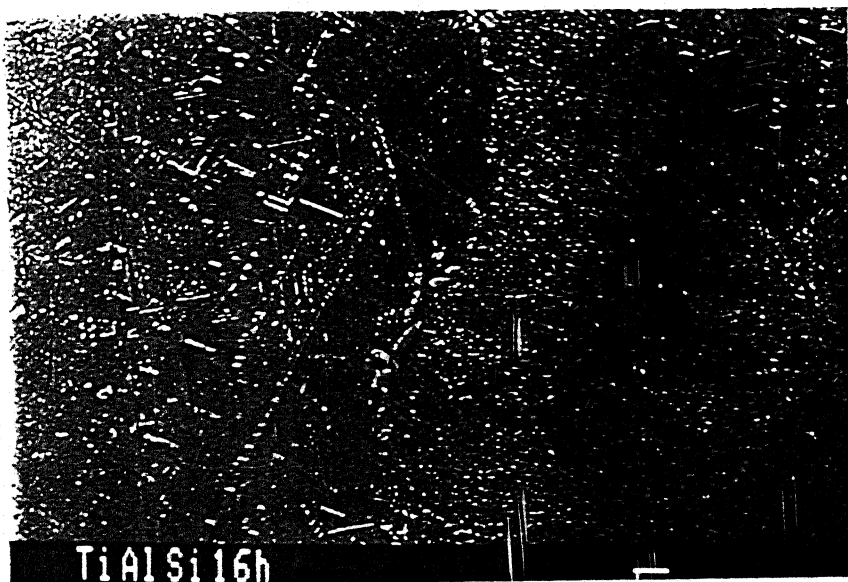
Figure 3.55: Ti_3Si precipitate on α Ti

librium with α (Ti) at 1000°C. β(Ti) is found near the interface as expected from the binary Ti-Al phase diagram . β(Ti) shows a clear habit plane and orientation relationship with matrix α(Ti). Again, α (Ti) matrix shows another type of precipitate morphology (Fig 3.55) ,which is identified to be Ti_3Si This is quite expected from Ti-Si phase diagram,Fig 3.56 .
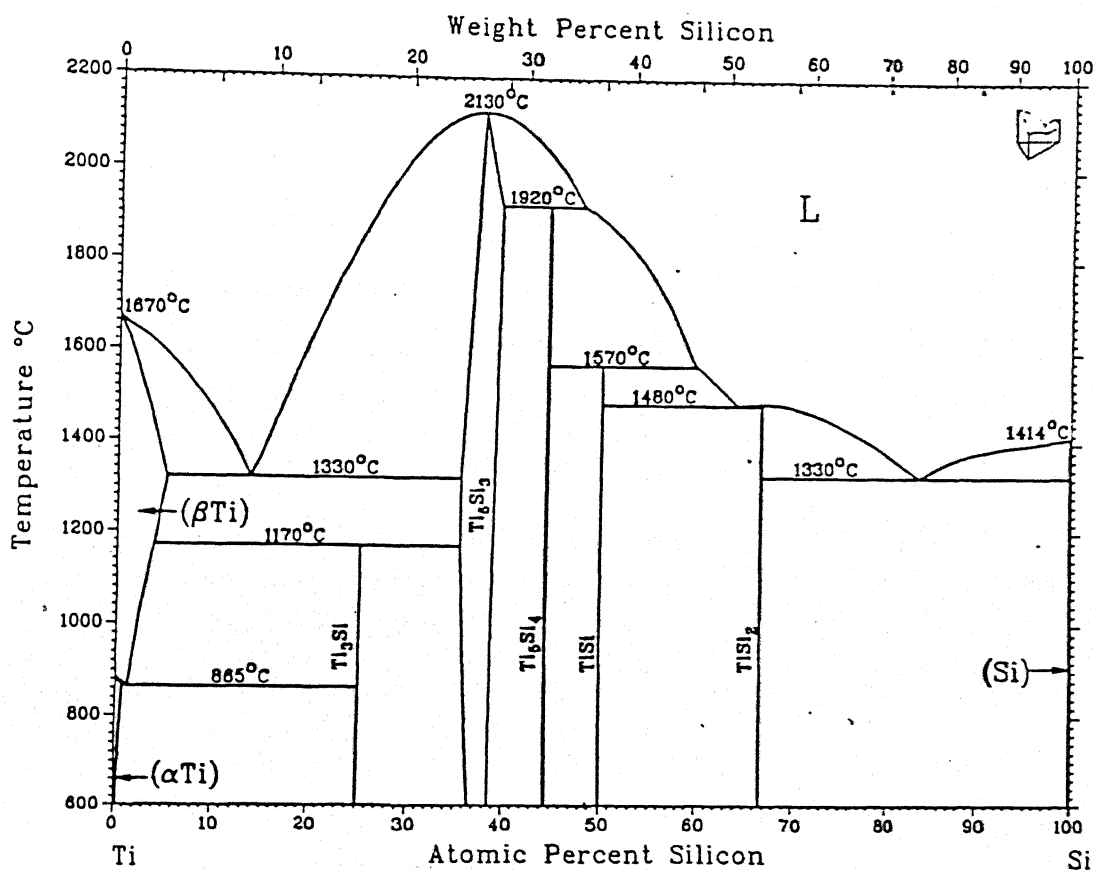
Figure 3.56: Ti-Si binary phase diagram (23)

to almost " zero " wt%Si at room temperature, so that α(Ti) throws out Si in the form of Ti_3Si. The Ti_3Si precipitates also has preferred orientation for growth and therefore maintains a rigid habit plane and direction with the α(Ti) matrix .

3.8 Composition of Binary Aluminides and (Ti) Solid Solution of Ti-Al-Si Diffusion Couple

The analysis of different titanium aluminides was carried out for Ti-Al-Si ternary diffusion couple, using EPMA unit. This is shown in table **3.7**. Analysis of Ti solid solution is shown in Table **3.8**. Si atoms preferentially go to Al sublattice. Except for the $Ti(Al_{1-x}Si_x)_3$ phase, the solubility of Si in the other titanium aluminides is upto 1-5 at %. The $Ti(Al_{1-x}Si_x)_3$ phase shows Si solubility upto 12.08 at % which is comparable to the observed value of upto 15 at % by Brukl et al (31). From the isothermal section compiled by Perot(28),it is noticed that the solubility of Si in $TiAl_2$ and TiAl is almost negligible. The solubility of Si in $TiAl_2$ and Ti_3Al has been observed to be 0.22 and 0.5984 at%, respectively. Sidorenko et al(54) observed that the TiAl phase dissolves less than 1 at% Si. But, our results show Si solubility upto 1.5830 at% for the TiAl phase. As we go towards the off stoichiometric i.e, towards Ti rich side of titanium aluminides, Ti is expected to go the Al sublattice (though it is a perfectly stoichiometric compound according to the binary Ti-Al phase diagram (23)) as antisite defects and therefore would decrease the Si solubility because it has already occupied the site of Si atoms. This general trend is quite clear from our analysis. The reverse is true for the other side of the perfect stoichiometry. Table 3.8 shows the solubility of Al and Si in α (Ti). Binary Ti-Si phase diagram (23) shows almost 'Zero' Si solubility in α (Ti), but it appears that non-equilibrium cooling condition may lead to supersaturated solid solution of α (Ti), which shows Si solubility upto 0.5160 at % .

Table 3.7: Compositions of intermetallics formed in the Ti-Al-Si system

Phase	Atomic%			
	Ti	Al	Si	x
$Ti(Al_{1-x}Si_x)_3$	21.9616	66.9335	11.1048	0.1481
	22.0244	66.8215	11.1541	0.1487
	22.0314	66.3096	7.7529	0.1034
	22.0448	66.6217	11.3334	0.1511
	22.1504	66.9784	10.8713	0.1449
	22.2268	71.6143	5.7230	0.0763
	22.8458	69.0670	8.0871	0.1078
	23.0370	69.2101	7.7529	0.1034
	23.1570	70.2768	6.5662	0.0875
	23.8964	68.5070	7.5966	0.1013
	24.2058	69.7896	6.0047	0.0801
	25.0038	71.2629	3.7333	0.0497
	26.0780	67.3655	6.5565	0.0874
$Ti(Al_{1-x}Si_x)_2$	31.4554	68.3218	0.2207	0.0014
$TiAl_{1-x}Si_x$	42.1856	57.3928	0.4275	0.0085
	46.0771	52.4006	1.5223	0.3045
	46.4040	52.1887	1.4073	0.0281
	47.7476	50.6694	1.5830	0.0316
$Ti_3(Al_{1-x}Si_x)$	63.3070	35.3403	0.3526	0.0141
	66.1470	33.2870	0.5660	0.0226
	69.2053	30.4067	0.388-	0.0155
	70.8464	28.4707	0.6829	0.0273
	72.7749	26.6266	0.5984	0.0239
	74.5268	24.8911	0.5821	0.0233

Table 3.8: Composition of the Ti solid solution of the Ti-Al-Si ternary system

Solid solution	Atomic %		
	Ti	Al	Si
Titanium	82.4005	17.4353	0.1643
	90.7060	8.8240	0.4700
	91.8175	7.8480	0.3344
	92.0072	7.4822	0.5106
	92.0735	7.4034	0.5231
	92.3088	7.3490	0.3422
	99.8291	0.0548	0.1161

Chapter 4

Conclusion

- The microstructure of the phases observed in binary and ternary diffusion couple is characterised.

- All the binary phases of Fe-Al and Ti-Al system were found in both the ternary diffusion couple. In Fe-Al-Si system τ_2, τ_4, τ_5 and τ_6 were found while in Ti-Al-Si system both τ_1 and τ_2 were found as ternary compounds besides Ti_5Si_3.

- Diffusion induced recrystallisation was observed at Fe_2Al_5/ $FeAl_3$ interface of Fe-Al binary diffusion couple.

- Kirkendall plane was present at (Fe)/FeAl and $FeAl/Fe_2Al_5$ interfaces in Fe-Al diffusion couple and was observed to move from the middle of FeAl to $Fe_2Al_5/FeAl_3$ interface in Fe-Al-Si diffusion couple as diffusion time was increased.

- Only the peritectic reaction P_5 was observed to occur in water quenched Fe-Al-Si ternary diffusion couple.

- The τ_6 phase was observed to have preffered orientation in Fe-Al-Si diffusion couple which was air cooled from 600°C.

- $TiAl_2$ has very low growth kinetics in the presence of Si.

- Diffusion path bends towards the binary systems Ti-Al or Fe-Al path through solid state diffusion products formed isothermally.

- The Si atoms substitute for the Al sublattice in intermetallics formed in Fe-Al-Si and Ti-Al-Si system.

References

[1] P. Lin, L. Thorvaldsson, G. L. Dunlop ;*Mater. Sci. Technol.*, 2, 1009 - 1018 (1986), (Crys. Structure, Experimental, 26)

[2] P. Sujerpe,*J. Microscopy*, 148, 33-50 (1987), (Crys. Structure, Experimental, Theory, 12)

[3] T. Turmezey,*Mater. Sci. Forum*, 13/14, 121-132 (1987), (Crys. Structure, Experimental, 12)

[4] P. Lin, G. L. Dunlop ;*Acta Metall.*, 36, 1481-1489 (1988), (Crys. Structure, Experimental, 20)

[5] F. J. J. Van Loo, G. D. Rieck ;*Acta Metall.*, 21 , Jan 1973

[6] A. Loisean, C. Vannuffer ;*Phys. Status solidi.*, A, 107, 665-671 (1988)

[7] J. C. Schuster, H. Ipsen ;*Z. Metallkd*, 81, 389-396 (1990)

[8] Y. I. Frenkel, M. I. Sergeev ;*J. Exp. Teor. Fiz.*, 9, 189 (1939)

[9] B. Ta. Lyubov, *Kinetic Theory and phase Transformation*, Nauka, Moscow, 1969

[10] P. J. Desri, A. R. Yavari ;*Phys. Rev. Lett.*, 1990, 64, 13

[11] P. J. Desri, A. R. Tavari ;*J. Alloy Comp.*, 1992

[12] A. M. Gusak, K. T. Grov ;*Solid State Phenomenon*, 1992, 23-24, 117-122

[13] U. Goselle, K. Tu ; J. Appl. Phys, 1982, 53, 32-52

[14] J. Philleert,*Defect and Diffusion Forum*, vol. 95 - 98, 1993. 495

[15] B. Pieraggi, R. Rapp ;*Acta Met.*, 1988, 36, 1281

[16] G. B. Stephenson,*Defect and Diffusion Forum*, vol. 95 - 98, 1993, 507

[17] F. J. J. Van Zoo, B. Pieraggi, R. A. Raps,*Acta Met. Mater.*, 38, 9, 1990, 1769

[18] J. B. Clark, F. N. Rhines ;*Trans of the ASM*, 51, 1959, 199

[19] R. Kao, Y. A. Chang ;*Acta Metall. Metar*, 41, 12, 1993, 3463

[20] F. J. J. Van Loo,*Proc. Solid. St. Chem.*, 20, 1990, 47

[21] X. L. Li, R. Hillel, F. Teyssandier, S. K. Choi, F. J. J. Van Loo ;*Acta Metall. Mater.*, 40, 11, 1992, 3149

[22] Beyong, Joo Lee ;*Acta Mater.*, 45, 10, 1997, 3993

[23] Massalaski,*Binary Phase Diagram*

[24] V. G. Rivlin, G. V. Ranjnov ;*International Metals Review*, 3, 1981, 133

[25] A. A. Katnelson, V. Ye Polishchnik ;*Phys. Met. Metallgr.*, 36, 2, 86-90, 1972

[26] M. Takahasi,*Kotai Butsuri*, 21, 1986, 259

[27] Gautam Ghosh,*Aluminium - Iron - Silicon* in Ternary Phase Diagram

[28] Pierre Perot,*Aluminium - Silicon - Titanium* in Ternary Phase Diagram

[29] F. A. Crosley, D. H. Turner ;*Trans. Met. Soc. AIME*, 212, 1958, 60

[30] C. Panseri, B. Guastalla ;*Aluminio*, 10, 1941, 202

[31] C. Brukl, H. Nowotony, O. Schob, F. Benezorvsky,*Montash Chem*, 92, 1961, 781

[32] K. Schubert, K. Frank, R. Gohle, A. Maldonado, A. G. Meissna, A. Rama, W. Rosstentscher ;*Naturwisserscheften*, 50, 1963, 41

[33] A. Raman, K. Schubert,*Z. Mettallkd*, 56,1965,44

[34] D. Liang, H. Jones ;*Materials Science and Engineering*, A173, 1993, 109-114

[35] D. Liang, H. Jones ;*Soc. Metall. Mater.*, 28, 1993, 7

[36] H. Biloni, W. J. Boetlinger,*"Solidification" from " Physical Metallurgy"*, Chap. 8 edited by R. W. Cahn& P. Haasen

[37] M. Hillert,*Scripta Metall*, 17, 1983, 237

[38] Y. A. Chang, J. P. Neumann ;*Prog. Solid St. Chem.*, 14, 1982, 221

[39] Smithells ;*Metals Refence Book* vol 1

[40] J. C. Brice,*The Growth of Crystals from Liquids*, 1973, P120

[41] M. C. Fleming, *Solidification Processes*, McGrawHill, 1974

[42] D. G. McCartney, J. D. Hunt, R. M. Jordan ;*Met. Trans.*, 1980, 1243

[43] R. S. Wagner,*Acta Met*, 8, 1960, 57

[44] D. R. Hamilton, R. G. Seidansticker ;*J. Appl. Phys.*, 31, 1960, 1165

[45] Maquiab Lin Baicheng, Li Runquin ;*Acta Metall. Mater.*, 42, 12, 1994, 4087

[46] A. A. Murieva, N. German, V. Zarechnyuk, E. V. Gladyschevski ; *Ternary Compounds of the Fe-Al-Si System*, Proc. second All - Union Conf. on the Crystal Chemistry of Intermetallic Compounds, L'bov, October, 35-36, 1974

[47] M. Armand, *Liquation and Equilb. Diagram : Application to the Diagram of Al-Fe-Si alloys*, Congress Internationale de l' Aluminium, Paris, 1954, vol. 1, Revue de l' Aluminium, 305-327, 1955

[48] C. Y. Sun, L. F. Mandolfo ; *J. Inst. Met.*, **95, 1967, 384**

[49] A. L. Dons, Z. Metallkd., **75, 1984, 170**

[50] P . Skjorpe *Met Trans A*,18A,1987,189

[51] V. Stefaniay, A. Guiger, T. Turmezey ; *J. Mater. Sci.*, **22, 1987, 539**

[52] G. R. Kidson, G. D. Miller ; *J. Nucl. Mater.*, **12, 1964, 61**

[53] G. F. Hancock,*Phys. Stat. Solidi.*, **7, 1971, 525**

[54] F. A. Siderenko, I. Z. Rodovskii, L. S. Chemerinskaya, P. V. Geld ; *Fiz. Svoistva Met. Splavov*, **1, 1976, 10**

A 126246

MME-1998-M-MAI-FOR